FABRICATION AND CHARACTERIZATION OF SOLID-STATE GAS SENSORS

A Thesis submitted to the University of North Bengal

For the Award of

Doctor of Philosophy

in

Physics

By

Aparna Ghosh

SUPERVISOR

Dr. Suman Chatterjee

Department of Physics
University of North Bengal

December 2020

Dedicated
TO
My Parents
&
Family members

DECLARATION

I declare that the thesis entitled **FABRICATION AND CHARACTERIZATION OF SOLID-STATE GAS SENSORS** has been prepared by me under the guidance of Dr. Suman Chatterjee, Associate Professor of Physics, University of North Bengal. No Part of this thesis has formed the basis for the award of any degree or fellowship previously.

Aparna Ghosh 21/12/2020

Aparna Ghosh
Department of Physics
University of North Bengal
Darjeeling, 734013
West Bengal, India

CERTIFICATE

I certify that **APARNA GHOSH** has prepared the thesis entitled, **FABRICATION AND CHARACTERIZATION OF SOLID-STATE GAS SENSORS** for the award of Ph.D. degree of the University of North Bengal, under the guidance of Dr. Suman Chatterjee. She has carried out the work at the Department of Physics, University of North Bengal. No part of this thesis has formed the basis for the award of any degree or fellowship previously.

Suman Chatterjee 21/12/2020

Dr. Suman Chatterjee
Department of Physics
University of North Bengal
Darjeeling 734013, India
E-mail: suman_chatterjee@hotmail.com

Associate Professor
Department of Physics
University of North Bengal

URKUND

Urkund Analysis Result

Analysed Document:	Aparna Ghosh_Physics.pdf (D64434662)
Submitted:	2/26/2020 9:19:00 AM
Submitted By:	nbuplg@nbu.ac.in
Significance:	1 %

Sources included in the report:

https://www.semanticscholar.org/paper/Metal-Oxide-Semi-Conductor-Gas-Sensors-in-Fine-Cavanagh/20404ecfb239a0084e97a944781f39d73fca4ef1
https://ir.library.oregonstate.edu/downloads/m039k896k
https://www.science.gov/topicpages/n/nanowire+gas+sensors

Instances where selected sources appear:

3

Aparna Ghosh
21/12/2020

Suman Chatterjee
21/12/2020

Associate Professor
Department of Physics
University of North Bengal

Suman Chatterjee
21/12/2020

Head
Department of Physics
University of North Bengal

ABSTRACT

The research work in this thesis entitled as **FABRICATION AND CHARACTERIZATION OF SOLID-STATE GAS SENSORS** is primarily focused on the development of gas sensing materials, their working principle, influence of defects inside the grains on sensor output, factors affecting gas sensor performance, their characterization by various methods like Scanning Electron Microscope, Powder XRD and their application towards the monitoring of tea quality. We also dealt with the band structure and its modification by the incorporation of defects. The shift of Fermi Level results an additional potential which affects the conductivity of gas sensor materials. The overall work delineated herein has been divided into five chapters.

The **Chapter I** covers a brief review on the recent fabrication procedure of gas sensing materials, transition metal oxide semiconductor gas sensors, their characterization, various gas sensing mechanism that includes potential barrier model, band bending model etc which deals with the surface of the grains, effect of doping, effect of microstructure, particle size on the sensor performance and finally application of these gas sensor materials in various fields.

Chapter II depicts the study of the responses with temperature of a p-type, La_2CuO_4 and a n-type, WO_3 semiconducting sensing element fabricated over YSZ substrate in NO gas atmosphere. The measurements in potentiometric and resistive modes revealed that for potentiometric mode the peak of the response curve shifts toward lower temperature region and for resistive mode the peak shifts towards higher temperature region which confirms more sensitivity of potentiometric mode at lower temperature region compared to resistive mode for both kind of sensing materials.

Chapter III illustrates the detection limit of solid state gas sensors are dependent on the size and average pore diameter of the sensing material which can be varied by sintering the materials at appropriate temperatures. In this paper, we report the fabrication and characterization of a potentiometric NO_x gas sensor based on La_2CuO_4 nanoparticles as efficient electrode material annealed at different temperatures. The synthesized nanoparticles were characterized by

scanning electron microscopy (SEM) and X-ray diffraction (XRD) which revealed that the particle size of the prepared nanomaterials increases with increasing the sintering temperature. It was observed that the smaller nanoparticles increases the contact surface area of the gas–solid interface and exhibited higher sensitivity at low gas concentrations. From voltage response curve, it has been observed that range of detection was maximum at intermediate particle size diameter and became least at large diameter nanoparticles. Planar sensor elements were fabricated over tape cast YSZ substrate with both the ceramic and metal electrodes screen printed on either side of the substrate. The dependence of sensitivity at different range of gas concentration with the pore size distribution of the sensing electrode has been studied in this investigation.

In **Chapter IV** the mechanism of NO adsorption on the WO_3 surface to improve the performance of gas sensing has been studied from a theoretical view point based on Density Functional Study. Different activation energies of the defect directly affect the surface chemistry of the sensing material. Here, the adsorption behaviour of NO on the sensor surface, including the perfect and WO_3 surfaces with defects have been studied. In this study it was revealed that surface oxygen vacancies induced by the adsorption of NO molecule on the defect free WO_3 surface increased the surface conductance of the sensing material. The WO_3 surface with defects was re-oxidized by the atmospheric O_2 molecules. During this step, charge transfer from the surface to O_2 molecule generates an active O_2 species which results in reduction of surface conductivity. This active O_2 species tends to react with the NO molecule and releases NO_2 molecule with the reproduction of perfect WO_3 surface. The difference between Fermi levels associated with above surface reactions were determined with the help of Density Functional study and was found to be 1.54 eV.

In **Chapter V** we have prepared various transition metal doped ZnO nanosensing material which have been successfully used to sense the flavor of Orthodox Darjeeling tea collected from various garden by electronic nose system. The application of E-nose system to determine tea quality is a new direction of research to develop better sensing material. Doping is a very good process which can modify the response signal of E-nose system to a better one. Research in this ground will significantly increase the quality of the sensor system which will obviously help to better differentiate the quality of various teas, foods etc.

PREFACE

Research on variety of transition metal oxide based gas sensor, their fabrication, characterization and various applications has revealed much attention now a days. Various gas sensing mechanism that includes potential barrier model, band bending model etc which deals with the surface of the grains, effect of doping, effect of microstructure, particle size on the sensor performance are very important. The research work discuss about the band structure and its modification by the incorporation of defects. The Fermi Level shift causes an additional potential that affects the conductivity of the gas sensor materials.

This thesis begins with **Chapter I**, which describes the fabrication, characterization of metal oxide based gas sensors, their working principle and their applications. **Chapter II** gives a brief review on temperature dependence of semiconducting gas sensors in potentiometric and resistive modes of measurements. **Chapter III** illustrates fabrication and characterization of NO_x gas sensor based on Lanthanum Copper Oxide (La_2CuO_4) nanoparticles annealed at different temperatures. **Chapter IV** deals with the investigation of sensing mechanism of NO oxidation on tungsten oxide (WO_3) surface using density functional analysis. **Chapter V** illustrates the application of electronic nose systems by array of nanostructured doped ZnO sensing material for assessing tea quality.

ACKNOWLEDGEMENT

This thesis is the outcome of a long rigorous journey in which I have been encouraged and supported by many peoples who actually make my dream possible. It is really pleasure moment for me to express my full gratitude for them.

Primarily, I would like to express my deep and sincere gratitude to my supervisor Dr. Suman Chatterjee, Associate Professor, Department of Physics, University of North Bengal, Darjeeling, for his Inspiring guidance, parental attitude, solicitude behaviour and constant encouragement throughout my work..

I wish to express my warm and sincere thanks to Nano-Structured Materials Division, CSIR-CGCRI, Kolkata, for their help to characterize our sensor materials.

I would like to thank my labmates Rajat Biswas, Chinmay Roy, Trinakshi Roy for their help and active co-oparation throughout my research period.

I would like to express my thanks to University of North Bengal for providing the infrastructural facilities and UGC, New Delhi for awarding NFOBC fellowship.

I express my full gratitude to Head and all respected teachers of Department of Physics, University of North Bengal.

I would like to thank my husband Sankar for his constant selflessness, love and support.

The single largest contribution in properly shaping me what I am today comes from the faith, hope and pride of my parents. Words are inadequate for expressing such feelings.

TABLE OF CONTENTS

		Page No.
Abstract		i-ii
Preface		iii
Acknowledgement		iv
List of Tables		x
List of Figures		xi-xiii
List of Appendices		xiv
Appendix A: List of Research Publications		xv
Appendix B: Oral and Poster Presentations		xvi
Abbreviation		xvii

CHAPTER I

General introduction to fabrication, characterization and application of solid state gas sensors 1-22

I.1.	Introduction	2
I.2.	List of solid state Gas Sensors and their Detection Principles	2
I.3.	Operating principle of the transition metal oxide semiconductor gas sensors	2-10
I.3.1.	Potential Barrier Model	3-5
I.3.2.	Band Bending	5-6

I.3.3. Electrical Conduction Mechanisms 7-10

I.4. Gas Sensing Mechanism 11-15

I.5. Criteria for the Choice of Sensor 15-18

I.6. Sensor Fabrication Methods 18-20

I.7. Applications of Chemiresistive Gas Sensors 20-22

I.8. Reference 22

CHAPTER II

Temperature dependence of Semiconducting Gas Sensors in different Modes of Measurement 23-36

II.1. Introduction 24

II.2. Background and Objectives 24-27

II.3. Present Work: Result and Discussion 27-35

II.3.1. Sensor fabrications and Characterizations 27-34

II.3.2. Experimental Details 34-35

II.3.2.1. Synthesis of the material 34

II.3.2.2. Sensor electrode preparation 34-35

II.3.2.3. Experimental setup 35

II.4. Conclusion 36

II.5. References 36

CHAPTER III

Fabrication and Characterization of La_2CuO_4 Nanoparticle Based NO_x Gas Sensors 37-48

III.1. Introduction 38-39

III.2. Background and Objectives 39-40

III.3. Present Work: Result and Discussion 40-48

III.3.1. Change of response magnitude with gas concentration 41-42

III.3.2. Sensitivity with pore size 43-47

III.3.3. Experimental Details 47-48

III.4. Conclusion 48

III.5. References 48

CHAPTER IV

Investigation of sensing mechanism of Oxidation of NO on the WO_3 surface by Density Functional Analysis 49-62

IV.1. Introduction 50

IV.2. Background and Objectives 50-52

IV.3. Present Work: Result and Discussion 52-61

IV.3.1. Synthesis of Sensing Material and Device Fabrication 52

IV.3.2. Characterization of sensing elements 52-53

IV.3.3. Fabrication and Measurements 54

IV.3.4. Dependence of oxygen partial pressure on sensor output 54-56

IV.3.5. Resistivity of WO_3 thin film with reducing gas 56-60

IV.3.6. Explanation with band structure calculations 60-61

IV.4. Conclusion 62

IV.5. References 62

CHAPTER V

Application of electronic nose systems by array of nanostructured doped ZnO sensing material for assessing tea quality 63-85

V.1. Introduction 64-66

V.2. Background and Objectives 67-70

V.3. Present Work: Result and Discussion 70-84

V.3.1. Steps for fabrication of ZnO based devices 71

V.3.2. Fabrication of ZnO Nanorods 71-73

V.3.3. Sensor Array and its Responses in Tea Infusion Vapour 73

V.3.4. E-Nose measurements 73

V.3.5. Correlating sensor signals with Tea-tasters scores 73-74

V.3.6. Characterization of ZnO 74-78

V.3.7. Measurement of sensor characteristics 78

V.3.8. Doped ZnO Materials for Four Different Sensors 79

V.3.9. E-nose Application of Doped ZnO Sensors for Tea Quality Estimation 80

V.3.10. Principal Component Analysis 80-82

V.3.11. Development of E-Nose response function 82-84

V.4. Conclusion 85

V.5. References 85

Bibliographic References

References for Chapter I	86-89
References for Chapter II	90-91
References for Chapter III	92-94
References for Chapter IV	95-96
References for Chapter V	97-100
Index	101-103

LIST OF TABLES

Table No.	Title	Page No.
Table II.1.	Sensing Parameters of sensing surfaces WO_3 and La_2CuO_4 in Resistive and Potentiometric modes.	29
Table II.2.	Span of Temperature for high response of sensing surfaces WO_3 and La_2CuO_4 in resistive and potentiometric modes.	33
Table V.1.	Properties of doped and undoped sensing elements	77
Table V.2.	Covariant Matrix formed from responses of four different sensor and its Eigen values	81
Table V.3.	Gradient of each sensor calculated from individual response	83-84

LIST OF FIGURES

Figure No.	Title	Page No.
Figure I.1.	a) Physical model and b) Band model showing the development of potential barrier on oxygen adsorption.	4
Figure I.2.	Band bending model showing semiconductor with a wide band gap	5
Figure I.3.	Schematic representation of a conductometric gas sensor with electrodes placed in the sensor face	7
Figure I.4.	Schematic diagram depicting compact sensing with geometry and band.	8
Figure I.5.	a) Open neck, b) Close neck, c) Schottky barrier models for conductance limited by intergrain connections	10
Figure I.6.	Mechanism of Electronic and Chemical sensitization process by metal/metal oxide additives	14
Figure II.1.	SEM Micrograph of sensing surfaces (a) WO_3 and (b) La_2CuO_4	27
Figure II.2.	X-Ray diffraction pattern of sensing surfaces (a) WO_3 and (b) La_2CuO_4	28
Figure II.3.	Response characteristics of sensing surfaces WO_3 and La_2CuO_4 in resistive and potentiometric modes.	30-31
Figure II.4.	Response with Temperature of sensing surfaces (a) WO_3 and (b) La_2CuO_4 in resistive and potentiometric modes.	32
Figure II.5.	Schematic Diagram of sensor designs (a) Potentiometric and (b) Resistive	35
Figure II.6.	Schematic Diagram of the Measurement setup.	35
Figure III.1.	Typical SEM images of prepared La_2CuO_4 nanoparticles sintered at (a) 750 °C, (b) 800 °C and (c) 900 °C.	41
Figure III.2.	Voltage response of three different types of prepared La_2CuO_4 nanoparticles sintered at 750 °C, 800 °C and 900 °C with step change in gas concentration	42

Figure III.3.	Voltage response of three different types of prepared La_2CuO_4 nanoparticles sintered at 750 °C, 800 °C and 900 °C with gas concentration at 450 ^oC	42
Figure III.4.	Schematic diagram of gas diffusion through different porous sensing surface.	44
Figure III.5.	Simulation of the sensitivity range for small, medium and large sized pores of sensing material.	46
Figure III.6.	X-ray diffraction pattern for the prepared La_2CuO_4 nanoparticles sintered at (a) 750 °C, (b) 800 °C and (c) 900 °C.	48
Figure IV.1.	SEM micrograph of sensing surface WO_3	53
Figure IV.2.	X-Ray diffraction pattern of sensing surface WO_3	53
Figure IV.3a.	Nyquist diagrams of WO_3 films in different P_{O_2} at 450 ºC	54
Figure IV.3b.	Nyquist diagrams of WO_3 films in different P_{O_2} at 650 ºC	55
Figure IV.3c.	Variation of resistance as a function of P_{O_2} plotted on logarithmic axes	55
Figure IV.4.	a. Response with Temperature of WO_3 sensing surfaces in resistive mode and b. corresponding to Arrhenius Plot.	58
Figure IV.5a.	Band structure of WO_3	60
Figure IV.5b.	Band structure of W_nO_{3n-1}	61
Figure IV.5c.	Variation of DOS with energy for WO_3 structure	61
Figure IV.5d.	Variation of DOS with energy for WO_3 with 5 % defect surface states	61
Figure V.1.	Flow chart for preparation of ZnO nano layer.	72
Figure V.2.	Sketch of the Electronic Nose system used for the study.	74
Figure	(a) X-ray diffraction patterns of ZnO thin film and (b) EDX analysis of	75

V.3.	ZnO Sample	
Figure V.4.	SEM images of (a) un-doped and doped ZnO thin films with (b) Fe doped ZnO (c) Co doped ZnO and (d) Ni doped ZnO	76
Figure V.5.	PCA results of training data obtained from sensor array.	82
Figure V.6.	Calculation of individual response gradient of four different sensor elements	82-83
Figure V.7.	Calibration of the sensors using a function built from individual sensor responses for Orthodox black tea.	84

APPENDICES

APPENDIX A:

List of Research Publications

APPENDIX B:

Oral and Poster Presentations

APPENDIX A:

List of Research Publications :

1. "Temperature Dependence of Semiconducting Gas Sensors in Potentiometric and Resistive Modes of Measurement", **Aparna Ghosh**, P. K. Mandal, Suman Chatterjee*, *Sensor Letters*, **2017**, 15(2), 137–141, DOI : 10.1166 /sl.2017.3788.
2. "Fabrication and Characterization of NO_x Gas Sensor Based on Lanthanum Copper Oxide (La_2CuO_4) Nanoparticles Annealed at Different Temperatures", Suman Chatterjee*, **Aparna Ghosh**, *Sensor Letters*, **2018**, 16(2), 116–122, DOI : 10.1166/sl.2018.3940.
3. "Investigation of Sensing Mechanism of NO Oxidation on WO_3 Surface Using Density Functional Analysis", Suman Chatterjee*, **Aparna Ghosh**, Chinmay Roy, *Sensor Letters*, **2018**, 16(9), 677–682, DOI : 10.1166/sl.2018.4009.
4. "Role of defects in electron band structure and gas sensor response of La_2CuO_4", Chinmay Roy, **Aparna Ghosh**, Suman Chatterjee*, *Sensor Review*, **2020**, 40(6), DOI : 10.1108/SR-12-2019-0319.

APPENDIX B

Oral & Poster Presentations :

1. "Fabrication and Measurement of WO_3 and ZnO Nanopowders and Measurement of Activation Energies for Application as Gas Sensor", National conference on "Modern Trends in Material Science–2015" organized by the Department of Physics, University of North Bengal, Darjeeling, India, February 5–6, 2015.
2. "Sensor for determination of tea quality using nanostructured sensing elements", Interdisciplinary (Science) National seminer on "Science and Mankind – A better Tomorrow", organized by the Department of Physics, A. B. N. Seal College, Cooch Behar, February 22–23, 2018.

ABBREVIATION

ADS	Auto damper system
ANN	Artificial neural network
BPNN	Back propagation neural network
^{o}C	Degree Celsius
CWAs	Chemical warefare agents
CTC	Cut Tear Curl
CDA	Canonical discriminate analysis
CA	Cluster analysis
DOS	Density of states
DMMP	Dimethyl methyl phosphonate
ev	Electron volt
EMF	Electromotive force
FTIR	Fourier transformed infrared spectra
HCs	Hydrocarbons
ITO	Indium tin oxide
KNN	K-nearest neighbours
MOS	Metal oxide sensor
MEMS	Micro electronic mechanical system
ppm	Parts per million
PEG	Polyethylene glycol
RBF	Radial basis functtion
S/N	Signal to noise
SEM	Scanning electron microscope
TM	Transition metal
VOC	Volatile organic compound
XRD	X–ray diffraction

Chapter I

General introduction to fabrication, characterization and application of solid state gas sensors

I.1. Introduction

A device which detects a change in the physical and/or chemical stimulus and converts it into an electrical signal that can be measured or recorded is known as ‘sensor’. A wide field of sensors have been developed with the growth of science and technology leading to the development of various sensing devices. This is an interdisciplinary branch involving physics, electronics, chemistry, sometimes biology involving biosensors. ‘Sensor’ and ‘transducer’ are two important words which are widely used now a days for the description of various measurement systems. Transducer is a device which transfers power in same or in different form from one system to another. Due to large number of sensors that may exist one may categorize sensors depending upon the principle of operation. Sensors are normally prepared in the amorphous, single crystalline, polycrystalline, as well as nanostructural forms. Finally, the newly emerged sensing technology is utilizing nanomaterials for very efficient low temperature gas sensing. In the present chapter, we will discuss about theoretical background of solid state semiconductor gas sensors, more particularly about metal oxide sensor (MOS).

I.2. List of solid state Gas Sensors and their Detection Principles

i) Chemiresistive : Change in the conductivity while exposure to different analyte gases.

ii) Potentiometric : Here the signal is measured as potential difference/voltage obtained between the working electrode and that of the reference electrode. The potential of working electrode must depend on the analyte gas concentration.

iii) Chemical field effect transistors : Current–Voltage (I-V) curves of this type are sensitive to a particular gas when it interacts with a gas.

iv) Calorimetric : Oxidation on a catalytic element results the rise in temperature which measures the concentration of a particular combustible gas.

I.3. Operating principle of the transition metal oxide semiconductor gas sensors

Surface of the sensing element and the microstructure of the same acts as receptor and transducer respectively for transition metal oxide semiconductor gas sensor . A change in output resistance occurs due to the receptor and transducer function of these active metal oxide layer of the gas sensor.

Under exposure of a reducing or oxidizing species sensor undergoes an exponential change in conductance across the sensing layer of the sensor under constant flow rate and operating temperature which is assumed to be the stationary condition. The response of semiconductor gas sensor materials towards the reducing gases are denoted by the change in the concentration of the adsorbed oxygen. Oxidizing species can interact with sensor surface by any of the two ways viz. interacting with the sensor surface directly which results an negatively charged ionosorbed species and also competes with the ionosorbed oxygen ions already present at the relative adsorption sites.[1,2] Conductance of sensing layer are modulated by the change in the height of potential barriers. Thus sensitivity depends upon the structural characteristic of the sensor materials, the working temperature. The surface with dopants or without dopant which are catalytically active plays an important role in determining the sensitivity. Brief review of various established models are depicted hereunder.

I.3.1. Potential Barrier Model

Potential barrier is the most authentic model for the semiconductor gas sensors operation, representing the simplified metal oxide grains chain model. According to the physical model (Figure I.a) the grains contain adsorbed oxygen in its surface, where the adsorbed oxygen contains trapped electrons coming from the subsurface grains region leading to an insulating surface layer. Moreover, it is assumed that electrons are more in bulk. Conduction occurs when electrons go from one grain to another through the insulating layer. Band model has been illustrated in the Figure I.b which well depicts the insulating layer with potential barrier. The adsorbed oxygen present at the surface removes electrons leaving a positively charged surface. Consequently, an electric field develops between the positively charged ions and the negatively charged oxygen ions present upon the surface.[3] To move to the neighbouring grain the barrier associated with the electric field must be overcome by the electrons present in conduction band. The potential barrier is indicated as qV_s. V_s increases proportionately with the concentration of O^-.[4] n_s represents the density of electrons having sufficient energy to cross the potential barrier. This is given by the Boltzmann equation:

$$n_s = N_d \exp\left(\frac{-qV_S}{kT}\right)$$

N_d is density of donors. With increasing concentration of oxygen on the surface the barrier increases. As a consequence transition of fewer electrons are possible increasing the resistance thereby. The adsorbed oxygen shows a capacity of 1 eV band bending at high coverage.

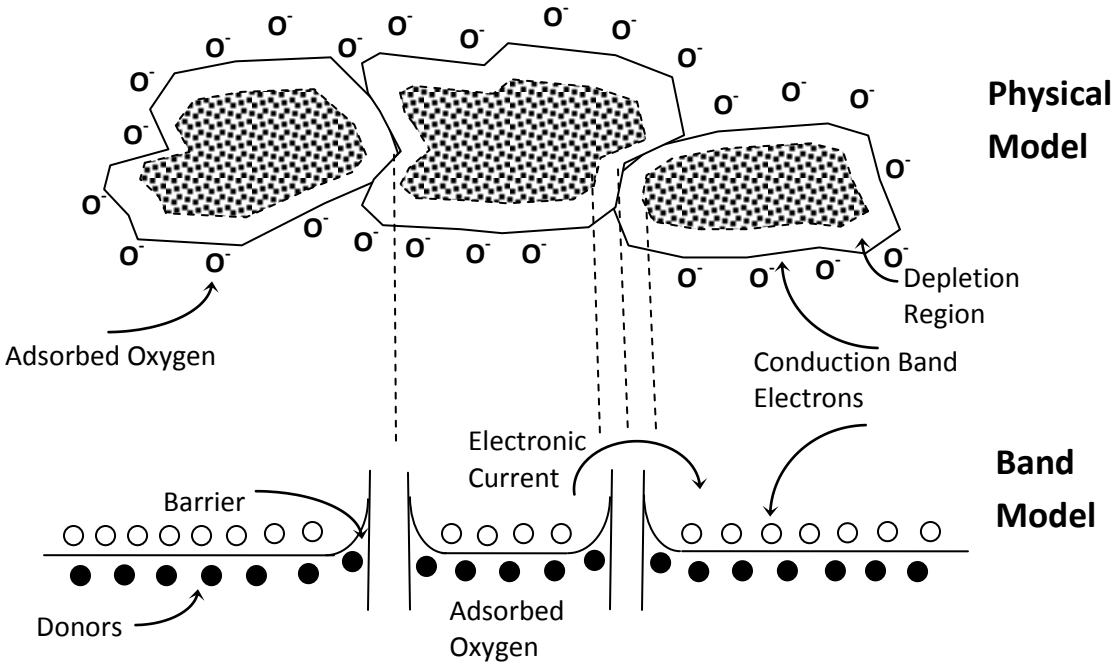

Figure I.1.a) Physical model and b) Band model showing the development of potential barrier on oxygen adsorption.

Relaxation of surface charge takes place when the surface comes in contact with reducing gas present in air due to reduction of the surface oxygen level to a steady state. That is oxygen is removed by the reducing gas from surface is proportional to the concentration of the gas. Hence decrease in the depletion region and also in resistance occur due to the reinjection of electrons into the bulk of the semiconductor material. These are represented by the reactions given below.[5]

$$O_2 + 2e^- \rightarrow 2O^-$$

$$RH_2 + 2O^- \rightarrow RO + H_2O + 2e^-$$

H_2O and gases are given up to the atmosphere. Surface layers enriched with charge carrier form a complex interlacing of conducting channels which determine the conductance of semiconductor.

I.3.2. Band Bending

Oxygen is ionosorbed on surface of the metal oxide in absence of humidity. The ionosorbed species can act as an electron acceptor due to their varrying relative energetic position about Fermi level, E_F as depicted by the Figure I.2. Absorption of oxygen on the surface depends on the temperature predominantly. In case of oxide(O^{2-}) ions the operating temperature is below 420 K and in case of superoxide (O^-) ions it is between 420-670 K. Above 670 K, formation of oxide (O^{2-}) occurs again and above 870 K it is directly impregnated to the lattice.[6] The electrons required for this process originates inherently from oxygen vacancies, they are extracted from unconduction band, E_C and trapped to the surface which leads to an electron-depleted region on the surface, widely known as the space-charge layer, Λ_{air}.[7-10] E_V, E_F and E_C represents the valence band energy, fermi level energy and conduction band energy respectively. Λ_{air} and $eV_{surface}$ indicates thickness of the space-charge layer and the potential barrier respectively. The e^- and (+) represents the conducting electrons and the donor sites respectively.

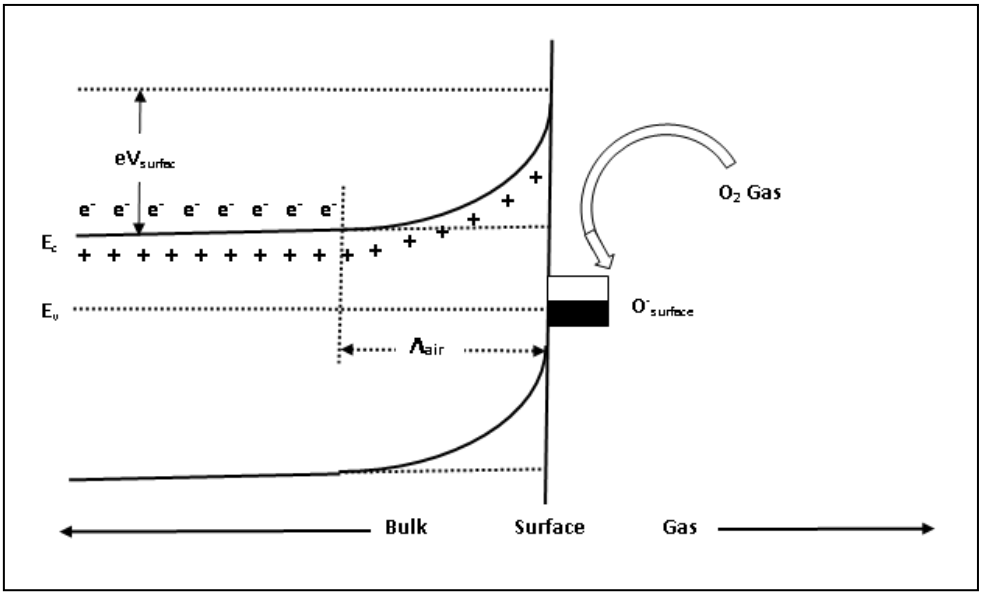

Figure I.2. Band bending model showing semiconductor with a wide band gap

Figure I.2 reveals that presence of negative charge on the surface leads band bending. It creates a surface potential barrier (expressed as $eV_{surface}$) with value 0.5 to 1.0 eV. $eV_{surface}$, Λ_{air} both are determined by the amount as well as type of the adsorbed oxygen and depend upon the surface charge.[11] Λ_{air} also depends upon L_D, the Debye length which is an important characteristic of semiconductor sensor material for any particular donor concentration. It is determined by the following equation,

$$L_D = \sqrt{\frac{\varepsilon\varepsilon_0 k_B T}{e^2 n_d}}$$

Here ,

k_B = Boltzmann's constant,

ε_0 = Permittivity of free space,

ε = Dielectric constant,

T = Operating temperature,

e = Charge of electron,

n_d = Concentration of carrier corresponding to the concentration of donor assuming complete ionization.

The ideal case does not involve any humidity in the surface. But under atmospheric conditions sensor performance may be altered by water molecules which form hydroxyl groups.

In case of polycrystalline sensing materials, the electronic conductivity occurs through the grain to grain contacts known as percolation path. Thus it depends upon the value of Schottky barrier, $eV_{surface}$ of neighbouring grains. Here the conductance G of sensing material is represented as[12] :

$$G \approx \exp\left(\frac{-eV_{surface}}{k_B T}\right)$$

CO, a reducing gas, react with the ionosorbed oxygen species to form bound carbonate groups either unidentately or bidentately and desorb as CO_2.[13,14] Hence the amount of adsorbed oxygen decrease considerably in the presence of traces of reducing gas. As a consequence the electrons trapped at the surface are pushed back to the bulk, which reduces the height of Schottky barrier. As a result, the conductance of entire sensing layer increases.

I.3.3. Electrical Conduction Mechanisms

How the surface reactions allow to detect a gas are determined by the microstructure of sensing layers for selected operational mode and transduced into output signal. The deposition technique mainly decides the microstructure, but addition of promoters, dopants etc also plays important role. Figure I.3 illustrates the energy profile diagram of a semiconductor between a pair of electrodes which possess energy barriers at the grain boundaries and at semiconductor interface. During adsorption of species like O_2, H_2O, CO, charge transfer takes place from the gas to sensor material or to the electrodes which leads to surface chemical reaction between chemisorbed oxygen species and CO. A simple difference between two different types of layers can be illustrated.[6,15] The interaction with chemical species in gas phase occurs at compact oxide layers, the geometrical one. Here electron flow is parallel to the depletion layer. The volume of the porous polycrystalline layer is accessible to gases and the active surface of this layer is greater than the previous one. These two varying behaviour can be easily differentiated for a particular compact layer, which depends upon the ratio between t (thickness of the layers) and x_o (width of the depletion layer (which is equivalent to Debye length $2L_D$).

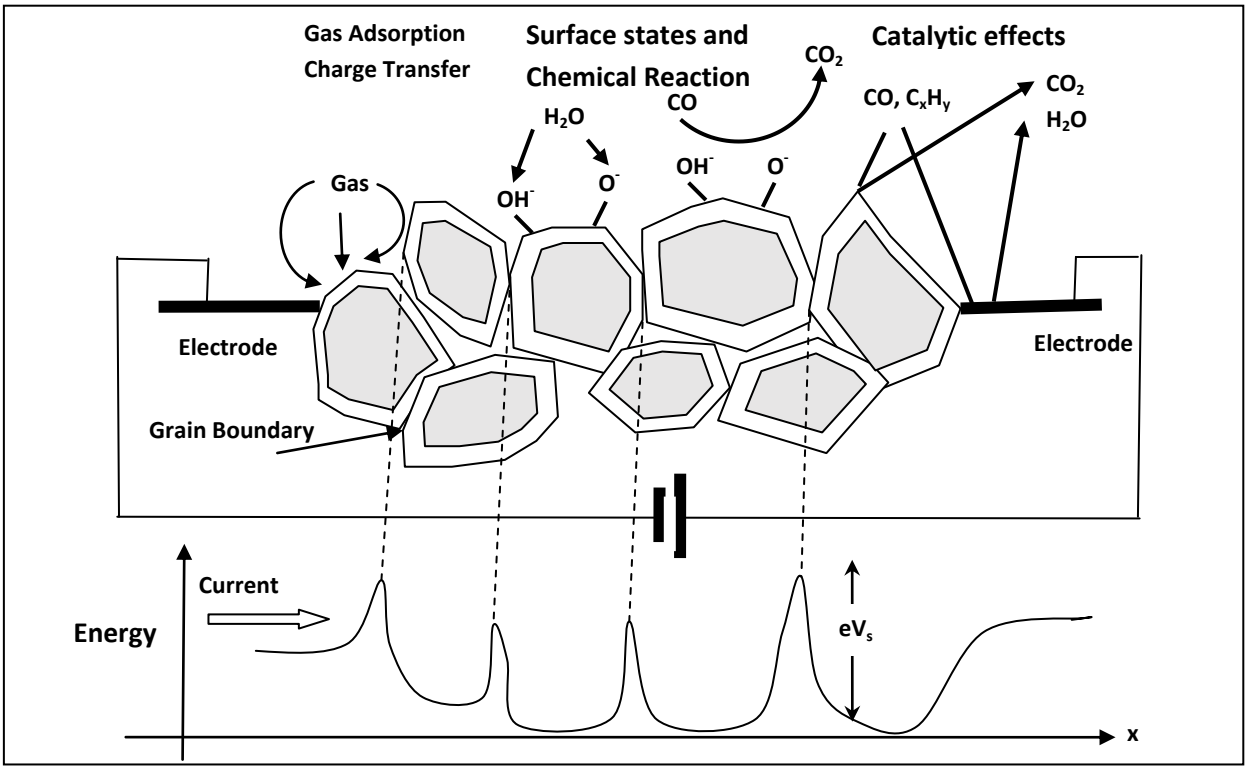

Figure I.3. Schematic representation of a conductometric gas sensor with electrodes placed in the sensor face

Surface traps restrict the conductance when the layer is fully depleted that is t ~ L_D. Here the electrons which are excited from the surface determine the conductance and the activation energy is equal to the surface-state energy (E_{SS}).

The surface reactions do not affect the conduction when the layer is partially depleted that is t > L_D. Here the conduction takes place by the electrons provided by the donor states in the bulk layer with variable width, ($t-x_o$) and the conductance is far more than the depleted layer. The energy E_D of the bulk donor acts as activation energy. The surface gas reactions and surface states change ($t-x_o$) i.e. conduction channel width which is also known as bulk trap-limited conduction (Figure I.4).

Here, x_0 = thickness of the surface layer,

t = thickness of the layer,

$e\Delta V_S$ = Height of the energy barrier.

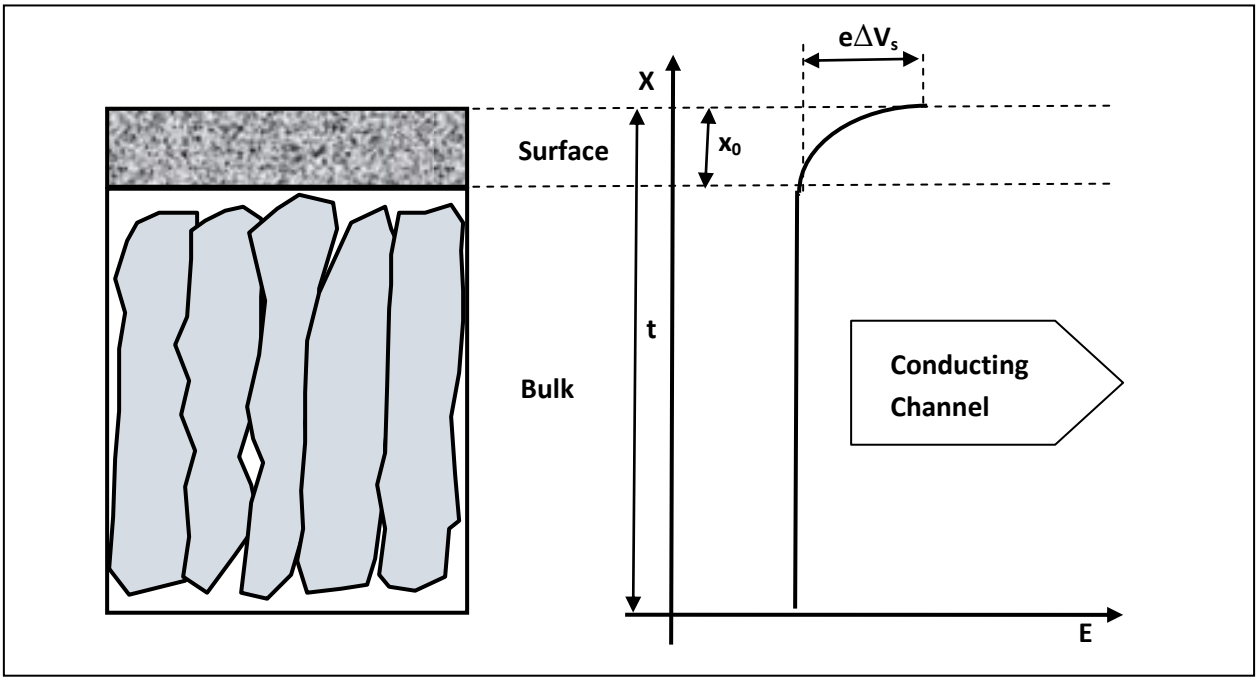

Figure I.4. Schematic diagram depicting compact sensing with geometry and band.

From, geometric considerations, conductance (G) of a thin single crystal layer is given by,

$$G = G_0\left(\frac{W_t}{L}\right)\left(1-\frac{x_0}{t}\right) \text{ where,}$$

$$x_0 = \sqrt{\frac{2e\Delta V_s \varepsilon\varepsilon_0}{e^2 N_D}}$$

Here, t = thickness , W = width, and L = length of the layer.

In case of partly depleted layer on exposure to reducing gases, the gases operate as switch to inject free electrons. Further, partly depleted layer turns to absolutely depleted layer, when it is exposed to oxidizing gases that operate as switch. But it is noteworthy that the sensitivity to gases is very poor in this state. Moreover, substantial sensitivity values can be obtained by the use of very thin sample. The conduction mechanism for porous nanocrystalline layers vary depending upon the existence of schottky barriers, necks between grains and on grain size. The nanocrystalline structure possess smaller resistance paths. There are three common cases regarding the degree of sintering for the sensor material which are well illustrated in the figure I.5.

Figure I.5a illustrates the case of a well-sintered material possessing an open neck between the adjacent grains. Depletion layers are extended by the surface states below the grains to the depth. This is marked by the dashed lines which is present in the both sides of neck. The conduction mechanism occurs in the bulk layer of variable width of ($Z_n - 2Z_o$). Furthermore the bulk layer is much more conductive compared to the depleted layer. The electrons are provided by the bulk donor states in the process. The activation energy is expressed as E_D. ($Z_n - 2Z_o$), conduction channel width is changed by the surface states and surface gas reactions.

Figure I.5b depicts a closed neck case where the depletion zones from surfaces of neighboring grains udergo overlap causing a path through the center with higher resistance. The geometry corresponds to less complete sintering which cause a narrower neck. Here the conductance is influenced directly by the gases that occupy the surface states. The conductance is measured by activation of electrons from surface states to conduction band.

Figure I.5c illustrates the case where a schottky barrier is formed. This barrier exists at the boundaries of the two adjacent grains and the conduction mechanism involved between the grains is through thermionic emission. The conductance G depends on the barrier height $e\Delta V_S$. This is given by,

$$G = G_b \exp\left[-\frac{e\Delta V_s}{kT} \right]$$

This conduction mechanism is different from the former two cases. $e\Delta V$ is the activation energy for the conductance and it is directly related to the surface charge. Changes in Schottky barrier leads to high gas sensitivity as it is a function of the sensing gaseous composition.

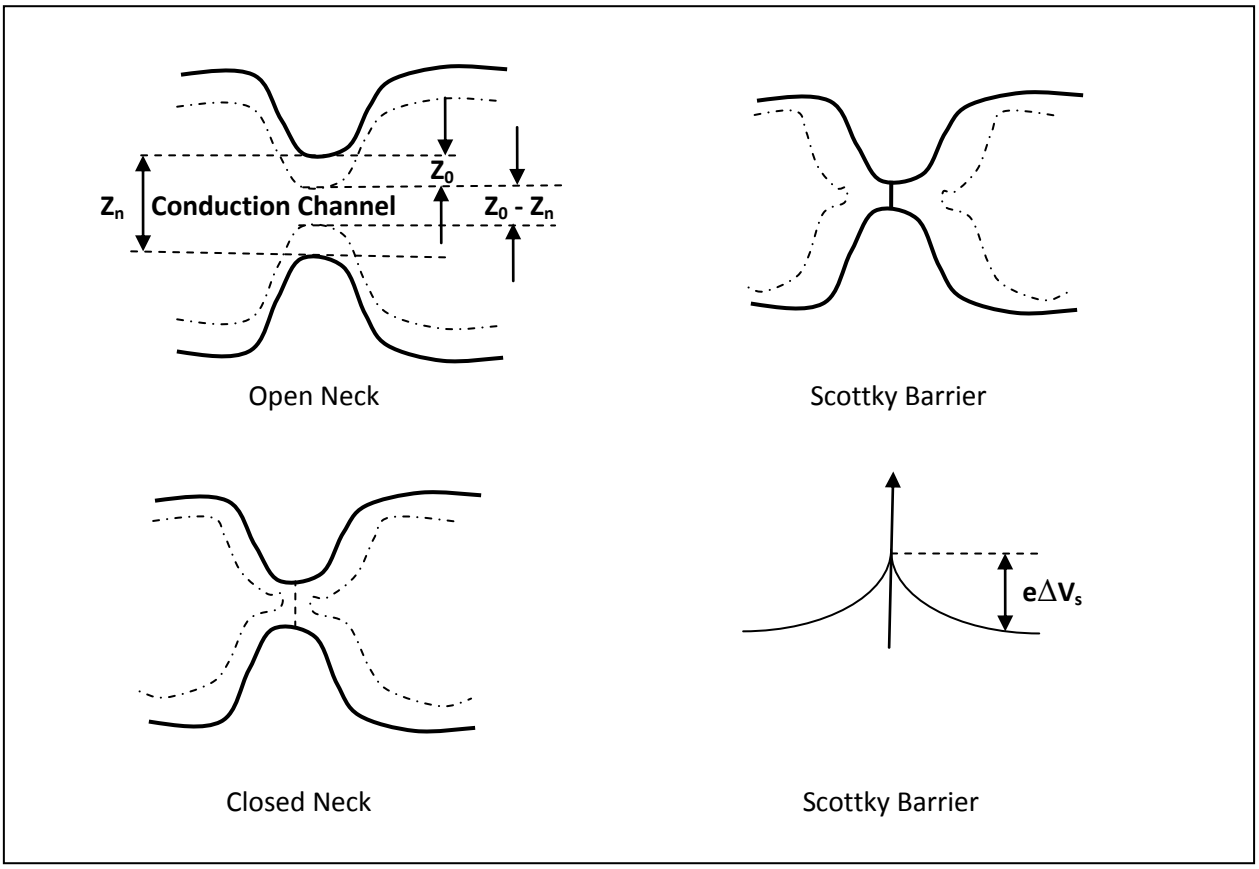

Figure I.5. a) Open neck, b) Close neck, c) Schottky barrier models for conductance limited by intergrain connections

I.4. Gas Sensing Mechanism

Though the working principle of the chemiresistive gas sensor is simple but the gas-sensing mechanism is a bit complex. The interaction between gas phase and gas sensing material are mainly two types.

I.4.1. Physisorption

This occurs due to the van der Waals' forces and solid-gas interaction is weak in this case. The adsorbent surface and adsorbed gas molecules become feebly polarized. Thus interaction due to this induced dipoles causes physisorption. The energy of interaction is very weak (~10–100 meV) in the physisorption process. Sensors based on physisorption are sensitive to wide range of gaseous species due to unselective character of adsorbate-adsorbent interaction.

I.4.2. Chemisorption

In this process activation energy is supplied thermally or by illumination. Chemisorption involves interaction which is often the formation of chemical bonds between adsorbates and the surface atoms of sensor materials. Thus the electronic structure of adsorbate as well as that of surface are modified which is mainly promoted by the surface defects. The energy of interaction is high. Interaction mechanism depends on the nature of material and on the operating conditions. The surface reactions of the gas sensors are well known example of heterogeneous catalysis. Usually the surface just provides a better place for a reaction between gaseous species to occur. However, during normal sensor operation all the products of reaction should desorb and thus the adsorption sites are freed and the sensor can be reused.

I.4.3. Mechanism of Gas Interaction

Metal oxide layers acting as gas sensor may undergo conductance changes in surface and/or bulk when come in contact of ambient gases. Electron transport processes cause change in surface conductance while ion transport is responsible for bulk conductance changes. Chemiresistive gas sensors find its application for the detection of concentrations of toxic as well as combustible gases present in air even in minute amount. Some groups has illustrated the gas sensing mechanisms so well that it can be well understood.[16,17] Becker et al. observed that sensor response reaches a maximum with increasing layer temperare and at higher temperatures it

aproaches towards zero.[18] Selectivity of the sensor can be controlled by the operating temperature of the analyte gas. Response variation to different concentration of sensed gases are also different. These sensors usually show low resolution towards high concentration and high resolution at low concentration. These sensors can be used to detect very low concentration of the toxic gases present in atmosphere as response times are fast. More important applications of these type of sensors include humidity sensors, oxygen sensors etc.[19, 20] The gas detection mechanism of these type of sensors usually requires oxygen in atmosphere and is also influenced by the presence of humidity in air. Oxygen is adsorbed from air and it creates surface states. For n-type metal oxide electrons are captured from the conduction band by the surface states and for p-type metal oxide it is from valance band in. The oxygen adsorption follows the steps below,

$$O_{2gas} \rightarrow O_{2ads}$$

$$O_{2gas} + e^{-} \rightarrow O^{-}_{2ads}$$

$$O^{-}_{2ads} + e^{-} \rightarrow 2O^{-}_{ads}$$

$$O^{-}_{ads} + e^{-} \rightarrow O^{2-}_{ads}$$

Brailford et al. described that the ionic forms of oxygen are function of operating temperature.[21] Oxygen shows $2O^{-}$, O^{-} and O^{2-} character at temperature less than 100 ºC, at temperature 100 ºC to 300 ºC and at temperature higher than 300 °C respectively. G. Bläser et al. showed oxygen adsorption with potential barrier formed due to the motion of charge carriers in terms of (a) physical and (b) band model (Figure I.1). [22] (, Physics A, 266, 218-223, 1999). Following reactions occurs when the gas sensor is exposed to a reducing gas represented as R.

$$R + O^{-}_{2ads} \rightarrow RO_{2gas} + e^{-}$$

$$R + O^{-}{}_{ads} \rightarrow RO_{gas} + e^{-}$$

$$R + O^{2-}_{ads} \rightarrow RO_{gas} + 2e^{-}$$

Removal of adsorbed oxygen takes place when it reacts with a reducing gas. It results lowering of potential barrier hence return of the captured electrons. As a result the conductivity increases for n-type metal oxides but the conductivity for p-type metal oxides tumbles. When oxidizing gases are used the changes are opposite. The sensing materials can be classified as n-type or p-type on the basis of these type of conductance change.[23]

I.4.4. Role of Defects

In semiconductors, surface defects play important role as active sites for the catalysis process and reaction occurs predominantly at these defects.[24] The basic theory of semiconductor materials possessing deviations from the ideal stoichiometric compositions, was developed by Wagner and Schottky.[25] A solid must be non-ideal and possess some defects for conduction process to occur as charge transfer is only possible in case of this type of solids. Entropy of solid is directly related to the defects. According to 2nd law of thermodynamics, zero entropy is only possible at temperature 0 K. But normally even at 0 K a finite concentration of defects exist hence entropy never becomes zero and does so for a perfectly arranged system. The solids that we operate possess certain defects that has made them special. Defects can be classified as line defects, impurities or vacancies and defects at grain boundaries. Line and point defects assume importance as gas sensing is surface phenomena. Point defects are important for the bulk. Insertion of the foreign particle in lattice causes extrinsic defects. Hence, adsorbed atoms are considered to be point defects. The interstitial positions may occupy excess metal ions and equal number of free electrons which are present in conduction band that leads to n-type semiconductivity. Whereas Cation vacancies lead to an equal number of positive holes present in valence band that are responsible for p-type conductivity

I.4.5. Role of Particle Size

Gas-sensor response mainly depends upon the reaction between metal oxide surface material and gas molecules present in the atmosphere. Generally nanocrystalline metal oxides possess large surface-to-bulk ratio. Hence they show an improved sensitivity compared to microcrystalline materials with a better response and recovery time. Sensitivity largely depends on the particle size and smaller particles sizes show improved sensitivity which results numerous structural and electronic defects. The conductance is proportional to the energy difference of E_F (that of Fermi level) and E_C, the conduction band.[10,26]

I.4.6. Influence of Microstructure

The microstructure specially film thickness and porosity play important role to control the response time and sensitivity. Oxygen and other analyte molecules penetrates the sensor surface layer. Thus it is essential that the diffusion rate of the analyte/oxygen would be fast.

which also depends on the working temperature and its mean pore size. Lower film thickness and higher porosity gives rise to faster response time and higher sensitivity.[27,28]

I.4.7. Effect of Surface Doping

Sensor performance is largely influenced by the doping with metals and/or oxides. Moreover, this doping process is different from that of the bulk doping of the semiconductors. Here the doping process accompanies addition of the base material to the catalytically active sites of the surface. The doping process increasing the sensitivity by improving sensor performance. Surface doping also enhances the thermal and long-term stability. Parameters which control the process include particle size, composition, redox state of the surface modifiers and their dispersion onto the metal oxide surface. The particle size effectively controls the temperature range and also the efficiency of a particular catalytic reaction.[29,30]

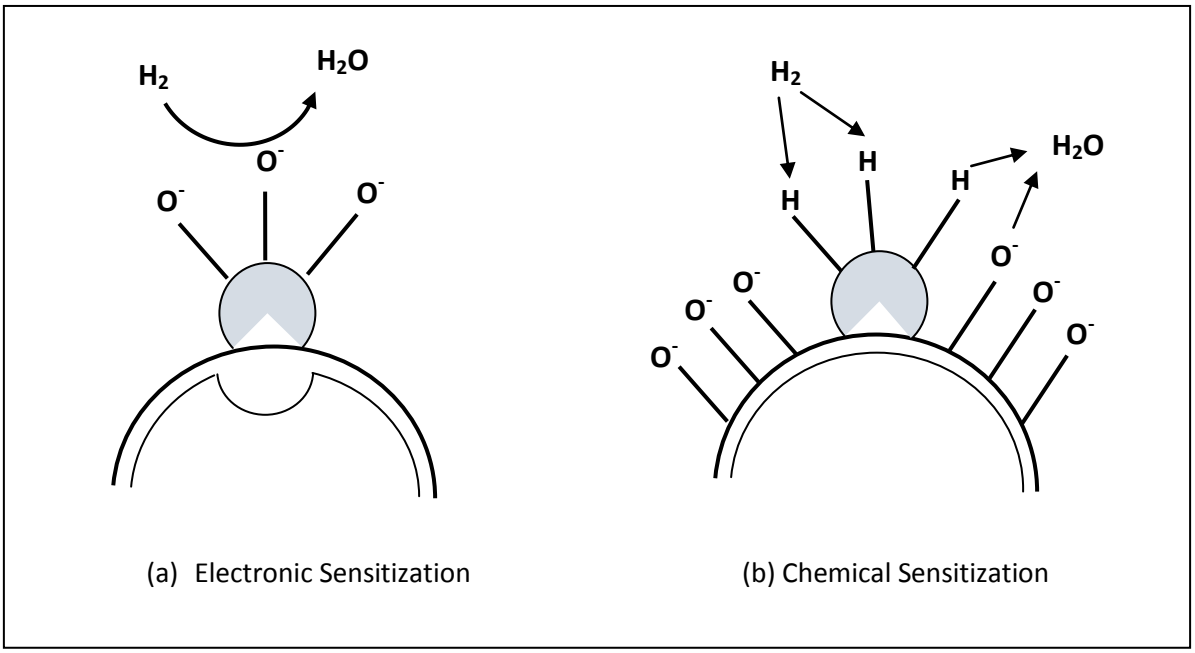

Figure I.6. Mechanism of Electronic and Chemical sensitization process by metal/metal oxide additives

Two different mechanisms, i.e, electronic and chemical sensitization are applied to illustrate the surface additive effect.[10, 11, 31–33] In case of electronic sensitization process, the electrons are accepted by the semiconductor metal ion in its particular oxidized state. As a result an electron depleted space-charge layer is induced near the interface. Figure I.6a illustrates the electronic sensitization, where the additive H_2 is an electron acceptor and the redox state or the chemical potential is modified by the reaction of analyte with the semiconductor.

The chemical sensitization results from the catalytic surface reaction. Figure I.6b shows chemical sensitization by the activation of the target analyte (H_2) which changes the surface oxygen concentration.[11] As a result, $eV_{surface}$, is reduced by the surface coverage of oxygen, which causes conductance change.

I.5. Criteria for the Choice of Sensor

An ideal sensor should have high sensitivity so that it can detect least quantity of gas with the variation of resistance. It should exhibit high selectivity for a particular gas and the response and recovery should be fast. Good sensor should have tolerance various adverse effect like humidity, temperature, acid, baser, dust etc. Moreover the sensing material should be safe and non-toxic. It should have high sturdiness and simple to operate. Low temperature operating miniaturized materials are preferred to couple the materials with electronic circuitry possessing low power consumption.

I.5.1. Types of Metal Oxide Sensors

The operating principle of the metal oxide sensors is that the conductance of the sensor material will change with the interaction of the gas. This change is proportional to the gas concentration. Two types of metal oxide sensors are there. The n-type such as ZnO, SnO_2, TiO_2, Fe_2O_3 etc which responds to the reducing gases and p-type like NiO, CoO etc that respond to oxidizing gases.[34] Oxygen in the air reacts with the surface of the n-type sensor which traps the free electrons on the material surface or it may be trapped at the grain boundaries of this metal oxide grains. Due to lack of the carriers large resistance is produced in these areas. The potential barriers produced in this process between the grains inhibit the mobility of the carrier. If the

sensor come in contact with the reducing gas such as hydrogen, methane, carbon monoxide etc. resistance drops due to the reaction of the gas with oxygen which releases electron and lowers the potential barrier thereby. It also allows the electrons to flow which increases the conductivity. Whereas p-type sensors respond to the oxidizing gases such as oxygen, nitrogen di oxide and chlorinre because these gases produce holes by releasing electrons. The reactions taking place at the surface can be represented as

$$\frac{1}{2}O_2 + e^- \rightarrow O^-(s)$$

$$R(g) + O^-(s) \rightarrow RO(g) + e^-$$

Where, R (g) = The reducing gas,
e = An electron from the oxide,
g = gas, s = surface.[34, 35]

I.5.2. Transition Metal Oxide Chemiresistive Sensor Materials

A consize discussion of such transition metal oxide based gas sensing material has been illustrated below:

i) Chromium Oxide (Cr_2O_3): Thermodynamic stability, hardness and resistance power towards chemical attack has made p-type Cr_2O_3 an importat material for sensors now a days.[36] It is sensitive towards H_2 and CH_4 gases.[37] TiO_2-doped Cr_2O_3 has been found to be sensitive towards the gases NO_2, O_2 and also towards humidity.[38, 39]

ii) Cobalt Oxide (Co_3O_4): It is very promising towards the gas sensing applications due to its catalytic activity towards oxidation reactions.[40] Co_3O_4 is very sensitive to a variety of gases like NH_3, CO, CH_4, C_3H_8, NO_2 and Cl_2.[41]

iii) Copper Oxide (CuO): Among the oxides of copper, only the cupric form of oxide (CuO) is sensitive towards gas. CuO is a p-type semiconductor and possess a band gap of 1.2 eV. It's electrical resistance is also low and is sensitive towards NO_2 and CO.[42, 43] CuO-doped SnO_2 has been found to be highly selective towards the sensing of H_2S.[44]

iv) Iron Oxide (FeO, Fe_3O_4, Fe_2O_3): There are three different polymorphic forms like FeO, Fe_3O_4 and Fe_2O_3 are possible for iron-oxide system. Among them only Fe_2O_3 is gas sensitive due to its good thermo-dynamic and structural stability. Three types of defect, viz, oxygen vacancies, Fe^{2+} interstitials, Fe^{3+} interstitials are present in the complex defect structure of Fe_2O_3. These defects gives rise to the semiconductor properties of the material. Fe_2O_3 has been found to be high sensitive towards various organic gases. ZnO doped Fe_2O_3 works as a selective NH_3 gas sensor which works at room temperature.[45] Au or Zn doped Fe_2O_3 is sensitive towards CO and NO_2.[46] When doped with Pt, Pd or RuO_2, Fe_2O_3 sensor can also detect acetone.

v) Molybdenum Trioxide (MoO_3): It is an n-type semiconductor having band gap 3.2 eV. Its selectivity and no cross-sensitivity are the main causes of its excellent use as a gas sensitive material. acts as a well-known catalyst towards the oxidation process of hydrocarbons and also towards the conversion of harmful NO_x gas to nitrogen. Currently the gas sensing properties of this material has been investigated.[47] It has been found that the sensitivity of MoO_3 sensing material for NH_3 can be enhanced considerably by using a coating of Ti over MoO_3 films

vi) Niobium Oxide (Nb_2O_5): Nb_2O_5 has been found to be a popular n-type semiconductor for the detection of H_2 gas.[48]

vii) Nickel oxide (NiO): NiO acts as a p-type semiconductor possessing band gap 4.2 eV. Good chemical stability and excellent optical as well as electrical properties are the causes of wide applicability of NiO. NiO has been found to be a good gas-sensing material for both thermoelectric and chemiresistive type gas sensors.[49, 50]

viii) Tantalum Oxide (Ta_2O_5): Ta_2O_5 is a good humidity sensor. It acts as a good promoter in gas sensors. An over layer of Ta_2O_5 improves the sensitivity, response time of $In_xO_yN_z$ films significantly towards the sensing of gases like CO, H_2, CH_4 etc.

ix) Titanium Dioxide (TiO_2): High thermal stability and tolerance to harsh environments has made TiO_2 an important gas sensing material with comparable thermal expansion coefficient

with Al_2O_3, which has also made it a suitable material for fabrication of thin film based sensors. TiO_2 is a high resistive n-type semiconductor. The addition of Chromium with TiO_2 alters the electronic conductivity from n-type to p-type that helps the development of the novel gas sensors.[51] These p-type materials which were obtained at appropriate conditions responded excellently with a sharp decrease in resistance when exposed towards diluted NO_2.

x) Tungsten Oxide (WO_3): Operability at high temperatures for long time has made WO_3 a potential and selective sensor towards various gases. It is an n-type semiconductor with wide band gap.[52] Mo, Mg, Au, Zn, Re etc. doped WO_3 films have been found to detect toxic gases selectively.[53] Surface of WO_3 films modified with Au and Pt were found to be more sensitive towards NH_3.[54]

xi) Vanadium Oxide (V_2O_5): V_2O_5 has been used extensively as catalyst in the oxidation reactions. This feature has made V_2O_5 a good promoter towards the enhancement of the sensitivity of sensors like TiO_2, MoO_3 and ZnO.[55]

I.6. Sensor Fabrication Methods

High performance gas sensors can be achieved by controling the structure of the sensing material. Particular sensing material, a heater which increases the temperature of the sensing material and the electrodes for measuring the resistance of the sensing element are required for the fabrication procedure. Different response characteristics are produced for different gas sensors by different techniques.It happens because different material structures can be achieved by applying different preparation techniques. For the fabrication procedure various methods are used which can be discussed hereunder.

I.6.1. Bulk Form

In this process the sensing element i.e. compressed pellets of metal oxide powder is by sintered at 900-1000 °C temperatures. Electrodes on sintered pellets in this type of sensors are prepared by depositing Au by thermal evaporation process. These sensors are very cheap to produce. But these sensors also possess several disadvantages like poor selectivity and sensitivity, slow response and recovery times, high power consumption at temperature greater than 200°C.

I.6.2. Thick Film Form

Thick film possess thickness of the order of microns. The powder form of semiconductor oxide material is mixed with binders like propandyol/terpineol to form a paste. Calcination of the binder is important to create porosity. This can also be done by adding some chemical substances to the paste which decomposes on thermal treatment. Fractures appearing in the sintering of powders increase sensor resistance. This can be reduced by addition of some Al_2O_3 powder with mean size 100 to 150 μm to the paste. The powders have a natural tendency to agglomerate. Hence the paste must be well mixed before the deposition process.

I.6.3. Thin Film Form

Thin films form possess different properties comparede to bulk form. The thickness are of the order of few nanometers to few microns for this kind of sensors. Sensors with high selectivity, small size and possessing low power consumption can be developed by silicon microelectronic technology. Thus thin film forms are found to be the most suitable. Thin films can be divided into two types namely single crystalline and polycrystalline, based on the structural properties. Single crystalline thin films do not possess grain boundaries and they show small variations of electrical resistance when they are brought to the contact of oxidizing or reducing gases. So they are not used as gas sensors.[56] Whereas in polycrystalline thin films charge transport across grain boundaries plays important role in developing the sensor response to gases.[57] That is why these are more suitable as gas sensors. In fact sensor response improves significantly as the grain size approaches nano form.

I.6.4. Nanostructure Form

Gas sensing is a surface phenomena and high surface area to volume ratio in the nanostructure form enhances the response. Hence different nanostructured forms like single nanowire, mat type, film, thick film technology[58-68] etc. have been used for dropcasting, di-electrophoresis, pick and place etc. approaches.

I.6.5. Substrates used in thick film technology

The substrates used in the thick film technology should possess the following criteria.

i) It should be able to support the circuit.

ii) It should be able to protect the circuit from any mechanical damage.

iii) It should be able to dissipate heat.

iv) It should be chemically inert and it can provide electrical isolation.

The properties like relative dielectric constant, resistivity, surface characteristics, chemical reactivity, strength, thermal expansions coefficient, thermal conductivity, dimensional stability etc. are important factors for the selection of the substrates for the above phenomena.

The polycrystalline ceramics are ideal for that prpose. Aluminum oxide, beryllium oxide, barium titanate etc. are popularly used materials. Beryllium oxide ceramics possess high relative dielectric constant because of high thermal conductivity. This substrates can be used to make high capacity devices. Al_2O_3 ceramics are popularly used with combination which gives the best performance. The unglazed Al_2O_3 substrates with 96% purity are widely used in thick film industry.[69]

I.7. Applications of Chemiresistive Gas Sensors

Several applications of the gas sensors are noteworthy. Some applications of chemiresistive gas sensors are illustrated below:

I.7.1. Environmental Monitoring

Volatile organic compounds (VOC's) and various toxic gases can be actively detected by these chemiresistive gas sensors. The present methods are very much costly and time consuming. High level of various gases, VOC's and ozone in atmosphere causes harm to human respiratory system by causing inflammation, congestion of respiratory tract. The O_3 level rises because of the interaction of sunlight with various chemicals excruited by the industries. Several materials based on WO_3,[70] SnO_2 [71] are useful to detect the ozone level in atmosphere, when fabricated. Thus chemiresistive gas sensors serve as efficient environment monitors owing to their simplicity in operation and low cost. Thus importance of research on this ground are increasing now a days.

I.7.2. Chemical Warfare

Gas sensors can be used for detecting toxic chemical warfare agents (CWAs) used in war as weapons for mass destruction. Spectroscopic techniques like FTIR[72], Raman[73] spectra have been employed to monitor CWAs. However, this procedure is costly and complex. Thus it is important to develop low cost, selective devices that will provide effective CWA detection quickly. Semiconductor metal oxides like SnO_2, ZnO, WO_3 etc. and their modified form effectively possess sensing property towards various CWAs. For example, SnO_2 is highly sensitive towards acetonitrile and dimethyl methyl phosphonate (DMMP)[74] which is the simulant molecule for sarin ($[(CH_3)_2CHO]CH_3P(O)F$), a liquid extensively used as chemical weapon.

I.7.3. Automobiles

Chemiresistive gas sensors are also applied in the car ventilation and filter control, alcohol breath test and gasoline vapor detection. Although cars are designed in such a fashion that outside air can constantly ventilate through the air inlets. Yet in the closed car, as the concentration of CO_2, smoke gets increased, the air quality becomes lowered. Chemiresistive gas sensors capable of detecting organic pollutants can be used as air quality sensor. In auto-damper system (ADS) these sensors can be also used which can monitor various inflammable gases like hydrocarbons, NO_x etc.

I.7.4. Safety

The functioning of fire alarms are basically smoke sensor or heat sensor based. Various inflammable gases result on the occasion of fire, however H_2 gas diffuses more rapidly compared to smoke and it is easy to detect than the conventional methods where sounding fire alarm is used widely. For this reason, conventional fire alarms now use chemiresistor gas sensor as an active component.[75]

I.7.5. Food and Beverage Industry

Analytical analysis of foodstuff and beverages can be done by using electronic nose of the chemiresistive sensors in the industry. Work on this ground that is on the tea quality detection has been discussed in the last chapter of this thesis.

I.7.6. Medicine

Chemiresistive sensors with electronic nose system can diagnose certain disease which can be an effective criteria in the medicinal ground. As for example, patients with certain kidney disorders produce some characteristic VOC, which can be detected using particular gas sensor and it can be a useful tool for the diagnosis and control of some renal disorder.[76] Also, studies non-selective gas sensors have been shown to be active in lung cancer detection by simple breath analysis.[77] In future electronic nose devices can be an effective tool for doctors, which can be used by them for rapid detection of specific diseases.

I.8. Reference

References are given in BIBLIOGRAPHY under Chapter I page no. 86-89.

Chapter II

Temperature dependence of Semiconducting Gas Sensors in different Modes of Measurement

II.1. Introduction

Air pollution is a serious problem in many heavily populated and industrial areas. Economic growth and industrialization are randomly growing on, accompanied by increasing emissions of air pollutants. Furthermore, since the kinds and quantities of pollution sources have been also increased dramatically, the development of methods to monitor the pollutants has become even more important. To prevent or minimize the damage caused by atmospheric pollution, suitable monitoring systems are required that can rapidly and reliably detect and quantify air pollutants. Nitric Oxide is one of the major air pollutant component which is heavily produced by many industrial systems. Metal oxide semiconductor gas sensors are utilized in a variety of different roles and industries. They are relatively inexpensive compared to other sensing technologies. They are also robust, lightweight, long lasting and beneficial from high material sensitivity and quick response times. That is why they have been used extensively to measure and monitor trace amounts of environmentally important gases such as carbon monoxide (CO), nitrogen dioxide (NO_2), Nitric Oxide (NO) etc. From literature survey, it has been shown that NO gas effects the conductivity of both the semiconductor sensing materials La_2CuO_4 and WO_3.[1,2,3,4] It is reported that sensors of the form La_2CuO_4|YSZ|Pt and WO_3|YSZ|Pt are very sensitive to NO in the temperature range of 400–600 °C[5] and 150–250 °C[6,7] respectively. Various works involving La_2CuO_4 electrodes for non–Nernstian potentiometric sensors with La_2CuO_4 electrodes illustrating the effect of the sensing electrode with varying grain size,[8] area[9] and thickness,[10] on the response of the potentiometric sensor are well reported. The effect of electrical contact configuration for the La_2CuO_4 sensing electrodes on the sensor response has also been studied.[11] But the comparative study of temperature sensitivity of these semiconducting sensing materials in resistive and potentiometric mode is not studied yet. Here we report a comparative study of resistive and potentiometric mode to find out the minimum temperature of operation for pollution monitoring. Out of these above said two methods we found that potentiometric mode is more sensitive at lower temperature towards NO gas.

II.2. Background and Objectives

Several behavioural tendencies have been established for the metal oxide sensor. Different gases and oxides possess different sensitivity to gases which also varies with temperature and shows

highest sensitivity at different temperatures with varying gases and metal oxides. Temperature also controls the response times (response times are shorter at high temperature), and the responses to gases are non-linear as a function of concentration. Temperature Changes also causes the sensor response to act differently. One more common feature is that water vapour influences both the conductance (resistance) in atmosphere and the response to other gases. That's why it is preferable to work in a controlled ambiance. Another alternative is to find materials that are less dependent on humidity or to compensate for this reliance by characterizing the sensor response to different humidity values. The sensor was characterized to find the optimum operating conditions, reproducibility and reliability of that very sensor. This involves determining the range of various operating parameters for different sensors and different working conditions, also ascertaining the stability of these parameters. There are different ways to measure the characteristics of the semiconductor devices. The presence of traces of impurities affects both the chemical and the physical properties of these semiconductors used as sensor materials. The surface reactions, on which the sensors are absolutely dependent, are also affected by variations in surface topography. The characteristics can be also changed by the fabrication method. The situation can be further complicated when additives are introduced into the oxide to improve some aspect of performance; both the amount of additive and the method of introduction can be critical.

The semiconductor sensor's characteristics are highly temperature dependent, thus the measurements should be taken at various temperatures. The temperature range would be different for various oxides and various analyte gases of interest. At lower temperatures conductance for some devices, often takes a long time to attain the steady state. Therefore, at a given temperature, measurement must be done after sufficient time so that conductance may reach a steady value. It has also been suggested that the performance of the sensor can be somewhat dependent on the recent history of the sensor. It is therefore worthwhile, at least in the early stages, to obtain data when temperature is both increasing and decreasing over the range of interest.

In temperature programming method, the temperature is such carefully chosen that the sensor can sense only a particular gas. The response of the gases at different temperature varies due to the temperature dependence of adsorption-desorption kinetics of gases. At very low temperature, the reaction between test gas and surface species is so low that the sensitivity is not good. At

higher temperature, sensitivity is low due to rapid desorption which causes, low concentration of the test gas at the sensor surface.

The response time and recovery of sensors are temperature dependent. Parameters like surface coverage, chemical decomposition and/or other surface reactions, co-adsorption etc. also depend on temperature, which results different static characteristics with varying temperatures. Moreover, temperature has a profound effect on various physical properties of semiconductor sensor materials like debye length, charge carrier concentration, work function etc. Ability of a sensor material to reduce/oxidize the target gas catalytically is indicated by the effective sensor response at the optimum range of temperature, which also changes the electrical properties of that very sensor material simultaneously. The reaction rate also depends upon the particular reducing agent used under study. It has been found that, there is a sensitivity peak for a particular reducing agent. At very low temperature, the reaction rate is so slow that it gives low sensitivity, whereas at high temperature, overall oxidation reaction occurs rapidly and the concentration of the reducing agent at the sensor surface becomes limited which results zero concentration. For each sensor-gas combination, an optimum temperature between these limits must be used. Sensors arrays can be used for these type of higher selectivity.[12-16] The overall target gas concentration which reaches the semiconductor sensor material surface can be reduced or oxidized at such temperatures, without accompanied by any electrical change on the material. Thus again the sensitivity becomes low. However, temperature should be kept high to allow any kind of gas reaction upon the material surface. To provide the highest sensitivity, the operating temperatures for the determinate gases are chosen empirically. Thus the whole gas sensing mechanism is understood by the relation between the sensing material, their catalytic properties and/or the electrical response of the sensing material. Hence potentiometric mode was chosen where substrate acts as catalyst there by reducing the temperature for highest sensitivity compared to the resistive mode. For each sensor-gas combination, an optimum temperature between these limits must be used. For higher degrees of selectivity, sensor arrays termed as "electronic noses" are used. In this procedure different response for different sensors are used to identify the particular gaseous species through pattern matching. For such type of sensor array, producing the signals of sensor devices of same kind at different operating temperatures and/or processing different device materials at same temperature can be used as procedure to overcome the lack of selectivity of single metal-oxide gas sensor.[17] The characteristics of semiconductor

sensor materials are highly temperature dependent. Different oxides and analyte gases have different temperature ranges. At lower temperatures conductance can take long time to reach steady state for some devices. Therefore, during the measurement, sufficient time should be allowed at a given temperature so that the conductance may reach a steady value. Most of the semiconductor chemical sensors work at an elevated temperature, although the number of sensors working at room temperature are very few. To find the optimum operating temperature for a gas at which the gas responses maximum, the variation of the response of the gas with the operating temperature is used. It is also used to characterize a sensor. The operating temperature is termed as the temperature at which sensor material shows maximum gas response for a particular gas.

II.3. Present work: Result and Discussion

II.3.1. Sensor fabrications and Characterizations:

The morphology of the samples was observed using a Scanning electron microscope (SEM).

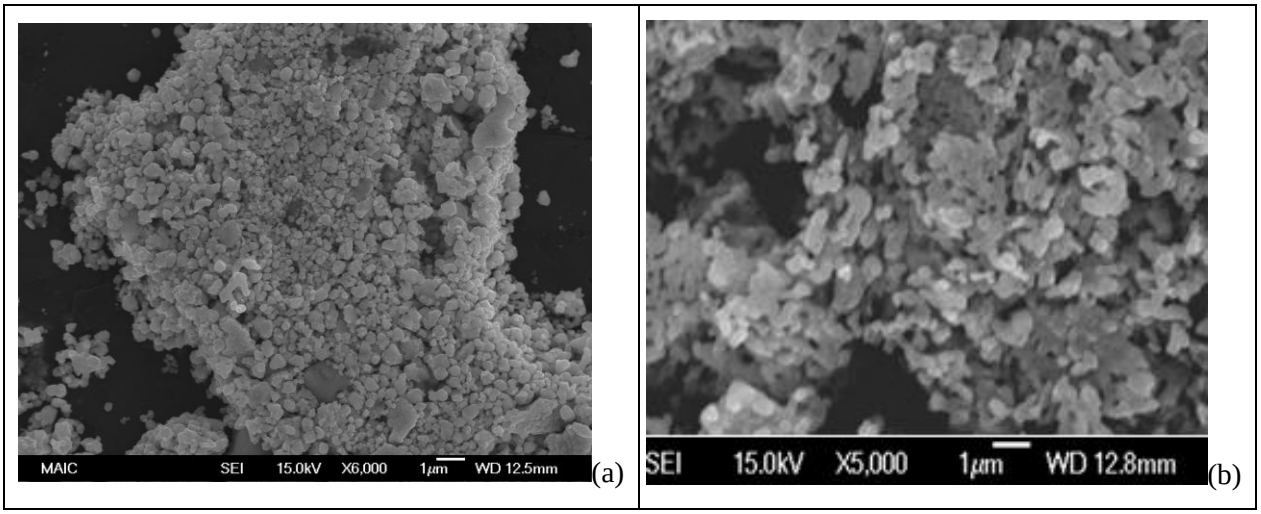

Figure II.1. SEM Micrograph of sensing surfaces (a) WO_3 and (b) La_2CuO_4

Figure II.1. shows the microstructure of two sensing surfaces. The particle size was around ~1 μm of both the films; however, for WO_3 the particle size appears to be smaller. For La_2CuO_4, the

particles appear to be sintered a little more than WO_3. The BET surface area of powders was found to be 16.3 for La_2CuO_4 and 11.2 for WO_3 powders.

X-ray diffraction patterns of both the sensing materials WO_3 and La_2CuO_4 were collected in the 2θ range of 5^o to 70^o and 10^o to 80^o respectively using a diffractometer as shown in figure IV.2. However, no departure was observed from pure substances.

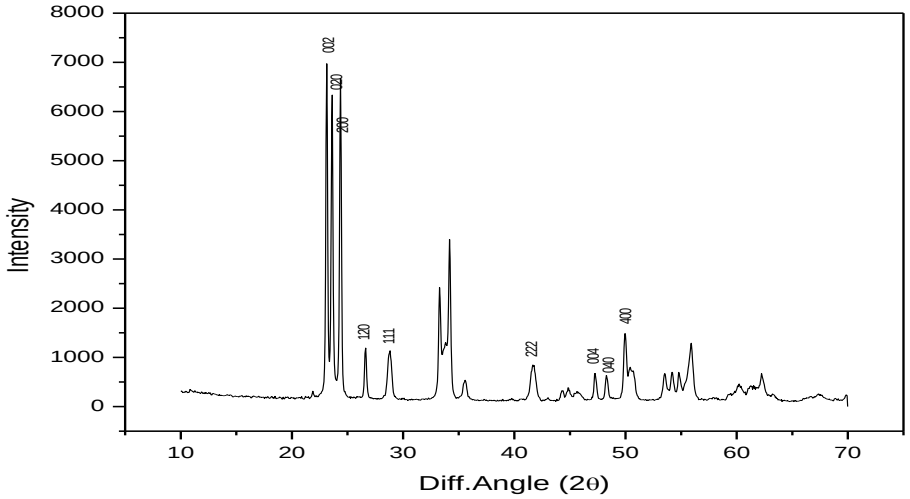

(a)

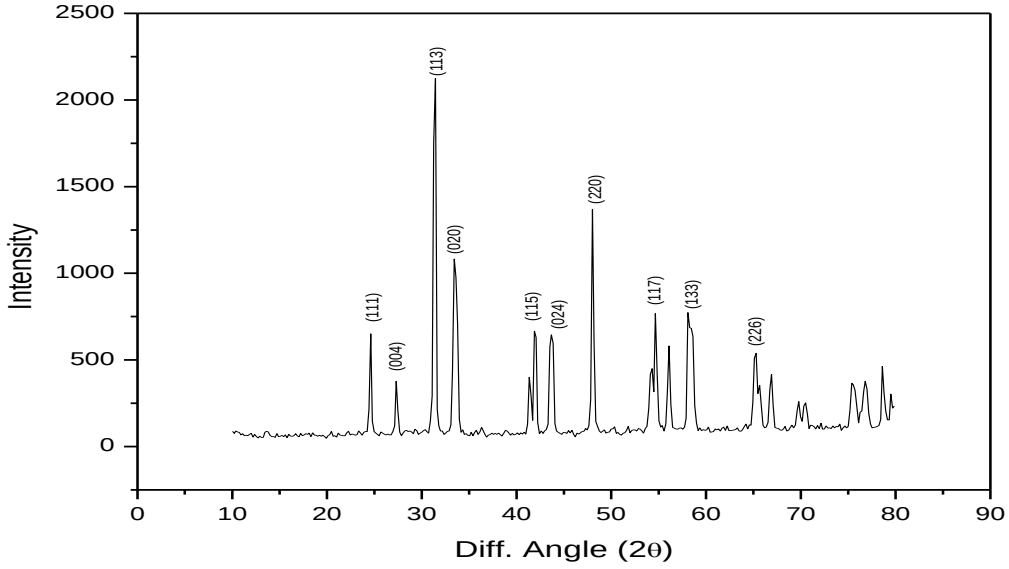

(b)

Figure II.2. X-Ray diffraction pattern of sensing surfaces (a) WO_3 and (b) La_2CuO_4

The response characteristics for one p-type and one n-type sensor in potentiometric and resistive mode of detection have been presented in the figures below. The voltage and resistance change is detected when NO gas (in N_2) concentration is raised from 0 to 650 ppm. The sensitivity of the maximum response shows that the response is much higher for potentiometric mode of measurement for two types of sensors. It also shows that the response for n-type and p-type materials are opposite in magnitude for both types of measurements. The response characteristics at different temperature in potentiometric mode indicates that stability of response improves at lower temperature of operation. From Table II.1 we observed that S/N ratio is small for resistive mode where as it is high for potentiometric mode. Very small value of S/N ratio in case of p-type resistive mode was obtained. The reason behind this small value of S/N ratio may be due to some fabrication error during screen-printing of the sensing substrate or counter electrode. The high magnitude of response indicates higher response sensitivity of the sensing element to NO. In this experiment La_2CuO_4 in potentiometric mode shows the higher response sensitivity to NO. While response time (time in which response reaches 90 % of its maximum value) is higher in resistive mode for both n-type and p-type material but it is lower in potentiometric mode for both the material. Among two type of material in potentiometric mode, n-type material shows the minimum response time.

		Resistive	Potentiometric
n-type	Sensitivity	3.02	4.35
	Stability (S/N ratio)	60.185	77.89
	Response time (90 %)	2.17 min	38.4 sec
p-type	Sensitivity	5.72	6.63
	Stability (S/N ratio)	2.64	66.95
	Response time (90 %)	4.68 min	4.36 min

Table II.1 Sensing Parameters of sensing surfaces WO_3 and La_2CuO_4 in Resistive and Potentiometric modes.

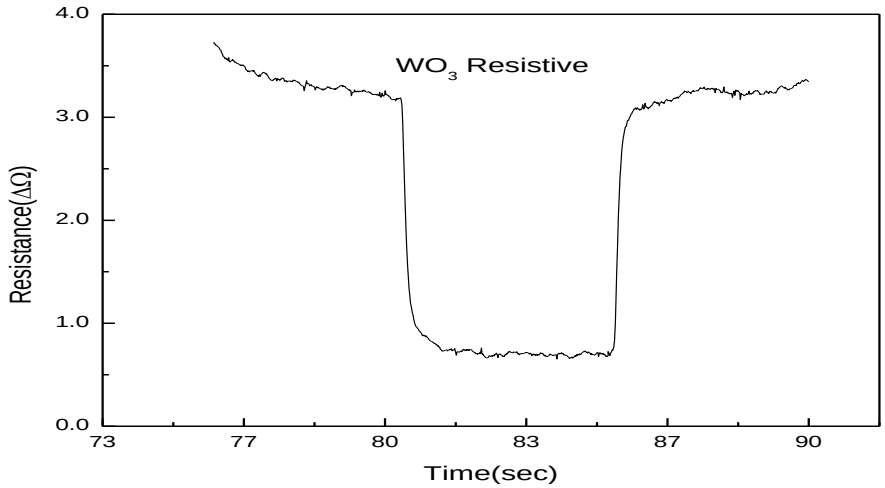
WO3 Resistive
Resistance(ΔΩ)
Time(sec)
4.0
3.0
2.0
1.0
0.0
73
77
80
83
87
90

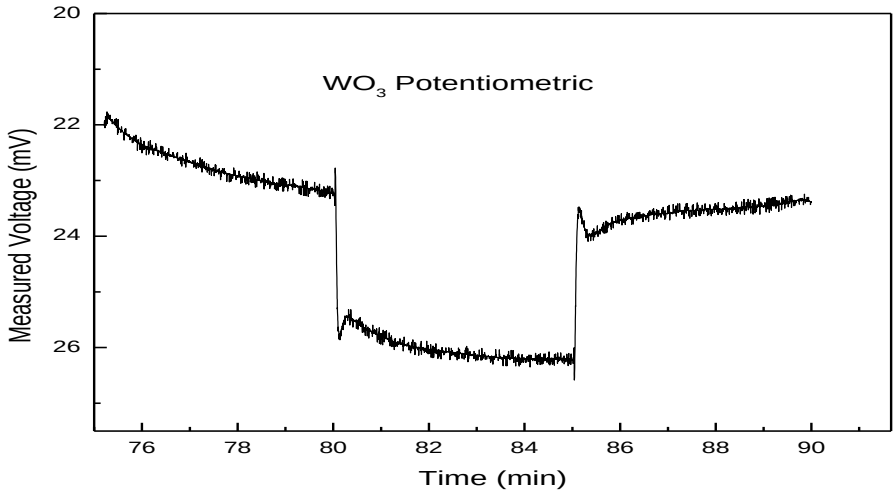
WO3 Potentiometric
Measured Voltage (mV)
Time (min)
20
22
24
26
76
78
80
82
84
86
88
90

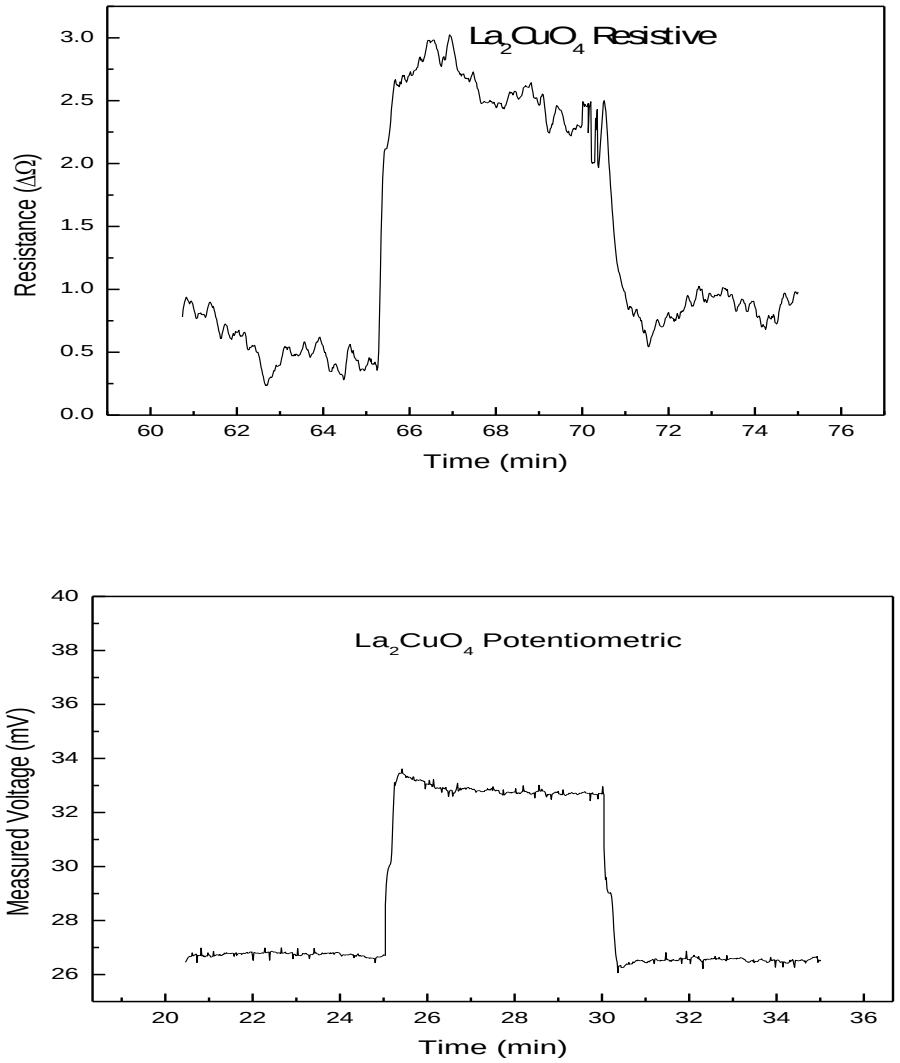

Figure II.3. Response characteristics of sensing surfaces WO_3 and La_2CuO_4 in resistive and potentiometric modes.

In case of La_2CuO_4 sensing element, for potentiometric mode, the minimum temperature of response was 290 °C and for resistive mode it was 320 °C while maximum temperature of response for potentiometric and resistive modes were around 420 °C and 530 °C respectively. Similarly, for WO_3 sensing element the minimum temperature of responses was 325 °C and 400 °C for potentiometric and resistive modes of operation respectively. While maximum temperature of responses was around 410 °C for potentiometric mode of operation and the

measurement at higher temperature up to 500 °C was possible for resistive mode of operation as shown in table II.2 below.

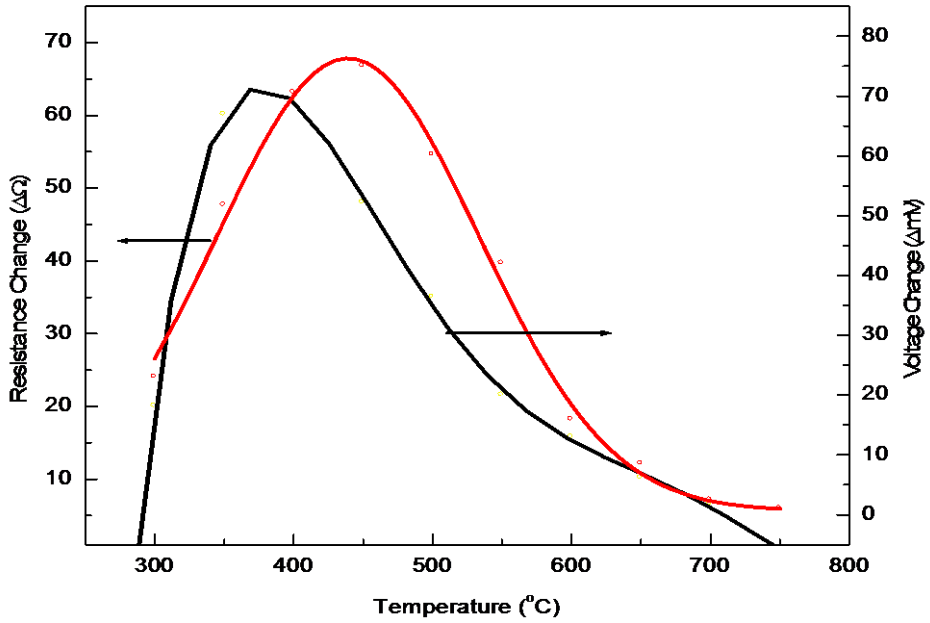

(a)

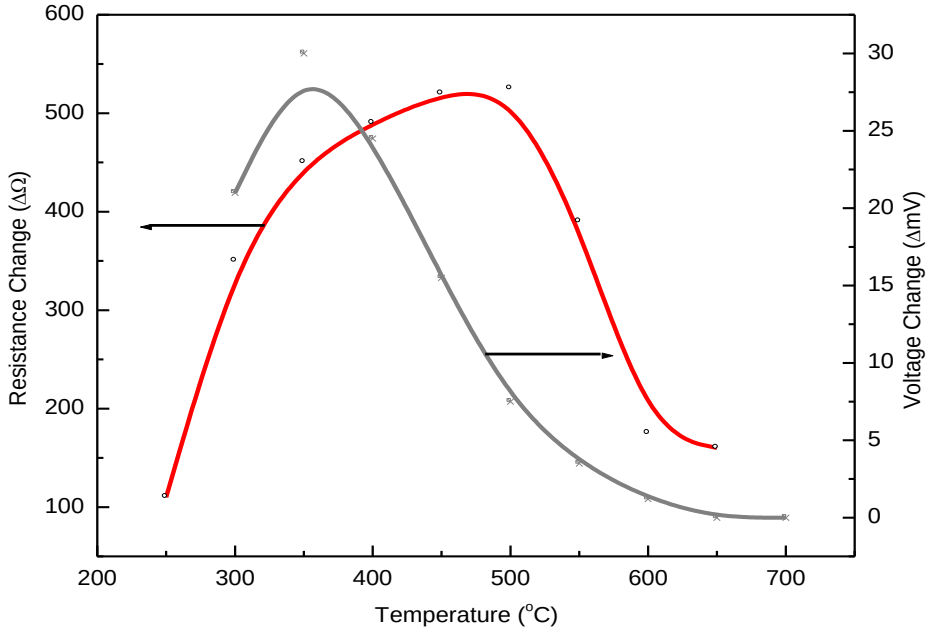

(b)

Figure II.4. Response with Temperature of sensing surfaces (a) WO_3 and (b) La_2CuO_4 in resistive and potentiometric modes.

Sensing material	Mode of Operation	Minimum Temperature	Maximum Temperature	Span of measurement	Reported in literature
WO_3, n-type	Potentiometric	325 °C	410 °C	85 °C	100 °C (ref 22)
	Resistive	400 °C	500 °C	100 °C	250 °C (ref 7)
La_2CuO_4, p-type	Potentiometric	290 °C	420 °C	130 °C	450-600 °C(ref 5)
	Resistive	320 °C	530 °C	210 °C	-

Table II.2. Span of Temperature for high response of sensing surfaces WO_3 and La_2CuO_4 in resistive and potentiometric modes.

The interaction between the sensor and the gas phase may involve physical adsorption (physisorption), chemical adsorption (chemisorption),[18] and formation or annihilation of surface and bulk defects.[19] The prevailing effect, or dominant reaction, depends on temperature, for the interaction between oxygen and the surface of ZnO.[20] This characteristic behavior is typical for many semiconducting metal oxides, with the transition from one region to another occurring at different temperatures for different materials. For most gas sensors operating at elevated temperatures, typically between 100 and 500 °C, chemisorption is the dominant effect controlling the sensing mechanism, while for resistive oxygen sensors operating at higher temperatures (typically above 700 °C), oxygen incorporation into the lattice is the dominant mechanism. This is beyond our measurement region.

For the n-type material span on maximum response is less for both potentiometric and resistive mode. This is because, NO being a reducing gas, can deliver electron more easily to the substrate. A p-type substrate can more easily adsorb this electron delivered by the NO gas. So, the span of measurement is higher for p-type substrate.

While comparing potentiometric and resistive modes, for resistive mode of measurement, span of maximum response is wider. This is because, for potentiometric mode the conductivity of electrolyte plays an important role, which diminishes at lower temperature, resulting in a shorter span of response. Whereas for resistive mode conductivity of the substrate play almost no significant role on the response. So, it gives high response for the entire range of temperature where gas adsorption is present.

Peak response for both n-type and p-type materials was found to be shifted towards lower temperature range in the potentiometric mode. This is because for potentiometric mode the physisorbed gas molecules only donate electrons for conduction through the substrate, while the chemisorbed molecules have bound electrons which do not take part in ionic conduction. The resistive mode of measurement gives higher response at higher temperature due to electrons contributed by the chemisorbed gas molecules.

II.3.2 Experimental Details

II.3.2.1. Synthesis of the material

La_2CuO_4 powder was synthesized by the auto ignition technique.[21] A stoichiometric mixture of $La(NO_3)_3 \cdot 6H_2O$ (Kanto chemical co., 99.99 %) and $Cu(NO_3)_2 \cdot xH_2O$ (Alfa Aesar, 99.999 %) was dissolved in deionized water and 0.25 mole % citric acid (Alfa Aesar, 99.5 %) was added to the mixture subsequently. The solution was heated at 70 ºC with constant stirring until a precipitate was formed, and the precipitate was then auto ignited with further heating at 90 ºC. The resulting powder was calcined at 600 ºC for 10 hours.

Tungsten oxide (WO_3, 99.8 % purity, Alfa Aesar) powder was purchased and the powder was dispersed in ethanol with polyethylene glycol 400 (PEG-400, Avocado Research Chemicals Ltd.), and mixed in a mortar for 3 hours. The mixed slurry was then heated at 60 ^oC for 10 hours. to remove the ethanol completely.

II.3.2.2. Sensor electrode preparation

For the preparation of a sensing electrode, Tungsten oxide or La_2CuO_4 powder was mixed thoroughly with solvent ethanol and plasticizer (0.01 %) ethylene glycol. The slurry was screen printed over one face of a Zirconia substrate.

For Potentiometric measurement, a square electrode of the sensing material was screen printed on one side of a YSZ substrate and a Pt electrode was printed directly opposite the sensing electrode. After that thin Pt wires were connected to both electrodes and finally, both the prepared sensors (La_2CuO_4 and WO_3) were sintered at 750 ^oC for 10 hours and at 400 °C for 12 hours respectively.

For resistive measurement, a square electrode of the sensing material was printed on one side of an YSZ substrate and it was fitted with Pt electrodes. In this case both the electrodes were in the same side. Finally, both the prepared sensors (La_2CuO_4 and WO_3) were sintered at 750 ^oC for 10 hours and at 400 °C for 12 hours respectively.

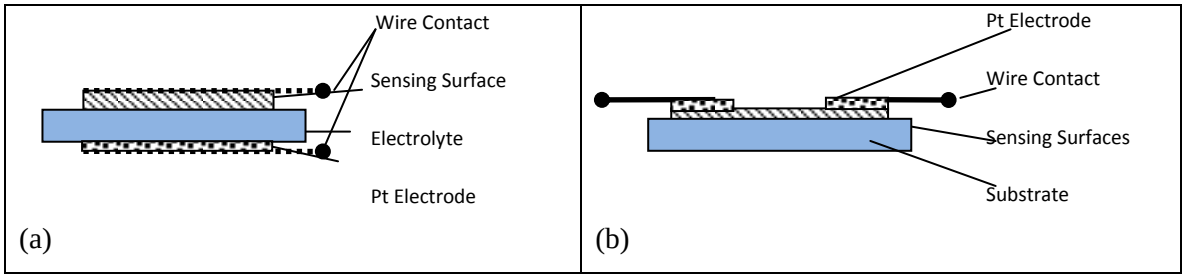

Figure II.5. Schematic Diagram of sensor designs (a) Potentiometric and (b) Resistive

II.3.2.3. Experimental setup

Sensing experiments were carried out with a gas flow system connected to a quartz tube which was inside of a furnace. Then the sensors were exposed to NO gas. For potentiometric and resistive measurement, the voltage and change in resistance between the two sensor electrodes was monitored using a digital source meter (2400 Keithley source meter) respectively.

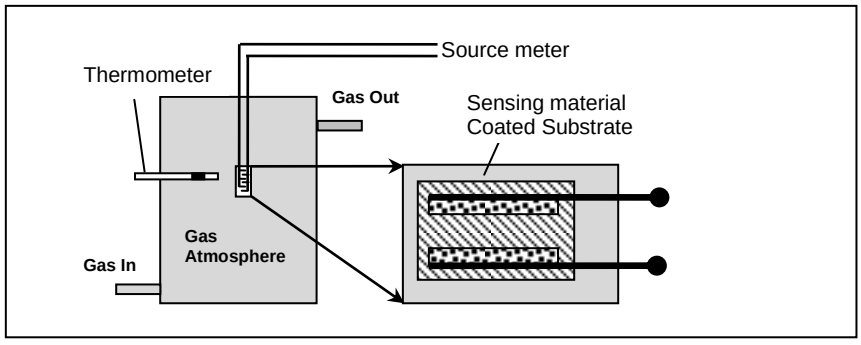

Figure II.6. Schematic Diagram of the Measurement setup.

II.4. Conclusion

This work has been attempted to compare the response curve shifts with temperature of the p-type, La_2CuO_4 and the n-type, WO_3 semiconducting sensing element fabricated over YSZ substrate in NO gas atmosphere. For La_2CuO_4 based sensing element, in potentiometric mode, the minimum temperature of response was 290 °C and in resistive mode it was 320 °C while maximum temperature of response for potentiometric and resistive modes were around 420 °C and 530 °C respectively. In case of WO_3 based sensing element the minimum temperature of responses was 325 °C for potentiometric mode and for resistive modes it was 400 °C. While maximum temperature of response was around 410 °C for Potentiometric mode and the measurement at higher temperature up to 500 °C was possible for resistive mode of measurement. From the experimental data, it has been observed that among potentiometric and resistive mode potentiometric mode was more sensitive at lower temperature range. Whereas for the resistive mode the sensors can be well operated upto higher temperature. Thus, potentiometric mode of operation can be used at lower temperature and the resistive mode can be utilized for higher temperature to detect the NO gas.

II.5. Reference

References are given in BIBLIOGRAPHY under chapter II page no. 90-91.

Chapter III

Fabrication and Characterization of La_2CuO_4 Nanoparticle Based NO_x Gas Sensors

III.1. Introduction

Metal oxide semiconductor gas sensor with finer microstructures are ideal candidates for low range detection because of its larger contact surface area between gas-solid interface. From the view point of today's demand, development of sensors, suitable for low range detection are necessary because of increase in environmental pollutants from different industrial exhaust and automobiles. There are already some legislation[1] based on low limit values for CO, NO_X and HCs from automotive emission. Several earlier investigations reported that sensitivity and response time depends on gas concentration profile.[2] The dependence of sensitivity at different range of gas concentration with the pore size distribution of the sensing electrode of YSZ based Potentiometric sensor has been studied in this investigation. Two theories have been proposed to explain the working mechanism of the potentiometric sensors: Mixed Potential Theory and Differential Electrode Equilibria Theory. Among them, Mixed Potential Theory originates from corrosion theory,[3] in which a pair of reduction and oxidation (redox) electrochemical reactions occur simultaneously to establish an equilibrium and there by produces a corrosion potential. This concept was first introduced in order to address potentiometric responses that deviated from the Nernst Equation.[4-12] According to Mixed Potential Theory, multiple gas reactions simultaneously come to equilibrium over the electrodes and each electrode establishes a mixed potential based on the equilibrium and rates of these reactions. For a NO sensor, the following equations represents the corresponding redox reactions:

$$2NO + 2O^{2-} \rightarrow 2NO_2 + 4e^- \quad (1)$$

$$O_2 + 4e^- \rightarrow 2O^{2-} \quad (2)$$

Since it measures the equilibrium level of NO, cannot describe NO sensing accurately. There are two limitations in Mixed Potential Theory, one of them is that NO does not come to thermodynamic equilibrium at sensor operating conditions because of the kinetic limitations and other is that at least one of the electrodes in a sensor must be a semiconducting material. To overcome these discrepancy Wachsman et al. introduced the idea of Differential Electrode Equilibria[13] to the gas sensing mechanism which is a more inclusive theory that takes into account multiple contributions as a cause for the difference in potential between two electrodes. Besides them additional contributions, namely the adsorptive and catalytic properties of

semiconducting oxides, including La_2CuO_4, have been thoroughly studied to potentiometric sensitivity in NO_x sensors. Upon adsorption of gas, semiconductors exhibit a change in Fermi Energy which lies between the valence and conduction bands and tends to bend under development of charge on the surface due to the adsorption.[14] Since Fermi Level is the localized electrochemical potential of electrons ($\mu_e = E_F$), the output (i.e. the difference between two electrodes) of a potentiometric sensor is affected by this phenomenon. Mixed Potential Theory that occurs over electrodes also does not take account for gas phase catalysis. So, sensitivity of semiconducting gas sensors in potentiometric mode can be explained with adsorption kinetics.

Earlier investigations with Potentiometric gas sensors indicate that electrode's microstructure affect the sensitivity and response time of the sensor[15-17] due to a large number of adsorption sites of microstructure electrode element which increases the surface to bulk ratio of microstructure electrode that extend the surface charging into the core of the microstructure. In previous work it was reported that response time decreases with microstructure of electrodes.[18] The NO_x sensors based on YSZ as a solid electrolyte has been reported in many publications.[19-27] From literature survey it has been observed that there are various sensors for NO_x detection in the form of Cr_2O_3|YSZ|Pt,[28] $La_{0.8}Sr_{0.2}FeO_3$ |YSZ| Pt,[29] NiO |YSZ| Pt,[30,31] $La_{0.8}Sr_{0.2}CrO_3$ |YSZ| Pt,[23] La_2CuO_4 |YSZ| Pt,[32] CuO |YSZ| Pt,[33] possess maximum range of detection 500 ppm, 20–1000 ppm, 10–400 ppm, 0–500 ppm, 50–400 ppm, 10–100 ppm respectively. But dependence of electrode's pore size with range of detection of a sensor is not discussed properly yet. Here we will discuss how detection of ultra–low ppm range is possible by using nano–crystalline microstructure electrode.

The experimental curve and simulated curve in this study both provide proofs of S–type nature of sensitivity with gas concentration with a definite shift in sensing range with average pore size of sensing layer. Microporous La_2CuO_4 based NO_x sensor also exhibit higher sensitivity at low gas concentration and low range(ppm) detection capability.

III.2. Background and Objectives

Although a large number of different oxides have been investigated for their gas sensing properties, commercially available gas sensors are mainly made of SnO_2 in the form of thick film, porous pellets or thin films. The effects of the microstructure, namely, ratio of surface area to volume, grain size and pore size of the metal oxide particles, as well as film thickness of the

sensor are well recognized. Lack of long-term stability and selectivity has until today prevented a widespread diffusion of this type of sensors. Gas sensors are employed in many applications including monitoring emissions from vehicles and other combustible processes, detection of toxic and combustible gases, Breadth analysis for medical diagnosis, and quality control in chemicals, food and cosmetic industries. Recently, by the application of Nanostructured sensing elements, issues like sensitivity and selectivity were reported by earlier workers and encouraging results were found. Higher sensitivity at lower concentration of gases is expected using sensing surface with finer microstructure. In this investigation, we propose, a systematic study of response with nano-structured sensing element which is expected to enhance the range of measurement up to ppb level.

III.3. Present work: Result and Discussion

Powder sintered at 750 ^{o}C, 800 ^{o}C and 1000 ^{o}C exhibit tiny, intermediate and macro grains respectively (reveals from Figure III.1). Again, it was observed from earlier literature that pores were usually comparable to their grain sizes.[34] With increasing sintering temperature, grains as well as pores began to fuse together,[35] produces a reduction of total porosity of the sensing material because of decreased surface area and modified surface structure.[36] In this regard, we optimized the sintering temperature at 1000 ^{o}C for macro pore and that sintered at 750 ^{o}C to yield micro pore, while 800 ^{o}C to yields mesoporous sensing surface.

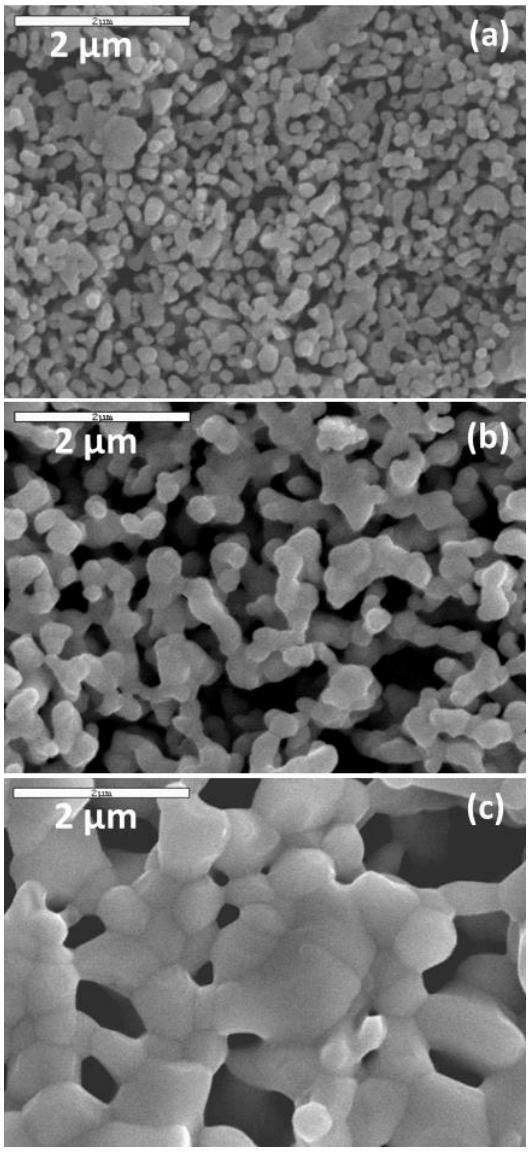

Fig.III.1. Typical SEM images of prepared La_2CuO_4 nanoparticles sintered at (a) 750 °C, (b) 800 °C and (c) 900 °C.

III.3.1. Change of response magnitude with gas concentration

The NO gas response of the potentiometric sensing element has been shown in Figure.III.2 where the response voltage is presented with changing gas concentrations in steps of 0, 50, 100, 200, 500 and 650 ppm. Under exposure of 650 ppm NO gas on the three types of porous sensing surfaces, gas response at a fixed temperature (450 ^{o}C) are different in magnitude and it is maximum for sensor which exhibit tiny pore, sintered at 750 ^{o}C and is minimum for that which exhibit macropore, sintered at 1000 ^{o}C. However, under close observation it was seen that the

sensitivity is not always same and it indicates a larger variation at the beginning for micropores and smaller variation at the begining for macropores. In order to understand the variation more closely, the sensitivity of three types of sensing surfaces are plotted in Figure III.3.

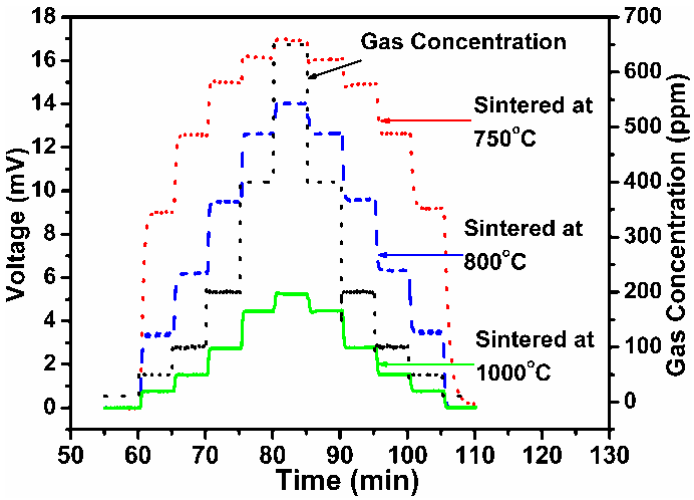

Fig.III.2. Voltage response of three different types of prepared La_2CuO_4 nanoparticles sintered at 750 °C, 800 °C and 900 °C with step change in gas concentration

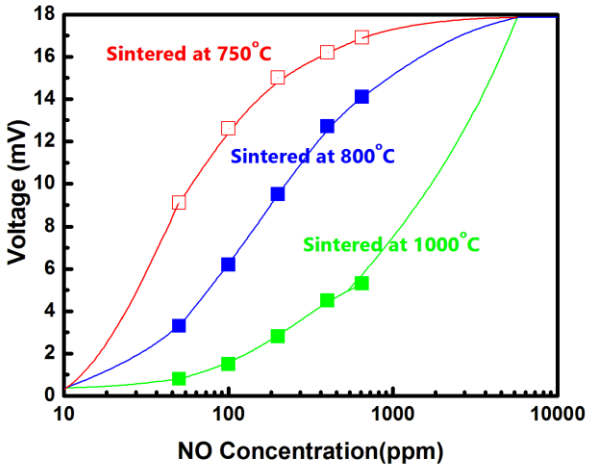

Fig.III.3. Voltage response of three different types of prepared La_2CuO_4 nanoparticles sintered at 750 °C, 800 °C and 900 °C with gas concentration at 450 °C

III.3.2. Sensitivity with pore size

Actually, with the increase in pore size following three types of diffusion occur at sensing material such as surface diffusion, Knudsen diffusion and molecular diffusion respectively,[36] which are responsible for gas sensing at different types of porous surfaces. For microporous material, pore sizes are too small to adsorb multiple layers of gas molecules and also, the pore edges are sharp. Due to these factors, the gas adsorption or surface forces are dominant so that adsorbed gas molecule cannot escape from force field of the surface. Due to small volume of pores, saturation of gas adsorption occurs at lower gas concentration ranges. This variation can be explained with the help of diffusion theory in nano porous media.[37] On the other hand, for mesoporous range, as the pore sizes are comparatively larger, capillary forces dominate over surface forces for their sensitivity in which pore condensation occur after multilayer adsorption of gas on the sensing material, as a result free volume of a mesopore decreased slowly than micropore after sorption treatment.[38,39] Again, from literature survey, Nitrogen adsorption isotherm for active charcoal showed that Nitrogen uptake at low relative pressure was mainly due to filling of micropores.[40] So, in case of mesoporous surface, sensitivity is smaller than that for microporous sensor in the low concentration range. The reason behind this may be due to an increased number of van der-waals interactions between gas molecules inside the confined space of capillary. For macro pore, molecular diffusion is responsible for their sensitivity,[39] in which transport properties of gas molecules through the macro pore is large but gas adsorption capacity is very small, and in this case interaction between gas molecules is significantly larger than the interaction between gas molecule to pore wall, that's why it exhibits a smallest sensitivity among them as shown in Fig III.4.

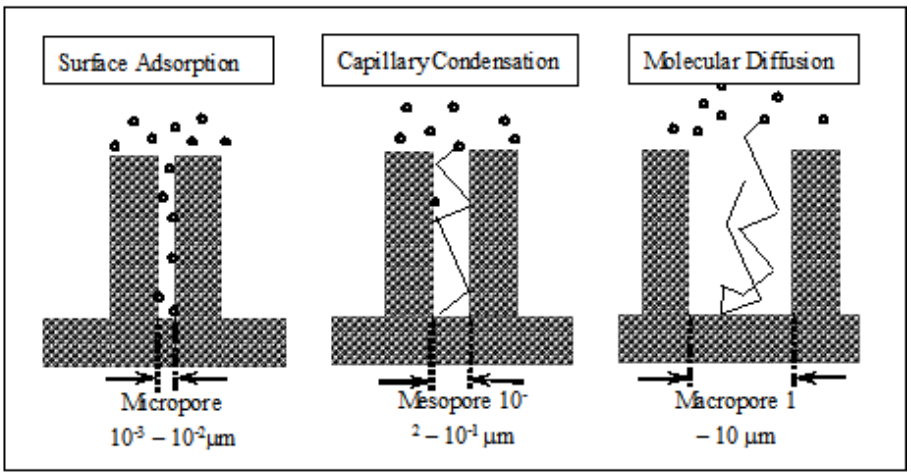

Fig III.4. Schematic diagram of gas diffusion through different porous sensing surface.

This can be explained with the concept of mean free path length. The gas diffusion coefficient is related linearly with its pore diameter as given in equation.

$$D_K = \tfrac{4}{3} r \sqrt{\frac{2RT}{\pi M}} \tag{3}$$

By using this diffusion constant and by solving the diffusion equation, one can estimate the amount of gas adsorbed (C_A) inside the sensing surface.

$$\frac{\partial C_A}{\partial t} = D_K \frac{\partial^2 C_A}{\partial x^2} - kC_A \tag{4}$$

$$C_A = C_{AS} \frac{\cosh\left[(L-x)\sqrt{k/D_K}\right]}{\cosh\left[L\sqrt{k/D_K}\right]} \tag{5}$$

Where, C_{AS} is the gas concentration outside the sensing layer, and L and x is the thickness of sensing layer and the diffusion length respectively. The different range of detection for micro, meso and macro-porous sensing surface can be explained with the help of this gas concentration profile inside this sensing surface, which again depends on pore size (from Equation 3) as well as surface reaction and rate of diffusion on surface of sensing material.[41,42] The gas concentration reduces with decrease in pore diameter. For micropores, volume of gas adsorbed is sufficiently low. This results in the gas molecules to reside closely near the sensing surface and further diffusion is restricted, reducing the chances of multilayer adsorption. Since micropores are in the

range of <1 nm, so it is assumed that a small concentration of target gas is sufficient to fill the pore.[43] Hence saturation region in this case came earlier than meso and macro-porous surfaces.

For macro-porous surfaces, the amount of gas adsorbed in sensing layer is sufficiently large, increasing the collision probability between gas molecules, results in lowering of mean free path length $\lambda_M = \frac{2kT}{\pi d^2 P}$, where d and P are the pore diameter and pressure concentration of applied gas. So, a large number of multilayer adsorption is required to fill up the pore volume of the sensing material. In macro pores, diffusion occurs mainly by bulk or molecular diffusion mechanism in which diffusion coefficient is inversely proportional to square of its pore diameter as given in Equation (6) below,

$$D_M = \tfrac{2}{3}\sqrt{\frac{kT}{\pi m}}\,\frac{kT}{\pi d^2 P} \tag{6}$$

So, with increasing pore diameter, rate of diffusion decreases and as a result high concentration of target gas is required to fill all the pores of bulk region. For this reason, saturation occur at high concentration range of the target gas.

In mesopore region, both the surface reaction as well as capillary forces are responsible for their wide detection range. In this case, the pore size is in intermediate range and so the volume of gas adsorbed will also be intermediate. Again, from Equation (5), it can be observed that the adsorbed gas concentration (C_A) decreases from surface after few diffusion layers. So, adsorption starts at higher gas concentration than microporous surface and saturation occurs after a small number of multilayer adsorption. Here the mean free path length for mesopore is $\lambda_m = \frac{1}{\sqrt{2}\pi\sigma^2}\frac{V}{N_A}$, where V is the gas molar volume at particular pressure and σ is the molecular cross section. In this case, collision probability between gas molecules are lower compared to collision probability with pore walls.

The profile of distribution of adsorbed molecules in subsequent layers can be obtained from Langmuir's isotherm equation for monolayer adsorption.[44] Considering evaporation in one layer and condensation in subsequent layer, the Langmuir's isotherm equation can be modified for nth layer as.

$$v = \frac{v_m c x}{(1-x)}\left[\frac{1-(n+1)x^n + nx^{n+1}}{1+(c-1)x - cx^{n+1}}\right] \tag{7}$$

Where, v is the volume of gas adsorbed when the entire adsorbent surface is covered with a complete unimolecular layer, $x=P/P_0$ and n is the number of layers of adsorbent v_m is the volume of the adsorbed gas in a monolayer of adsorbent. With the help of equation 7, the s-type nature of our experimental graph could be simulated and is presented in Figure III.5.

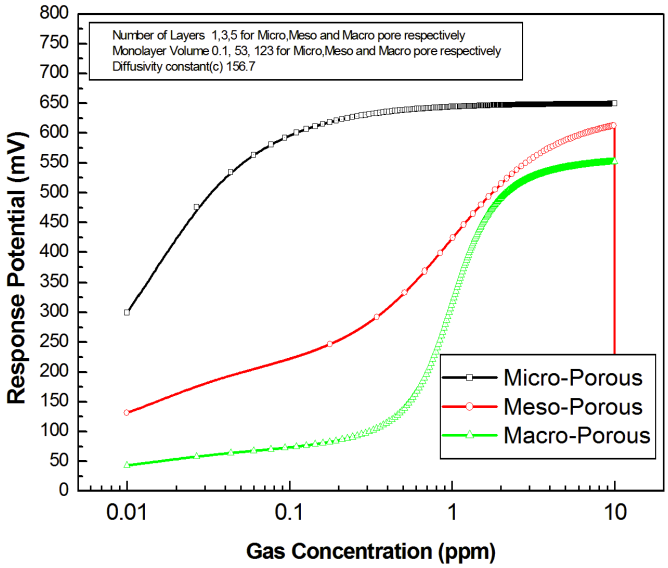

Figure III.5. Simulation of the sensitivity range for small, medium and large sized pores of sensing material.

To explain the exponential rise in sensitivity at very low gas pressure range, following factors may be responsible. It is highly probable that some surface complex containing carbon, hydrogen, and oxygen remained at the sensing surface. These can decompose into CO_2, CO, and H_2 by continued thermal treatment. Some of this complex could be removed during the outgassing at 450 °C, but an appreciable portion always remained in the adsorbent. The presence of this residual complex could have a major influence on the observed steady-state pressure in the range of very low pressures. The experimental results suggest that one of the factors responsible for the behaviour observed at low pressures may be directly related to the residual complex. Another factor of influence is associated with the diffusion of gas molecules at low pressures. Because of the intricate structure of the porous material, more time is required for the adsorbate to locate the adsorption sites of minimum potential energy which reduces the surface coverage. A similar argument may be valid in connection with surface diffusion phenomena.

This helps to explain the fact that even relatively well out gassed adsorbents (400 °C for 16 hour) required long periods to attain equilibrium in the low-pressure range.[45] With larger pore sizes, this equilibration time should be much larger. More and more be the gas pressure, the equilibration time became faster.

III.3.3. Experimental Details

In this study to fabricate a sensor ,tape cast YSZ (20mm×10mm×0.15mm) was taken as substrate and La_2CuO_4 as one of the electrode which were prepared through Auto-ignition technique,[46] where nitrate salts of constituent elements were taken and citric acid was added in appropriate proportion and subsequently heated with thorough mixing to form a gel, which was burnt to ashes which depends on the citrate-nitrate ratio, and was the key parameter in determining the powder morphology and the prepared La_2CuO_4 were calcined in air at 750 ºC, 800 ºC and 1000 ºC and mixed with appropriate amounts of solvents and ball-milled for 10 hours. The slurry thus obtained was screen-printed on one face of the substrate and Pt was pasted on the other. Thin platinum wires were connected to both the electrodes using Pt paste for ohmic contact. Finally, after drying of the printed electrode slurry, the sensor was sintered at appropriate temperature. The synthesized nanoparticles were characterized by X-ray diffraction (XRD) (Figure III.6) and scanning electron microscopy (SEM) (Figure III.1), which revealed that the particle size of the prepared nano materials increases with increasing the annealing temperature. The phase identification of all three perovskite oxides showed only the peaks of orthorhombic perovskite-type La_2CuO_4 phases.

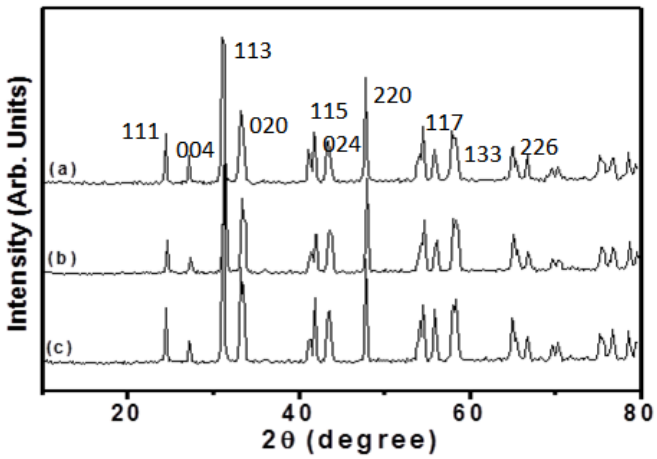

Figure III.6. X-ray diffraction pattern for the prepared La_2CuO_4 nanoparticles sintered at (a) 750 °C, (b) 800 °C and (c) 900 °C.

Prepared La_2CuO_4 perovskite-based sensor was systematically evaluated for NO reduction activity in Nitrogen (N_2 as carrier gas and the sensing experiments were carried out in a gas-flow system with a controlled heating facility. The sensors were exposed to step change of 50, 100, 200, 400 and 650 ppm of the NO gas to be sensed, in simulated combustion environment, at the total flow rate of 300 ml/min, in the temperature range between 400 and 700 °C. Electromotive force (EMF) measurements were performed between the two electrodes of the sensors using a Keithley 2400, digital voltmeter. During the EMF measurements, the electrode with the oxide coating was always kept at the positive terminal of the electrometer and both the electrodes were exposed to the same gas environment.

III.4. Conclusion

In conclusion, this study shows that the sensitivity of different microstructures are different in magnitude and they exhibit a shift in detection range, which has got definite correlation with pore size of the sensing layer. Larger pores have got higher sensitivity at higher concentration of gas whereas smaller pores have higher sensitivity at lower concentration of gas. Considering adsorption in one layer and condensation in subsequent layers and mean free path of gas molecules, we simulated the sensitivity profile. Simulation shows S-type nature of sensitivity with gas concentration with a definite shift in sensing range with average pore size of sensing layer. It was concluded that very large pore diameter reduced the adsorption sites and very small pore diameter reduced the probability of penetration. So, for the detection of higher concentrations one may use sensing material with larger pores and for low ppm detection one may use the sensor with micro pores.

III.5. Reference

References are given in BIBLIOGRAPHY under chapter III page no. 92-94.

CHAPTER IV

Investigation of sensing mechanism of Oxidation of NO on the WO_3 surface by Density Functional Analysis

I.1. Introduction

For environmental pollution levels measurement, gas sensors are hopeful candidates because of their low cost, fast response, high sensitivity, and direct electronic interface. Metal oxides are used as gas sensitive materials, due to their reproducibility and typical surface properties which are suitable for gas detection. They are robust, lightweight, long lasting and beneficial from high material sensitivity and quick response times and also relatively inexpensive compared to other sensing technologies. Tungsten oxide (WO_3) is one of these oxide elements studied extensively as NO_x sensors.[1] The functioning of these sensing devices can be attributed to the defects present in the surface of the material.[2,3] Material and surface properties are strongly dependent on the nature, concentration, and arrangement of defects like pores, voids, impurities, and vacancies. In our early studies we have presented n-type, WO_3 semiconducting sensing element fabricated over YSZ substrate in NO gas atmosphere,[4] since NO is one of the major air pollutant gas and also reducing in nature. To analyze the air quality, the development of NO sensing materials has become an important subject of current research. Concentration of electrons increases when a reducing gas is exposed on an n-type semiconductor surface. The change of resistivity of sensor surface is associated with oxidation–reduction kinetics of adsorbed gas.[5] It has been shown in earlier literature that NO gas affects the conductivity of the semiconductor sensing materials WO_3.[6-9] So, a theoretical study is very essential to understand the sensing mechanism of metal oxide material WO_3 with oxidation of NO on the surface. However, such theoretical analysis, compared with experimental results are lacking so far. Recently Tian's group have performed a series of first principle calculations.[10,11] Recent theoretical studies mainly focus on the adsorption behaviour of NO at WO_3 surfaces,[12] where surface resistivity of sensing material is related to the change of oxygen vacancy concentration (V_O). A dramatic effect on the electronic structure of WO_{3-x} has observed at higher V_O concentration (4%) where defect states become dispersed and then merge with the conduction band, that gives the metallic character of the sensing material.[13,14] In this work, the role of oxygen vacancies (V_O) on the performance of NO sensing by through the material WO_3 have been studied.

IV.2. Background and Objective

An outstanding research effort has been undertaken to address the environmental issues generated from environmental pollution and as a consequence health issues over the past two

decades. Particularly, the oxygen sensors plays an important role to control the pollution by optimizing industrial boilers, through automobile engine management, also in cement, steel industries and in the food processing plants.[15] The partial pressure and concentration of oxygen in a particular environment can be determined by several measuring principles. Ceramic-based sensors are used for the measurement of oxygen at high temperature. These are known as potentiometric sensors and the sensor output of these type of sensors vary with oxygen partial pressure logarithmically. Semiconductor based sensors can also measure oxygen indicated by the changes in the electrical conductance arising due to the alteration of the defect in the sensor surface by the chemisorption process of oxygen. Monitoring dissolved oxygen under ambient conditions is necessary in food processing, medical and waste management industries. Sensitivity, selectivity and response time are the three important parameters which characterize a sensor. The ability of a gas sensor to measure the test gas quantitatively under a given condition is known as the sensitivity of the gas sensor. Gas sensitivity is governed by the inherent physical as well as chemical properties of the used sensing material. The ability of a gas sensor to sense a particular gas is called its selectivity. The maximum signal change achieved with the changes in gas concentration is the response time of a particular gas sensor. Other factors like reversibility, size, long term stability, power consumption etc. also influences the overall performance of a gas sensor. The air-to-fuel ratio (λ) in the gasoline run automobiles is controlled by the oxygen sensors. The emissions of toxic gases like CO, NO_x, and hydrocarbons (HC) also depend upon the λ point at which a particular engine works. The emission of CO and HC is greater in the fuel rich region and NO_x emission is more in the lean region.[16] These gases are converted to the non-toxic gases like CO_2, N_2 and H_2O by the exhaust system. The potentiometric and planar O_2 sensors works well around the stoichiometric air to fuel ratio that is $\lambda = 1$. To improve the fuel economy, the best way is to run the engine under fuel lean conditions. Under the appropriate fuel lean conditions like air to fuel ratio 18:1 or 22:1, emission of green house gases is the least.[17] Now a days an advancement in the development of new sensor materials, micro electronic mechanical system (MEMS) devices, miniaturization etc have been offered by the semiconducting oxide sensor technology.[18] Electrical properties of most of the semiconducting oxide materials vary with the reacting gas species present in the atmosphere. The sensitivity of many oxide semiconductors towards the reducing gases like CO, NO, H_2, CH_4, hydrocarbons (HCs) etc. are mainly based on the surface reaction of the sensing material with the gas

species.[19, 20] Moreover, the bulk defect phenomena are mainly associated with the oxygen ion vacancies as well as metal ion interstitials and/or vacancies and electrons/holes present in the lattice. The common semiconducting metal oxides are TiO_2, Nb_2O_5, CeO_2, $SrTiO_3$ etc.[21-24] The change in the concentration of oxygen in the bulk is the cause of the change in conductance of the semiconductor material when it is exposed to the test gas. It is also a reflection of the defect structure present in the material.[19, 25] The major defects in the oxide semiconductor systems are the oxygen vacancies. At elevated temperatures, oxygen are adsorbed on the surface of these oxide semiconductors. TiO_2 is an *n*-type semiconductor which is one of the most widely used semiconductor material for the oxygen and other gas sensing applications.[26, 27] The rutile crystal structure of TiO_2 allows oxygen vacancies, and Ti^{4+} or Ti^{3+} exists in interstitial position of the lattice.[28] WO_3 is a good metal oxide sensor due to the defects present in the surface of the material. We have already studied n-type, WO_3 semiconducting sensing element fabricated over YSZ substrate in NO gas atmosphere,[4] in the present study the mechanism of NO adsorption on the WO_3 surface to improve the performance of gas sensing has been studied from a theoretical view point based on Density Functional Study.

IV.3. Present work: Result and Discussion

IV.3.1. Synthesis of Sensing Material and Device Fabrication

For the preparation of a sensing electrode, Tungsten oxide powder was mixed thoroughly with solvent ethanol and plasticizer (0.01%) ethylene glycol. For resistive measurement, a square electrode of the sensing material was printed on one side of an YSZ substrate and it was fitted with Pt electrodes. In this case both the electrodes were in the same side. Finally, the prepared sensors sintered at 400ºC for 12 hours. To study the sensing mechanism with the help of density functional theory, we remove one oxygen atom from WO_3 to produce defect with creation of single oxygen vacancy.

IV.3.2. Characterization of sensing elements

The morphology of the sample was observed using a Scanning electron microscope (SEM). Figure IV.1 shows the microstructure of sensing surfaces.

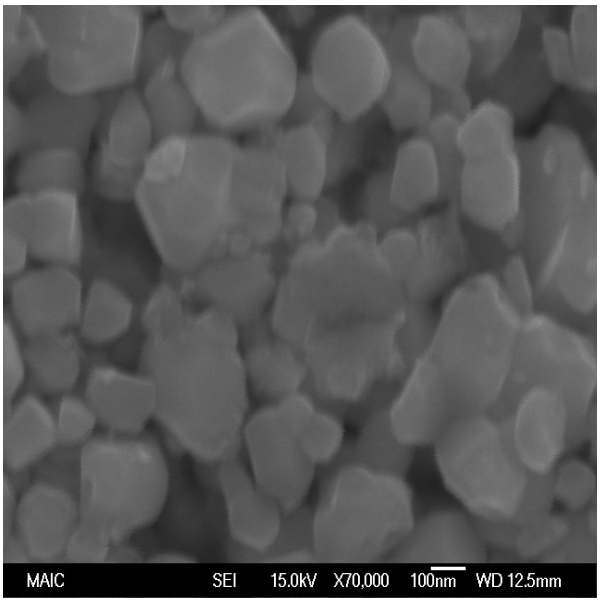

Figure IV.1. SEM micrograph of sensing surface WO_3

The particle size was around ~100nm for the films. The BET surface area of powders was found to be 11.2 for WO_3 powders. X-ray diffraction patterns of both the sensing materials WO_3 was collected in the 2θ range of 5 °C to 70 °C as presented in Figure IV.2, which shows complete formation of WO_3 phase.

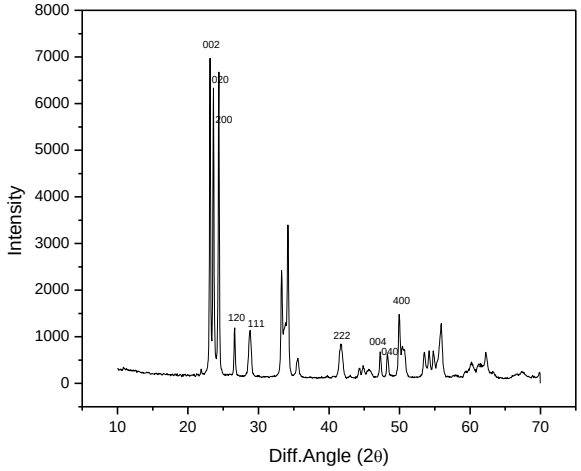

Figure IV.2. X-Ray diffraction pattern of sensing surface WO_3

IV.3.3. Fabrication and Measurements

Sensing experiments were carried out with a gas flow system connected to a quartz tube which was inside of a furnace. Then the sensors were exposed to NO gas. For resistive measurement, the change in resistance between the two sensor electrodes was monitored using a digital source meter (2400 Keithley source meter). Computational methods using density functional analysis are taken to illustrate the experimental output.

IV.3.4. Dependence of oxygen partial pressure on sensor output

The defect phenomena at two temperature ranges results in introduction of defect only in high temperatures and defect free substrate at low temperatures. This is further confirmed through impedance analysis.

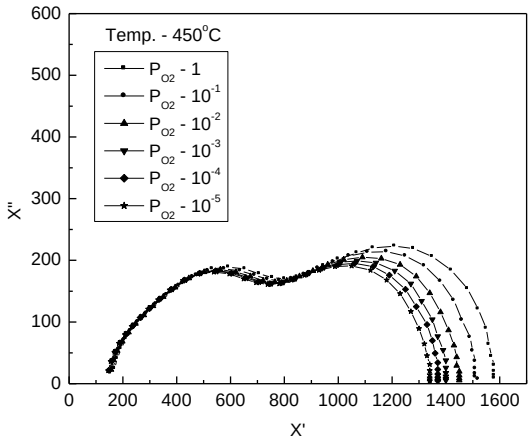

Figure IV.3a. Nyquist diagrams of WO_3 films in different P_{O_2} at 450 ºC

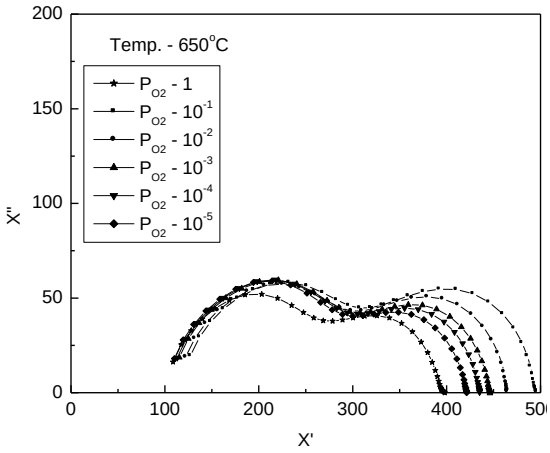

Figure IV.3b. Nyquist diagrams of WO_3 films in different P_{O_2} at 650 ºC

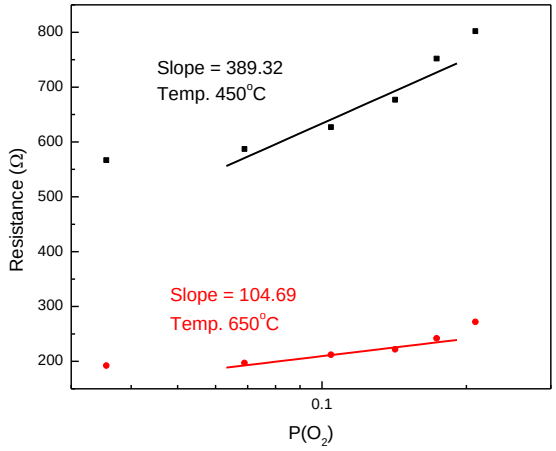

Figure IV.3c. Variation of resistance as a function of P_{O_2} plotted on logarithmic axes

Figure 3a and 3b, represent the variation of Im(x) with Re(x) at different partial pressure at two different temperature, is a circle whose right intercept with the x axis represent device resistance at $\omega \rightarrow 0$ and it is related by an equation

$$Re(x) = R/(1+ \omega^2R^2C^2) \quad (1)$$

From Figure 3a and 3b, it is seen that with increasing partial pressure of oxygen, resistance of the sample increases which is also true for Figure 3c and it agrees with the relation[29-32]

$$R = R_O P_{O_2}{}^{\beta} \tag{2}$$

where R_O is the sensor resistance in pure O_2 and β is the power law coefficient, which demands that the sensing material is n-type. And it is also seen that at temperature 450 ºC the value of real part of resistance is much larger than that at 650 ºC. It implies that at 450 ºC, oxygen adsorption plays a significant role in sensing mechanism than at higher temperature 650 ºC. Actually, at low P_{O_2} there occurs a loss of oxygen from semiconductor bulk and at high temperature there occur a lattice vacancy by releasing conduction band electrons. From Figure 3c, it is seen that, slope of the resistivity vs log **(** P_{O_2} **)** graph at 450 ºC is much higher than that at 650 ºC, which implies that at low temperature region activation energy is higher than that at high temperature region, where the relation between conductivity and P_{O_2} with E_g at a fixed temperature is given by

$$\sigma \infty P_{O_2}{}^{-1/6} \times e^{-E_g/kT} \tag{3}$$

This difference in activation energies at two temperature ranges results in introduction of defects only in high temperatures and defect free substrates in low temperatures.

IV.3.5. Resistivity of WO_3 thin film with reducing gas

Figure 4a shows the resistance variation with temperature at a gas concentration of 650 ppm of NO, for WO_3 film fired between 300 ºC to 800 ºC temperature in NO gas atmosphere. Variation of resistance with temperature obeys the relation

$$R=R_0\, e^{(-\Delta E/KT)} \tag{4}$$

and this curve consist of three distinct regions indicating different conduction regions with different slopes. At the high temperature range, the decrease in resistance with increasing temperature indicates the semiconductor behavior of the WO_3 thin film.[33]

Figure 4b shows the activation energy derived from Figure 4a. From Figure 4a, we see that at very low temperature region, between 300 ºC to 450 ºC, the resistivity of sensing material is

high. This is due to oxygen atoms pre-adsorbed on the surface which can be explained by the equation

$$(WO_3+e^-)+1/2O_2 \rightleftharpoons WO_3(O^-)_{ad} \quad (5)$$

and further NO adsorption is not possible so high activation energy is required in this region. In the intermediate range, between 450 ºC to 600 ºC, the activation energy is lower, allowing NO adsorption by replacing oxygen atoms on surface which can be explained by the equation

$$WO_3(O^-)_{ad}+NO \rightarrow (WO_3+e^-)+ NO_2 \quad (6)$$

From equation (5) it is clear that the ionosorption of atmospheric oxygen consume conduction band electrons which again become free by removal of O^- surface species by reducing gas NO. The net rate of return of electrons to the conduction band depends on oxygen partial pressure by a relation

$$\frac{dn}{dt} = K_2 P_{NO} - K_1\sqrt{P_{O_2}} \quad (7)$$

where K_1 and K_2 are rate constant for the processes involved in equation (5) and (6) respectively. This equation again confirms that with decreasing P_{O_2} the net rate of return of electrons to the conduction band must increase, provided P_{NO} remains constant Whereas, at high temperature range, between 600 ºC to 800 ºC, the activation again rises as shown in Figure 4b, since all gas molecules gets expelled from the surface and conductivity is determined by solid-state ionic equilibria.

The reduction of activation energy in the intermediate temperature range which is mainly due to the release of electron which can be further explained with the help of defect equation,[34]

$$W_nO_{3n} + NO = W_nO_{3n-1} + V_{O'} + NO_2 + e^- \quad (8)$$

Accumulation of these electrons create a donor level which reduces the activation energy.

The WO_3 surface with defect was further re-oxidized by the atmospheric O_2 molecules following the defect equation,

$$W_nO_{3n-1} + NO + O_2 = W_nO_{3n} + NO_2 \quad (9)$$

at very high temperature region. During this step, charge transfer from the surface to O_2 molecule generates an active O_2 species resulting in a reduction in surface conductivity. This active O_2 species tends to react with the NO and releases NO_2 with the reproduction of perfect WO_3 surface. With increasing concentration of gas, the number of oxygen vacancy is increased and such oxygen vacancies changes of the surface structure significantly.[35]

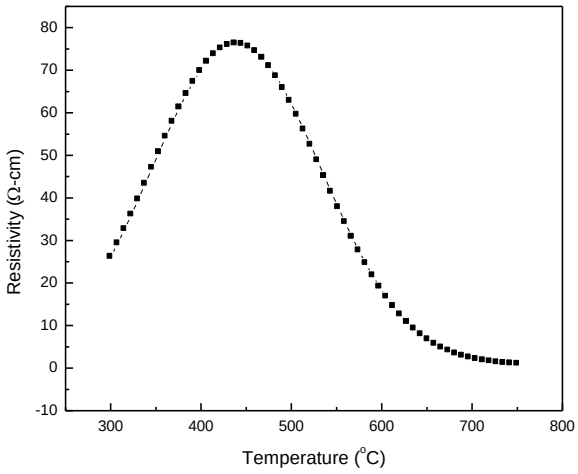

(a)

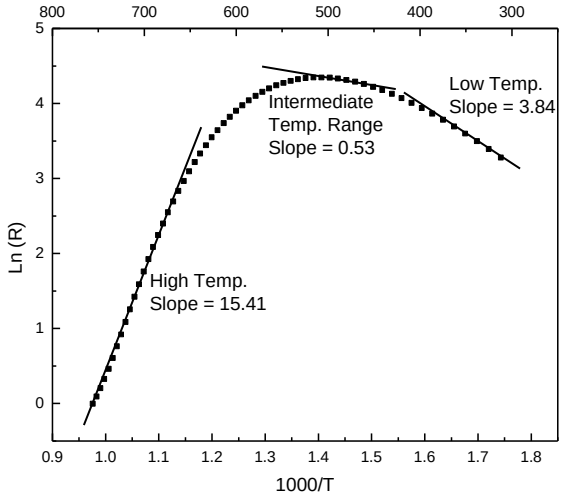

(b)

Figure IV.4a. Response with Temperature of WO_3 sensing surfaces in resistive mode and 4b. corresponding to Arrhenius Plot.

Resistivity of WO_3 thin films against the reciprocal temperature are represented by Arrhenius curves, the slopes of which depend on environment conditions of the sample. And the variation of conductivity σ with temperature is normally interpreted using Arrhenius equation

$$\sigma=\sigma_o \exp(-E_o/Kt) \quad (10)$$

where σ is the conductivity and E_o, the activation energy for electrical conduction and k the Boltzmann constant. The activation energy deduced from this equation corresponds to the slopes of the Arrhenius curves.

The conductivity of tungsten oxide films is controlled by the non-stoichiometry of n-type WO_3 and originates only from oxygen vacancies was assumed. The creation of oxygen vacancies in WO_3 can be expressed by a chemical equilibrium,

$$O_o^x \Leftrightarrow V_o^x + (\tfrac{1}{2} O_2)_g \quad (11)$$

Where, O_o^x is the neutral oxygen atom in an oxide site and V_o^x is the neutral oxygen vacancy with two trapped electrons giving rise to a donor level in the gap. When the temperature is increased, the donors are successively ionized with an activation energy E_a, generating free electrons e in the conduction band. This process is expressed by

$$V_o^x \Leftrightarrow V_o^{2+} + 2e^- \quad (12)$$

Where, V_o^{2+} represents a doubly ionized oxygen vacancy and subsequently, the total equilibrium for carrier generation is

$$O_o^x \Leftrightarrow V_o^x + 2e + (\tfrac{1}{2} O_2)_g \quad (13)$$

When the defect levels concentration increases, the donor orbitals overlap and lead to the formation of band which lessens the gap required for carrier ionization. For high defect concentration the ‘‘defect band’’ broadens sufficiently so that the gap disappears. Such a ‘‘defect band’’ model can be applied to the conductivity results that we obtain on WO_3 where the defects are surface oxygen vacancies. When the oxygen pressure decreases the density of oxygen vacancies, increases up to a c(2×2) structure for some parts of the sample. So according to the model of ‘‘defect band’’ the activation energy for electron generation decreases as the density of vacancies increase with decreasing oxygen partial pressure and drop to zero when the WO_3 sample is annealed in vacuum.[36-39]

In fact, there are many other parameters consider, in particular the grain size with the barrier at the grain boundaries should play an important role in the conduction mechanism. However, we suppose that the most important phenomenon in our experimental conditions is the oxygen vacancy formation.

IV.3.6. Explanation with band structure calculations

The Band structure of WO_3 samples with and without defect was plotted in Figure 5a and 5b and the DOS for these two types of samples are plotted in Figure 5c and 5d. From Band structure it was noted that the Fermi level lies above the band gap for both the defect free and WO_3 structure with oxygen vacancies and hence the material is n-type all through the concentration level of the adsorbed gas. There is a clear rise in the Fermi energy for WO_3 with defect surface (E_F = -4.87 eV) than WO_3 with defect free surface formed (E_F = -6.41 eV) due to gas adsorption and creation of donor levels. From the DOS it was seen that the density of states near the Fermi level is quite large for samples with defect. This variation of DOS plays a significant role in sensor output.

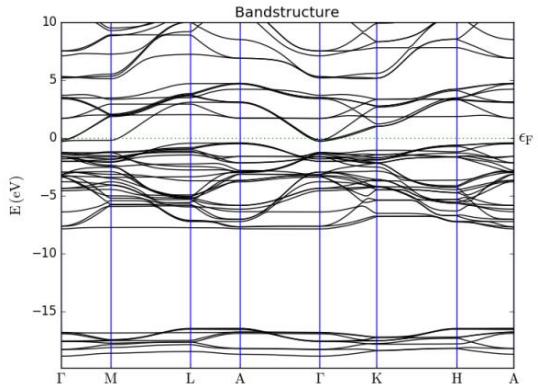

Figure IV.5a. Band structure of WO_3

(Fermi level = -6.41 ev)

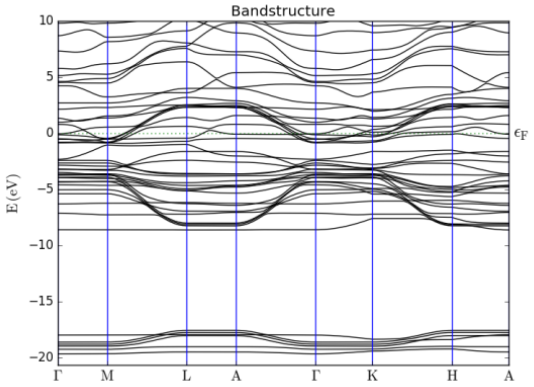

Figure 5b. Band structure of W_nO_{3n-1}

(Fermi level = -4.87 ev)

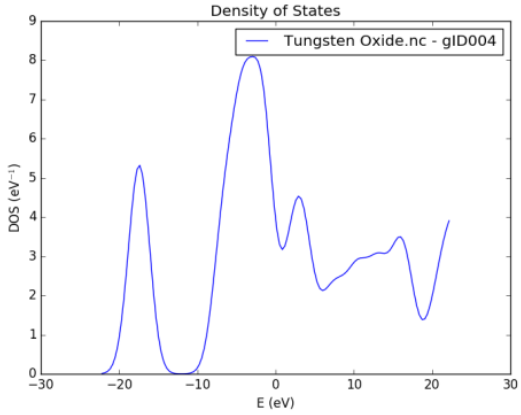

Figure 5c. Variation of DOS with energy for WO_3 structure

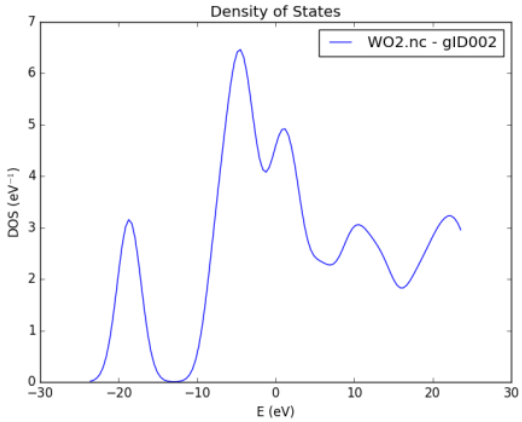

Figure 5d. Variation of DOS with energy for WO_3 with 5 % defect surface states.

IV.4. Conclusion

Our work demand that defect may affect the electrical transport by changing the band gap and density of states (DOS) of sensing material. For perfect structure the Fermi level positioned at -6.41 eV and for defect structure that positioned at -4.87 eV. This shift in Fermi energy is due to creation of large number electron at the conduction band of metal after formation of oxygen deficient surface. Practically when reducing gas (NO) exposed on a transition metal oxide (WO_3) based sensing material it become oxidized to NO_2 gas by creating oxygen vacancy on the surface and there by formed oxygen deficient surface and release electrons. The total number of oxygen vacancies is strongly related with defect density. So, sensor output must depend on defect density. Here, we generate 5% oxygen vacancy by removing oxygen atoms from WO_3 surface that gives a change in Fermi level between perfect and structure with defects, whose value is 1.54eV. Actually, after creation of oxygen vacancy, magnitude of DOS decreases and Fermi level shifts towards higher energy states due to large concentration of electrons at conduction band of metal so that several partly occupied energy bands appeared at the Fermi level. These differences in Fermi level and DOS are responsible for resistive sensor output.

IV.5. Reference

References are given in Bibliography under chapter IV page no. 95-96.

Chapter V

Application of electronic nose systems by array of nanostructured doped ZnO sensing material for assessing tea quality

V.1. Introduction

Application of nanoscience involving the use of various nanomaterials and nanosize components is known as nanotechnology. Nanotechnology is used to design custom made materials, nanoelectronic components, various types of sensors and solar cell systems.[1] There is a tremendous progress in nanotechnology which has been done by researchers in the past few decades. Materials with basic structural units/ grains/ particles/ fibers with particle size smaller than 100 nm in at least one dimension are known as nanomaterials.[2] These nanomaterial found various applications like improvement of conversion efficiency of solar cells, disease prevention, diagnosis and/or treatment. Nanomaterials include nanoclusters, nanotubes, nanocrystals, nanofibers, nanorods, nanowires, nanofilms etc. Various nanofabrication technologies like electro-spinning, phase separation, thin film deposition, self-assembly processes, chemical vapour deposition, nano imprinting, electron beam or nanosphere lithographies etc.[3] These processes help to synthesize various nanomaterials with ordered and/or random nanotopographies. When the material size is decreased into nanoscale, the surface area and surface area to volume ratios can be adjusted leading to superior physiochemical properties such as mechanical, electrical, optical, magnetic, catalytic properties.[4] That is why, nanomaterials have been extensively investigated with wide range of applications, like medicine, electronic devices, solar cells and in particular sensor devices. Thus nanodevices find its huge impact on ability to enhance energy conversion, control pollution and improve human health. The benifits of the applications in sensitivity is due to the presence of large surface area of nanostructured sensing material. Also selectivity of sensors depends upon the nanomaterials used.[5] The present work includes synthesis of ZnO nanorods by sol-gel technique, application of these fabricated nanorods as sensors for the detection of volatile organic component (VOC) for the detection of flavor in orthodox darjeeling tea. A special technology named electronic nose was adopted to detect the organic flavor. An array of sensors are used in the sensing technology of this electronic nose for the simultaneous detection of the signal and analysis of signals, so that the contribution of individual component can be known through sophisticated analysis techniques.

E-nose system is a technology based on sensors. It possess the total headspace full of volatiles and it creates a unique smell print. E-nose does not resolve the volatiles of a sample into individual components, but it responds to the total set of volatiles with a unique digital pattern.

These patterns denote a particular set of aromatic compounds. For each application, a certain database of digitized patterns is created which is called training set. For testing when an unknown sample possessing VOC is exposed to this E-nose sensor system, it digitizes first the volatiles of the sample and then compares the pattern with the existing training set.

From a practical point of view, in the last decade, this E-nose technology has opened a new field which helped to exploit the information related to different application fields. The E-nose ican be used to predict the optimal harvest date by sensing the aroma. Commercially available E-noses consist an array of sensors combined with the pattern recognition software. There are several reports of the application of electronic sensing in the food industry,[6] also in the discrimination of several fruits of different quality and/or ripeness, like oranges,[7] apples,[8-10] tomatoes,[11] grain[12] etc. Few literatures are also available regarding fruit shelf life and quality attribute.[13] The objectives of the present study were to monitor first the flavor in orthodox Darjeeling tea using doped ZnO fabricated electronic-nose sensor and analyze the response by using Principle Component Analysis (PCA); secondly to correlate the analyzed response data with the standard tea testers' scores to generate a calibration system which helps to predict the quality of unknown tea sample.

Zinc oxide (ZnO) is one of the most widely used oxide semiconductor based gas sensing material.[14-17] It is an n-type semiconductor with band gap E_g 3.2 eV. The electrical conductivity of ZnO is due to the intrinsic and extrinsic defects present in the lattice. Pure ZnO has the conductivity due to the former defects such as zinc excess at the interstitial position and oxygen vacancy. ZnO has been alloyed with various 3d transition metal (TM) to explore its applicability as gas sensor.[18-19] The transition metal oxide adhered to the surface of pure ZnO thus widening the depletion layer and increasing the resistance of gas film. The response is increased when test gas comes in contact with the metal oxide particles thereby decreasing the resistance for the wider depletion layer.

Absorption of oxide in the films decrease the electrical conductivity as pure ZnO thin films are sensitive to oxidation. But the electrical properties are enhanced by extrinsic defects in doped ZnO with different dopants and trials have been made in this respect.[20-24] Moreover the electrical properties of ZnO could also be modified by thermal treatment in the reducing atmosphere.[25] Surface morphology mainly affects the optical properties of ZnO and heavy doping changes the

optical energy band gap.[26] Thermal treatment in a reducing atmosphere[27] and appropriate doping process also modified surface morphology.[28] Ohyama *et al.* reported that the use of high boiling point solvent 2-methoxyethanol and monoethanolamine (MEA) resulted transparent ZnO films.[29] Further better electrical and optical properties were obtained by 0.5 at.% aluminium doped ZnO thin films treated with heat in reducing atmosphere.[20] Nunes *et al.* found superior electrical and optical properties with doped ZnO, where doping concentrations of Aluminium, Indium and Gallium were 1, 1 and 2 at. %, respectively.[30] The resistive response of the sensing material varies with band gap energy of the substrate. Krylov[31] *et al.* found the activity order of the metal oxide as follows, MnO_2>CoO>Co_3O_4>MnO>CdO>Ag_2O>CuO>NiO>SnO_2>>Cu_2O>Co_2O_3>ZnO>TiO_2>Fe_2O_3>ZrO_2>Cr_2O_3>CeO2>>V_2O_5>>HgO>WO_3>ThO_2>BeO>MgO>Al_2O_3>SiO_2. The potential between the sensor material and the gas molecule depends on the electro negativity difference between them. So variation in the band-gap energy of the sensing material imparts larger cross-sensitivity among various species of gases. When various transition metal ion was doped in ZnO blue and red shifts in band gaps were observed.[32] Thus three transitional elements Iron, Cobalt and Nickel having largest variation in band gap energy were selected.[32] For the preparation of ZnO thin films several deposition techniques, such as pulsed-laser deposition,[33] chemical vapor deposition,[34] RF magnet ron sputtering,[35] spray pyrolysis,[36] sol–gel process[37] etc, it is possible to prepare a small as well as large-area coating of ZnO thin films by the sol–gel technique. X-ray diffraction (XRD) and scanning electron microscopy (SEM) reveals that the ZnO exhibits a hexagonal wurtzite structure. Figure V.1 shows the XRD pattern of the ZnO nanowire growth on an ITO coated glass substrate by using the spin coating sol-gel method and EDX analysis of ZnO, wheras Figure V.2a is the SEM image of undoped ZnO. A dominant diffraction peak for (002) indicates a high degree of orientation with the c-axis vertical to the substrate surface. The hexagonal wurtzite structure of the ZnO nanorods was assured by both XRD and SEM. In this study, we present the growth of ZnO nano rod structures by sol-gel spin coating technique and detection of the tea aroma and their gas sensing properties with the E-nose prepared by doped ZnO nanomaterials . The effects of dopants and their doping concentration on the microstructure and electrical properties of doped ZnO thin films were also investigated.

V.2. Background and Objectives

V.2.1. Detection of Tea Aroma

Tea is one of the most most aromatic beverage and popular drink worldwide. Among various types of tea such as green tea, black tea, oolong tea etc black tea is most common beverage. Mainly two types of black teas are there namely Orthodox and CTC tea. The quality of tea is influenced by the amount of time a tea is stored in Almacafe's warehouses. The quality and the purchase price of tea are mainly determined by some protocols. The factors which are important to assess a tea sample are appearance, good condition and proper size of the tea grains. For further assurance tests are done in the cup or by the tasters.

Traditional methods where professional tea tasters were employed are still being practiced for quality of tea measurement. Unfortunately, no instrumental methods are still not in use in the industry. These tasters assess the quality of tea based on their experience and judgment and the price of the tea is fixed accordingly. The tea-tasters give mark ranging from 1 to 10 each for leaf quality, infusion and liquor for a particular sample.[38] This method is very much subjective and error-prone. Thus, industry demands a low-cost and portable instrument for the quality evaluation of the black tea. Electronic nose has been well demonstrated to serve the purpose.[39] To obtain a standard product analysts have developed different types of analysis for CTC, orthodox and green tea. Tea quality index could be correlated well with electronic nose (E-nose) signal. Few literatures illustrates a model using signal of E-nose system which predicts the quality of tea. One of the most important sensory attributes of tea is aroma. The flavor in different organic products like tea, coffee, etc. arises from Volatile organic compounds (VOC) which are emitted during infusion. Sensing of VOC's has attracted much interest focused on several factors like detection, monitoring and analysis. Tea flavor is sensitive due to the compositional alterations of VOCs present in tea. The VOCs which are the cause of tea flavor are produced during ripening, harvest, post-harvest and storage procedures. Many research groups are working now a days on the detection of volatile VOCs that produce aroma in various food products. As a consequence, E-nose technology have been introduced. However, selectivity of sensor material is very much important for the accuracy of the detection procedure. To overcome this problem, various researchers illustrated a number of statistical techniques such as linear multiple regression, principal component analysis (PCA) etc. However to improve the

selectivity of the sensors, designing new sensing elements attract much attention. Primarily porous oxide nanomaterials like ZnO and SnO_2 have been studied for detection of inorganic gases.[40] Due to the fine physical, chemical and optical properties ZnO has been used as potential semiconductor materials as sensor.[41-43] ZnO nanowire is much appreciating for fabricating sensors which detects various VOCs.[43] Very recently, ZnO nanomaterial gas sensors have attracted much attention for their capability of detecting pollutants, toxic gases, alcohols etc. Also various food's freshness such as fish freshness[44] can be detected using gas-sensing films integrated on one chip which is known as "electronic nose".[45] The sensitivities of the gas sensors can be greatly enhanced by doping transition metal ions like Fe^{+3}, Co^{+3} and Ni^{+2}. Very recently, identification of various components of the flavour of chinese liquors was carried out by the use of doped nano ZnO gas sensor array and their classification ability were compared using several statistical technique. Some research groups were able to analyse some flavour components by pattern recognition analysis of an E-nose system,[46-48] that possess broadly tuned nonspecific array of sensors. It represents the olfactory sensing mechanism, that has been developed by the use of variety of odour sensitive biological/chemical materials that can be used in food product evaluation. The E-nose system addresses fast and cost effective solution to the problems of tea quality determination which is based on organoleptic study and chemical analysis. The E-nose system consists of an array of gas sensors that record the characteristic response for any particular odour. The pattern recognition methodologies are in the form of software which identify particular odour by sensor response data set.[48] The odour molecules are carried to the sensor array by different sampling techniques like diffusion methods, head space sampling, pre-connectors. The sensing materials suffer some physico-chemical changes when it comes in contact with the odour molecules which leads to the change in their conductivity. Difference in the responses result as different sensor in the array responds to the different odour molecule with varying degree. The total set of responses from all the sensors are used for pattern recognition after transduction into electrical signals.[49-50] Depending upon the chemical composition of the odour/odour mixtures a variety of sensors such as conductivity sensors, intrinsically conducting polymers, conducting polymer composite sensors, metal oxide sensors, surface acoustic wave sensor, piezoelectric sensors, optical sensors, metal-oxide-semiconductor field-effect transistor sensor etc are usually used in the array of modern E-nose systems. Odour gas molecules which contains VOCs interact with thin/thick films of sensor materials by adsorption or chemical

reactions and with solid state sensors by absorption process. These changes in the sensing materials of E-nose are measured as electrical signals which are considered to be responses.

Inert gases like nitrogen is flushed through the array of sensors as reference gas in the very first stage of the odour analysis by E-nose system. After that the odour is allowed to reach the sensors. The reference gas is again allowed through the sensors when the data recording is completed. The reference gas is allowed to flush before and after the analysis which is necessary to prepare the base line of the responses. The period of time for which the sensors are exposed to the odour is called response time and the recovery time is the time for which reference gas is passed through the sensor array. After recording the responses, it is then processed for the pattern recognition after base line correction.[49] The basic data analysis techniques for pattern recognition in the E-nose system are,

(i) Graphical analysis: Bar chart, profile, polar and offset polar plots.

(ii) Multivariate data analysis (MDA): Principal component analysis (PCA), canonical discriminate analysis (CDA), featured within (FW) and cluster analysis (CA).

(iii) Network analysis: Artificial neural network (ANN), radial basis function (RBF).

Choice among the abovementioned methods depend on the type of responses obtained and the purpose of its use.[51]

V.2.2. Quality determination of Orthodox Tea by E-nose systems

For quality grading a neural network based E-nose which comprises an array of four SnO_2 gas sensors can assist the monitoring of tea quality. Different aroma profiles were visualised using the Principal Component Analysis (PCA) method.[52] In addition, Kohonen's Self Organising Map (SOM) cluster analysis was also done. Other analytical methods such as, Radial Basis Function (RBF) network, Multi Layer Perceptron (MLP) network and Constructive Probabilistic Neural Network (CPNN) were used for the classification of various aroma.[48-49]

Dutta *et al.* proposed a metal-oxide sensor (MOS) based electronic nose (EN) to analyze five tea samples possessing different qualities viz. over-fermented, overfired, under-fermented, etc using an array of four MOSs, each of which possess electrical resistance having partial sensitivity to the headspace of the tea and a suitable interface circuitry for the signal conditioning.[39] The data

obtained were processed by Principal Components Analysis (PCA) and Fuzzy C means algorithm (FCM) method.

Chen *et al.* proposed that a support vector machine algorithm is superior to KNN and ANN model for quality gradation of green tea by E-nose system comprised with MOS sensors. It can also be successfully used in the discrimination of green tea's quality.[53] This study was applied to classify four different grades of green tea. PCA and three different linear or nonlinear classification tools namely, K-nearest neighbors (KNN), support vector machine (SVM) and artificial neural network (ANN) were compared to develop the discrimination model.[53]

Yu *et al*. applied BPNN, PNN and cluster analysis (CA)for the electronic nose (E-nose) analysis which was employed for identification of the quality grades of the green tea.[54] It is evident from the results of CA that the classification of different green tea samples is possible by analysing the response signals obtained from E-nose. BP neural network gives better experimental results. The classification success rates for two neural networks BPNN (back propagation neural network) and PNN (probabilistic neural network) were reported to be 100% and 98.7% for the training sets and 88% and 85.3% for the testing sets respectively. The overall results of the experiment reported that both the neural networks are usable for the identification of different green tea samples.[55]

Tudu *et al.* proposed incremental learning fuzzy model which is a promising one to versatile pattern classification algorithm for the discrimination of black tea grade by using E-nose system.[55] It has been tested in some tea gardens of northeast India and the results obtained were encouraging.[56]

V.3. Present work: Result and Discussion

In our study, doped and un-doped ZnO nanorods based sensor have been developed and characterized. The fabricated sensor element was tested for its resistive response for evaluation of quality of two different types of tea infusion Orthodox. The performance of the sensor elements was characterized in different temperature of operation of the sensor element and different sensor characteristics were evaluated. Keeping in view of the small variation of the

resistivity with changing gas environment, the response was detected through an appropriate circuit in order to improve its sensitivity.

V.3.1. Steps for fabrication of ZnO based devices

Main steps followed to study zinc oxide based materials, both as nanorods and thin films are:

i. Synthesis of ZnO nano-rods using sol-gel spin coating methods.
ii. Coating electrodes by screen printing technique for Sensors.
iii. Fabrication of doped ZnO nanorod sensors for electronic nose.

V.3.2. Fabrication of ZnO Nanorods

Synthesis of ZnO nanorod Spin-coating is a simple method for preparing ZnO nanoparticles from Zinc acetate solution. In this process, we prepared 5mM solution of Zinc acetate dehydrate, $(CH_3COO)_2Zn$, $2H_2O$, (98% Merck) with methanol. The mixture was well mixed using an ultrasonic bath for 1 hour and then the resultant paste was dropped over a glass plate and the solution spun at 1000 rpm for 30s using a Programmable Spin Coater (Apex Technologies, Model SCU-2008C). Thus the nano layer of Zinc acetate solution is spread uniformly on a rotating substrate.[57] The coated substrates were heated to 350 °C in conventional oven for 30 min to yield layers of ZnO islands with their (100) plane parallel to the substrate surface.[57] After evaporation of solvent, a thin ZnO film was formed whose thickness can be controlled by repeating the above process. Concentration of the solution in the spin coater and spinning rate of the substrate also play important roles in adjusting the thickness of the formed seed layer. For preparing ZnO nanorods standard sol-gel protocol was used.[58] ZnO nanoseed were immersed in a solution with Zinc acetate and Hexamine in same proportion and kept at 90 °C for 2 hours for growth of nanorods. This forms an array of vertically aligned ZnO nanorods on the substrate surface. The coated substrate is rinsed and electrode with silver paste for further analysis.

ZnO thin films were prepared by the sol-gel spin coating method. As a starting material, zinc acetate dehydrate [$Zn(CH_3COO)_2$, H_2O] was used. 2-methoxyethanol and MEA were used as a solvent and stabilizer, respectively. The dopant sources of Fe, Co and Ni were Fe- Acetate, Co-Acetate and Ni-Acetate respectively. Zinc acetate dihydrate and a dopant were first dissolved in a mixture of 2-methoxyethanol and MEA solution at room temperature. The molar ratio of MEA to zinc acetate was maintained at 1.0 and the concentration of zinc acetate was 0.35 M. The

solution was stirred at 60 °C for 2 hours to yield a clear and homogeneous solution, which served as the coating solution after cooling to room temperature. The coating was usually made 2 days after the solution was prepared.

The solution was dropped onto glass substrates, which were rotated at 3000 rpm for 30 sec. After depositing by spin coating, the films were dried at 350 °C for 30 min over a conventional furnace to evaporate the solvent and remove organic residuals. The procedures from coating to drying were repeated six times until the thickness of the sintered films was approximately 200 nm.

The crystallinity of each ZnO film was measured using an X-ray diffractometer with CuKα radiation. The surface and cross-section of the films were observed with a scanning electron microscope (SEM). The electrical resistance was measured by a four-point probe method. Optical transmittance measurements were carried out using a UV–VIS spectrophotometer.

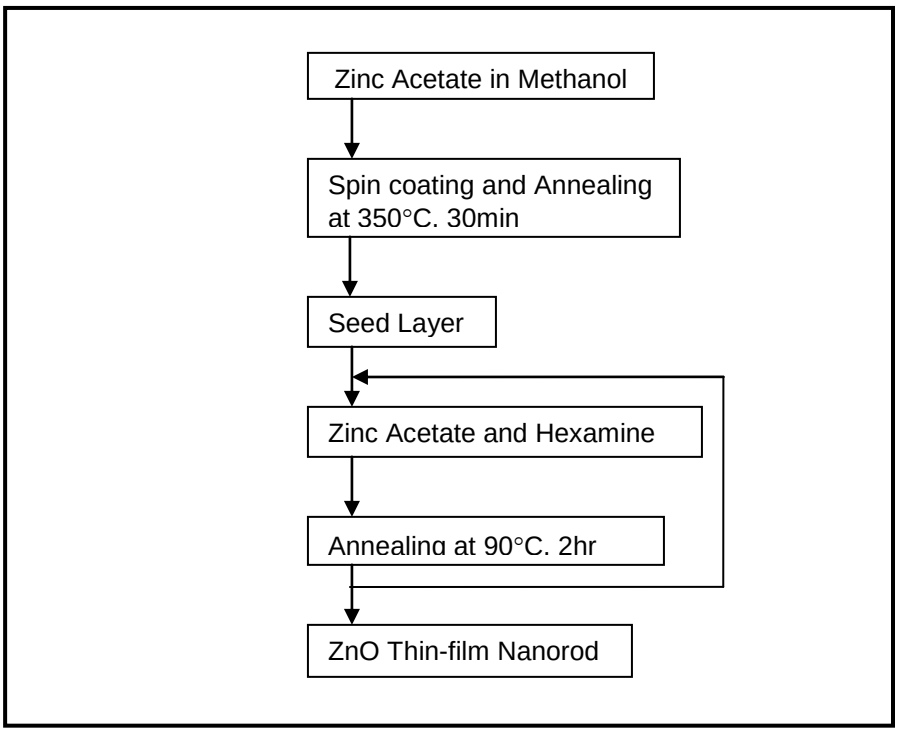

Figure V.1. Flow chart for preparation of ZnO nano layer.

A flow diagram of total synthesis process of ZnO nanolayer as presented in Figure V.1. The formation of phases were ascertained through study of X-ray diffraction pattern of the film calcined at various temperatures. Results showed pure ZnO phase formed at 350 °C and above.

For proper microstructure of sensor element, 350 °C was taken as optimum sintering temperature. The fabricate sensor material is characterized through SEM and the picture Figure V.4 shows clear ZnO nano rods aligned vertically perpendicular to substrate plane. Fabrication of device structure and measurement two interpenetrating comb like electrode structures were made with silver paste on the deposited film and was cured at 150 °C. Finally, two electrodes were soldered with copper wires for connecting with Whetstone Bridge circuit for measurement of off-balance voltage due to resistance change of the element.

For preparation of doped ZnO, Fe-Acetate, Co-Acetate and Ni-Acetate were added with Zinc acetate with appropriate proportion with further steps being identical to fabrication of the undoped one. The resulting nano-layer produced in this method over the substrate was electrode and connected to a digital multimeter for measureing the simultaneous resistance change in an atmosphere whose flavour (VOC composition) has to be determined.

V.3.3. Sensor Array and its Responses in Tea Infusion Vapour

For fabrication of E-nose, four such sensor measurement units, one of pure ZnO, one doped with iron, one doped with cobalt and one doped with nickel were incorporated at the same time in tea infusion vapour and the change of resistances of individual sensor were detected simultaneously. Four major grades of Orthodox black tea samples, Leaf, Broken, Fannings and Dust, were collected from fourteen Darjeeling tea gardens.

V.3.4. E-Nose measurements

This includes investigation on various sensors and sensor arrays useful for detection of smell and visual appearance of black tea liquor by electronic means using the system. Four similar systems pure ZnO, one doped with iron, one doped with cobalt and one doped with nickel were inserted in infusion vapour for simultaneous measurement. These E-Nose sensor responses of Volatile Organic Components (VOC) emitted from heated tea samples were analyzed through a Principle Component Analysis as presented in details in the results section.

V.3.5. Correlating sensor signals with Tea-tasters scores

The made tea samples were sent to selected professional tea tasters for organoleptic evaluation,

and scores (between 1 to 10) were obtained for strength, aroma, and colour of the liquors. The evaluation included estimation of following parameters: Colour with milk, Colour without milk, Colour of Infused Leaf, Strength, Flavour and Price/Kg. The calibration of sensing parameters and the scores of tea taster are outlined by the flowchart given as Figure V.2.

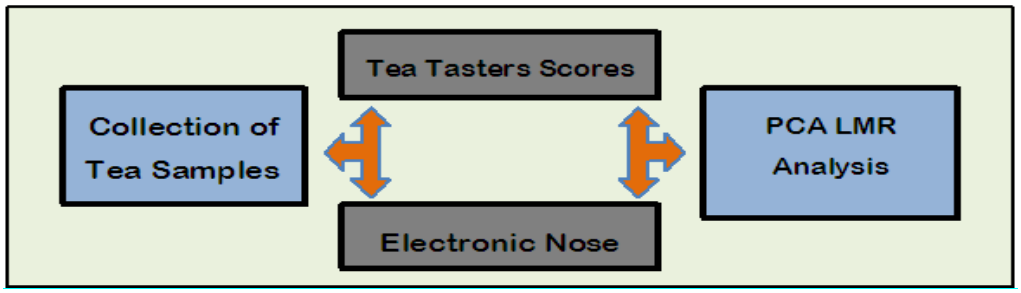

Figure V.2. Sketch of the Electronic Nose system used for the study.

V.3.6. Characterization of ZnO

V.3.6.1. X-ray Diffraction Analysis

The ZnO thin film crystal structure was investigated by X-ray diffraction analysis (Philips X'Pert Pro Alpha1 MPD diffractometer), utilizing Cu-Kα_1 radiation (λ=0.15406 nm). Figure V.3. shows the X-ray diffraction patterns of ZnO thin film. The EDAX analysis of selected area of SEM image was also studied for analysis of purity and identification of phases. Analysis shows a little impurity containing La ions. X-ray diffractrogram of ZnO films doped with iron, cobalt and nickel were also studied. However, no significant departure in the diffractogram from that of pure ZnO was noticed.

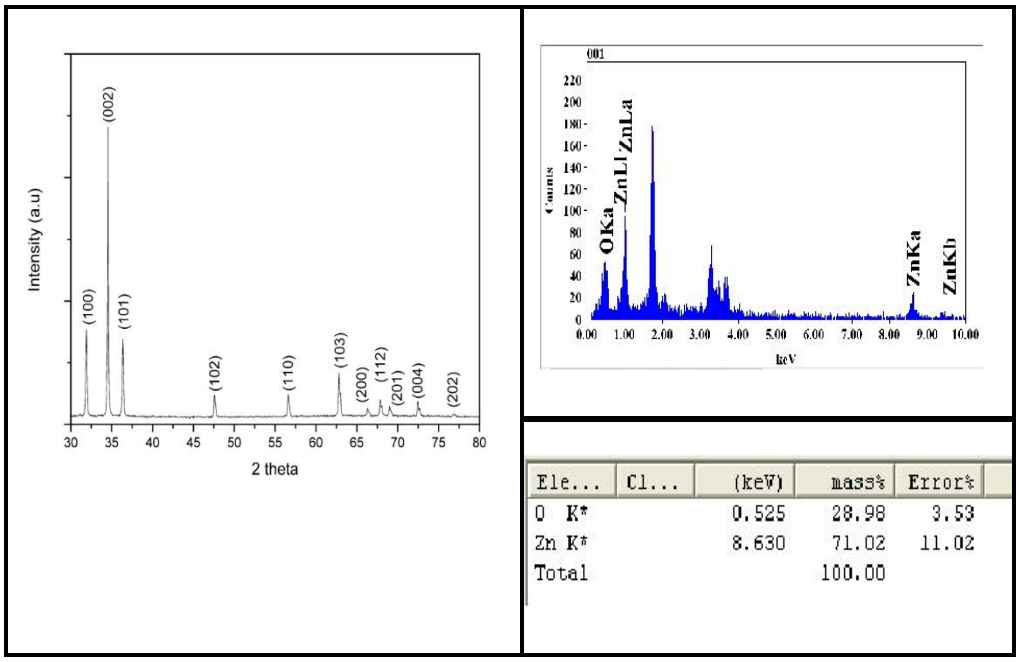

Figure V.3.(a) X-ray diffraction patterns of ZnO thin film and (b) EDX analysis of ZnO Sample

V.3.6.2. Effect of Dopant Concentration

The surface morphology of the films and its dependency on the type and concentration of the dopant are displayed in Figure V.4. A particular structure was observed in SEM images of doped and un-doped ZnO thin films on glass substrates for all films. The particle size of films doped with 1 at.% for all dopants was somewhat larger than that of the un-doped film. In the case of Co doping, the film doped with 1 at.% exhibited a porous structure and had grain sizes of 150 nm on the average. The microstructure of the films consisted of many round shaped particles. In addition, the films had a smooth surface morphology.

For the Fe doped films, the film have even larger grains. The grain size of the 1 at.% Fe doped film reduced a little, but the packing density of the film increased due to disappearing gaps between particles. The grains are more flaky in nature reducing the overall surface area.

For Co-doped films, particles with different shapes and sizes were mixed. Additionally, a microstructure with a larger difference in size between the large and small particles, similar to the case of Ni-doped film was observed. In the cases of films doped with Co and Ni with a smaller ionic radius than zinc, particles forming a matrix became smaller with increased doping

concentration because grain growth was disturbed by compression stresses due to the difference in ionic radii between zinc and Co or Ni. The change in particle size with an increase in doping concentration was observed more in the Co-doped films than in the Ni doped films. This is due to a higher difference in ionic radius between zinc and Co than that of the radii of zinc and Ni. However, since the ionic radius of Fe was larger than that of zinc, the change in particle size with an increased dopant concentration for Fe was less than that for the other dopants.

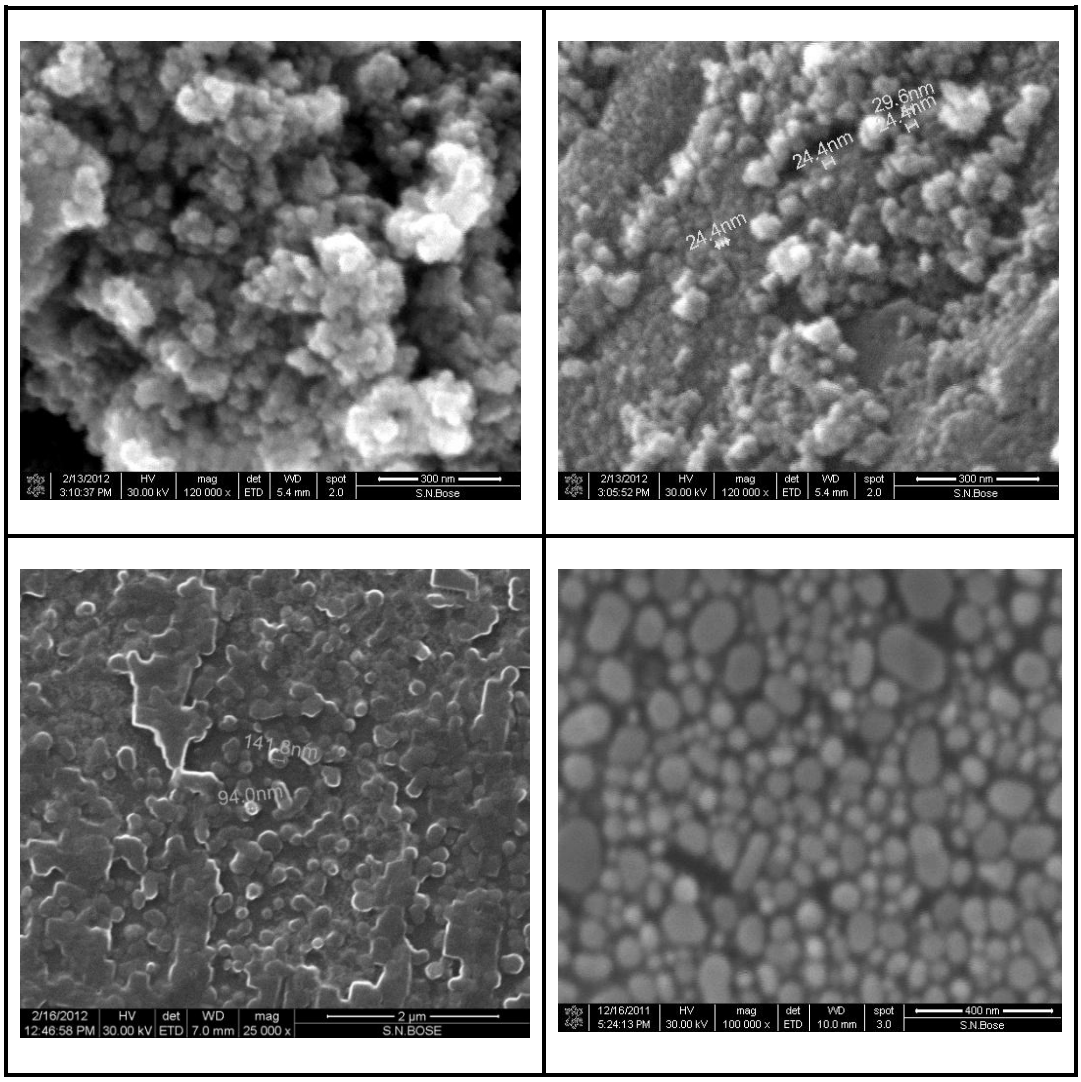

Figure V.4. SEM images of (a) un-doped and doped ZnO thin films with (b) Fe doped ZnO (c) Co doped ZnO and (d) Ni doped ZnO

The electrical resistivity of doped films was decreased by an increase in the carrier concentration. The lowest electrical resistivity values of the doped films were found out to be 1.1

x 10^{-1}, 4.8 x 10^{-1} and 5.6 x 10^{-1}Ωcm for Fe, Co and Ni, respectively. However, the increase in the electrical resistivity of doped films with increasing doping concentration may be due to a decrease in mobility of carriers caused by segregation of dopants at the grain boundary. Doped materials were acting as an electrical dopant at initial doping concentration but as an impurity at more doping concentrations having the lowest electrical resistivity values. Additionally, the electrical resistivity value of film was inversely proportional to a (0 0 2) preferred orientation of film. The resistance was measured using a Keithley 2400 multimeter configured in the two-wire mode. The main electrical characteristics: conductivity, carrier concentration, and mobility were derived from Hall measurements.[59]

Table V.1. Properties of doped and undoped sensing elements

	ZnO Film	**Fe doped ZnO**	**Co doped ZnO**	**Ni doped ZnO**
Average Grain Size (nm**)**	120	120	200	150
SurfaceResistivity(Ω-cm)	2.4 x 10^{-1}	1.1 x 10^{-1}	4.8 x 10^{-1}	5.6 x 10^{-1}
Electronmobility(cm^2/V s)	17.1	14.3	12.1	11.2
Conductivity(Ω cm)$^{-1}$	0.015	21.981	1.651	0.001
Electron concentration (cm^{-3})	5.8×10^{15}	9.1×10^{18}	8.6×10^{17}	9.73×10^{14}
Semiconductor Band Gap (from UV-Vizabs. spectra) (eV)	3.31	3.27	3.29	3.27

The UV-Vis absorprion spectra, carried out between wavelengths from 300 to 800 nm, of the un-doped and doped ZnO thin films. The band gap were measured through the general formula given by Davis and Mott[60] for optical band gap E_g is

$$\alpha h\nu = [\, B(h\nu - E_g)\,]r \qquad 5.1$$

where, r = index taking different values depending on the mechanism of the interband transition (usually 2 for ceramic system), B = constant called band tailing parameter and hν = incident photon energy.

Therefore for undoped and doped ZnO equation 5.1 becomes

$$\alpha h\nu = [\, B(h\nu - E_g)\,]^2$$

or,
$$(\alpha h\nu)^{1/2} = Bh\nu - BE_g$$

Variation of $(\alpha h\nu)^{1/2}$ with hν will be straight line with slope m = B and intercept c = BE_g

Therefore, $E_g = BE_g / B = c/m$ = intercept/ slope

The results of Hall measurements band gap studies were presented in Table V.1.

V.3.7. Measurement of sensor characteristics

The sensitivity of ZnO based nanosensor is defined as:

$$S = \frac{(R_g - R_a)}{R_a} = \frac{\Delta R}{R_a} \qquad 5.2$$

where R_a and R_g are the resistance of the sensing film in the atmosphere to be measured and the atmosphere that are referenced, respectively. In our case percentage change in output voltage can give an indication of sensitivity of the sensing system. Response time is the time taken by the sensing element to reach 90% of the final stable value of the response while the Signal-to-noise ratio was measured by the signal response divided by the mean fluctuation of results from its average value.

V.3.8. Doped ZnO Materials for Four Different Sensors

Tea is a non-alcoholic beverage consumed worldwide with an endlessly extending market. Like other food items, it also needs to be passed through the food safety and quality criteria.[61] Professional tea tasters have been traditionally assessing the physical quality attributes of tea by visual and nose approximations, which suffer from inconsistency and variability. So, there is a need for more accurate quality evaluation system.[62] Bio-chemical methods are available for assessment of tea quality applying modern analytical tools like high-performance liquid chromatography, gas chromatography, etc which are more accurate than human assessments, but these are time-consuming, and the results are often inconsistent with sensory evaluation. An application of electronic nose and vision coupled with multivariate data analysis in the analysis of foodstuffs has been increasing in last few years. The electronic testing devices are comprised of three principal components, sensor array, the equipment receiving signals and pattern recognition. In place of a single sensor, an array of sensors is solving the purpose more efficiently.

This is done by using array of sensors with partially overlapping selectivity and treating the data obtained by multivariate methods. E-noses have been used for identification of tea grade, prediction of tea quality, and monitoring of black tea fermentation process.[63] E-nose devices have also been successfully applied to different fields particularly in food and beverage industries, such as tomato, and coffee.[64] Computer vision systems are also gaining significant popularity in food industry because of their cost effectiveness, consistency, superior speed and accuracy. Also, the methods used so far for estimation of tea quality parameters have their own merits and demerits as they have been developed independently.[62] In the present study, an attempt has been made to integrate the three types of tea quality measurement techniques viz., taster's scoring, biochemical analysis and electronic sensor based studies, to find a correlation between them. This would be used to standardize the electronic sensor based study of Darjeeling Orthodox black tea quality, to contribute to the process of simplification as well as enhancing accuracy in determination of tea quality.

V.3.9. E-nose Application of Doped ZnO Sensors for Tea Quality Estimation

The E-nose was developed in order to mimic human olfaction that functions as a non-separative mechanism: i.e. an odor / flavor is perceived as a global fingerprint. Essentially the instrument consists of headspace sampling, sensor array, and pattern recognition modules, to generate signal pattern that are used for characterizing odors.

Electronic noses include three major parts: a sample delivery system, a detection system, a computing system.The sample delivery system enables the generation of the headspace (volatile compounds) of a sample, which is the fraction analyzed. The system then injects this headspace into the detection system of the electronic nose. The sample delivery system is essential to guarantee constant operating conditions.

The detection system, which consists of a sensor set, is the "reactive" part of the instrument. When in contact with volatile compounds, the sensors react, which means they experience a change of electrical properties.

In most electronic noses, each sensor is sensitive to all volatile molecules but each in their specific way. However, in bio-electronic noses, receptor proteins which respond to specific odor molecules are used. Most electronic noses use sensor arrays that react to volatile compounds on contact: the adsorption of volatile compounds on the sensor surface causes a physical change of the sensor. A specific response is recorded by the electronic interface transforming the signal into a digital value. Recorded data are then computed based on statistical models.[65]

In our case, there are four sensors and there are various Volatile Organic Components arising in tea infusion has to be detected. The contribution to individual gas component can be isolated through Principal Component Analysis (PCA).

V.3.10. Principal Component Analysis

PCA reduces the data dimension to some principal components and enables the extraction of the differences between samples and the main variables. The data of 51 samples were analyzed by PCA. PCA is a linear method that has been proved to be effective for discriminating the response of gas sensor array to simple and complex odours. Considering the differences of sensitivities of

gas sensors, all data have been normalized before analyzed by PCA. Figure V.5 shows PCA results of training data set projected onto their first two principle components.

Table V.2. Covariant Matrix formed from responses of four different sensor and its Eigen values

(a) The Covariant Matrix

0.0025	0.0013	0.0087	0.0141
0.0013	0.0011	0.0035	0.0056
0.0087	0.0035	0.0455	0.0669
0.0141	0.0056	0.0669	0.1170

(b) Eigen values of Covariant Matrix

Eigen value-1	**Eigen value-2**	**Eigen value-3**	**Eigen value-4**
0.1592	0.0054	0.0014	0.0002

Four eigen values of covariance matrix are listed in Table V.2b. It was found that the first eigen value appears to be the largest and other eigen values are smaller by an order of 10^2.

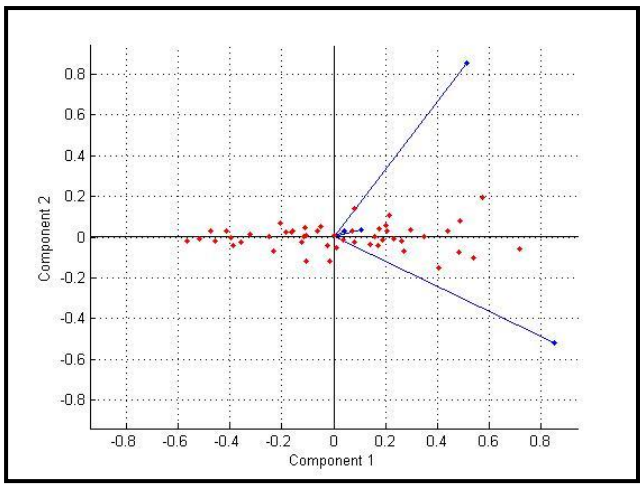

Figure V.5. PCA results of training data obtained from sensor array.

Therefore, the response data were greatly aligned along first principal component. In other words, the aroma in Darjeeling Orthodox tea liquor arises mostly from a single component. This is also evident from the PCA result shown in Figure V.5. Where all data were mostly aligned in the direction of first principle component.

V.3.11. Development of E-Nose response function

Response of individual sensors will have either positive correlation or negative correlation with individual flavour component i.e. some sensors have positive response with a particular flavour component, whereas, some exhibits negative response.

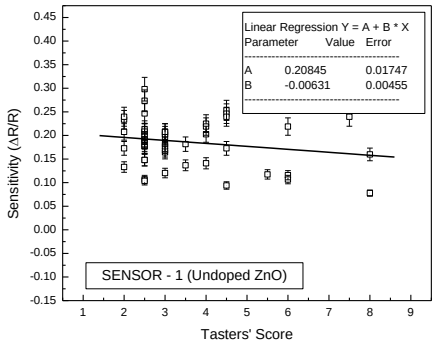

(a) Response of Sensor-1 (Undoped ZnO)

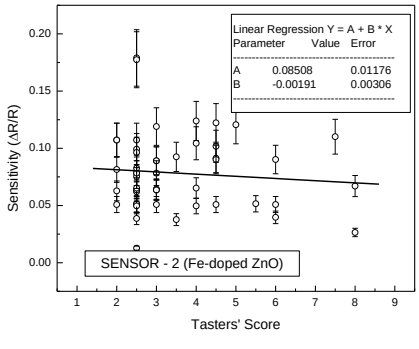

(b) Response of Sensor-2 (Fe-doped ZnO)

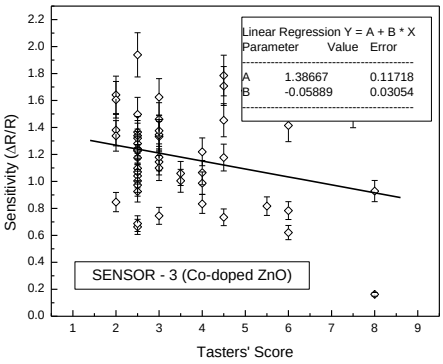

(c) Response of Sensor-3 (Co-doped ZnO)

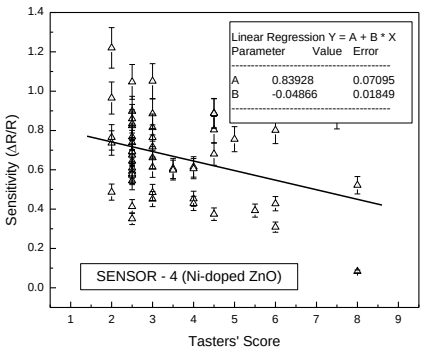

(d) Response of Sensor-4 (Ni-doped ZnO)

Figure V.6. Calculation of individual response gradient of four different sensor elements

Also, the contribution of individual response due to flavour component will be proportional to the sum for a particular sensor's response.[66] So, a function is constructed for the total sensor response (S) which is a linear sum of individual response multiplied by the individual gradient value of each sensor response.

$$S = \sum_{i=1}^{4} R_i \times \left| M_{Si} \right| \qquad 5.3$$

where, M_{Si} (i = 1 to 4) is the individual response of each attributes factor, and R_i is the weight coefficient corresponding to each attribute. The gradients of individual responses are taken as the weight coefficient of that sensor element.

The response from each sensor is plotted with tasters flavour score and the gradient is noted and presented in Table V.3.

Table V.3. Gradient of each sensor calculated from individual response.

Sensors	**Un-doped**	**Fe-doped**	**Co-doped**	**Ni-doped**

Response (R_i)	R_1	R_2	R_3	R_4
Gradient (M_{Si})	-0.00631	-0.00191	-0.04866	-0.05889

The resulting function is plotted with the Taster's scores obtained for orthodox tea. Figure V.7 shows the calibration of the sensors using a new function built appropriately from individual sensor responses as presented in Equation 5.2 where the weight coefficient of four individual sensing elements was built through multiple regression equation of four sensor data versus the tasters flavour score.

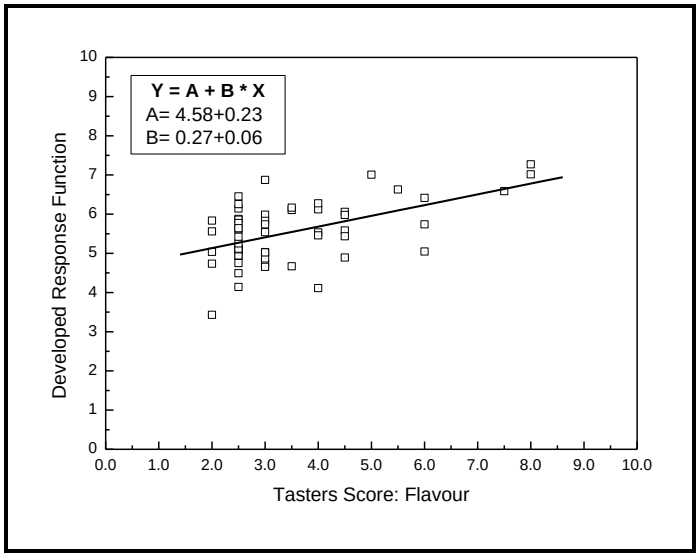

Figure V.7. Calibration of the sensors using a function built from individual sensor responses for Orthodox black tea.

When this newly developed function is plotted with the tasters' flavor score, a very good linear relationship is observed with very small scattered data exhibiting a significantly high value of the gradient as presented in Figure V.7.

V.4. Conclusion

In our study we have prepared various transition metal doped ZnO nanosensing material which have been successfully used to sense the flavor of Orthodox Darjeeling tea collected from various garden by electronic nose system. The application of E-nose system to determine tea quality is a new direction of research to develop better sensing material. Doping is a very good process which can modify the response signal of E-nose system to a better one. Research in this ground will significantly increase the quality of the sensor system which will obviously help to better differentiate the quality of various teas, foods etc.Our research in this ground to develop further sensing material is underprocess.

V.5. Reference

References are given in BIBLIOGRAPHY under chapter V page no. 97-100.

BIBLIOGRAPHY

CHAPTER I

1. W. Gopel, *Prog. Surf. Sci.*, 9–103, *20*, 1985.
2. B. Ruhland, T. Becker, G. Muller, *Sensor and Actuators B*, 85, *50*, 1998.
3. S. R. Morrison, *Sensor and Actuators B*, 425, *12*, 1987.
4. S. R. Morrison, *Surf. Sci.*, 20, *45*, 1974.
5. T. G. Nenov, S. P. Yordanov, *"Ceramic Sensors: Technology and Applications", Technomic Pub. Lancaster*, 1996.
6. N. Barsan, M. Schweizer-Berberich, W. Gopel, *J. Anal. Chem.*, 287, *365*, 1999.
7. S. Samson, C. G. Fonstad, *J. Appl. Phys.*, 4618, *44*, 1973.
8. Z. M. Jarzebski, J. P. Marton, *J. Electrochem. Soc.*, 299C, *123*, 1976.
9. J. Maier, W. Gopel, *J. Solid State Chem.*, 293, *72*, 1988.
10. W. Gopel, K. D. Schierbaum, *Sensor and Actuators B*, 26–27, *1*, 1995.
11. N. Yamazoe, G. Sakai, K. Shimanoe, *Catal. Surv. Asia*, 63, *7*, 2003.
12. M. J. Madou, S. R. Morrison, *Chemical Sensing with Solid State Devices, Academic Press, New York*, 1989.
13. S. Lenaerts, M. Honore, G. Huyberechts, J. Roggen, G. Maes, *Sensor and Actuators B*, 478, *18*, 1994.
14. M. I. Baraton, L. Merhari, H. Ferkerl, J. F. Castagnet, *Mater. Sci. Eng. C*, 315, *19*, 2002.
15. N. Barsan, U. Weimar, *J. Electroceram.*, 143, *7*, 2001.
16. J. Watson, *Sensor review*, 20–23, *14(1)*, 1993.
17. N. Barsan, U. Weimer, *Journal of physics:condensed matter*, *15(20)*, 2003.
18. T. Becker, G. Muller, *Sensor and Actuators B: Chemical*, 55–61, *77(1)*, 2001.
19. K. S. Chou, T. K. Lee, F. J. Liu, *Sensor and Actuators B: Chemical*, 106–111, *56*, 1999.
20. S. Zhang, K. P. Sandow, F. Adolf, W Gopel, *Sensor and Actuators B: Chemical*, 25–29, *70(1–3)*, 2000.
21. A. D. Brailford, E. M. Logothetics, W. Gopel, *Sensor and Actuators B: Chemical*, 39–67, *7*, 1985.
22. G. Bläser, *Physics A*, 218–223, *266*, 1999.
23. K. J. Williams, R. D. Esman, *Journal of lightwave technology*, 1443–1454, *17*, 1999.

24. A. Zangwill, *Physics at Surfaces, Cambridge university press*, 1988.
25. Wagner and Schottky, *Journal of Physical Chemistry*, 163, *B11*, 1930.
26. K. D. Schierbaum, U. Weimar, W. Gopel, R. Kowalkowski, *Sensor and Actuators B*, 205, *3*, 1991.
27. G. Sakai, N. Matsunaga, K. Shimanoe, N. Yamazoe, *Sensor and Actuators B*, 125, *80*, 2001.
28. N. Matsunaga, G. Sakai, K. Shimanoe, N. Yamazoe, *Sensor and Actuators B*, 226, *96*, 2003.
29. S. Abbet, U. Heiz, *The Chemistry of Nanomaterials, (Eds.: C. N. R. Rao, A. Muller, A. K. Cheetham), Wiley-VCH, Weinheim*, 551, *2*, 2004.
30. Q. Wang, A. E. Ostafin, *"Metal Nanoparticles in Catalysis" in Encyclopedia of Nanoscience and Nanotechnology, (Ed.: H. S. Nalwa), American Scientific*, 475, *5*, 2004.
31. S. R. Morrison, *Sensor and Actuators B*, 425, *12*, 1987.
32. D. Kohl, *Sensor and Actuators B*, 158, *1*, 1990.
33. N. Yamazoe, *Sensor and Actuators B*, 7, *5*, 1991.
34. T. C. Pearce, S. S. Schiffman, H. T. Nagle, J. W. Gardner, *Handbook of Machine Olfaction, Wiley-VCH, Weinheim*, 2003.
35. K. J. Albert, N. S. Lewis, *Chem. Rev.*, 2595, *100*, 2000.
36. G. An, Y. Zhang, Z. Liu, Z. Miao, *Nanotechnology*, 035504, *19(3)*, 2008.
37. B. K. Miremadi, R. C. Sing, Z. Chen, S. R. Morrison, K. Colbow, *Sensors and Actuators B: Chemical*, 21, *1*, 1994.
38. Y. Li, W. Wlodarski, K. Galatsis, S. H. Moslih, *Sensors and Actuators B: Chemical*, 160–163, *83(1)*, 2002.
39. G. Neri, *Recent Patents on Materials Science*, 146–158, *4(2)*, 2011.
40. J. Wöllenstein, M. Burgmair, G. Plescher, T. Sulima, *Sensors and Actuators B: Chemical*, 442–443, *93(1*), 2003.
41. C. Cantalini, A. Martucci, *Sensors and Actuators B: Chemical*, 184–192, *108(1–2*), 2005.
42. M. Frietsch, F. Zudock, J. Goschinick, M. Bruns, *Sensors and Actuators B: Chemical*, 379–381, *65(1*), 2000.
43. A. Cruccolini, R. Narducci, R. Palombari, *Sensors and Actuators B: Chemical*, 227–232, *98(2*), 2004.

44. V. R. Katti, A. K. Debnath, K. Muthi, M. Kaur, *Sensors and Actuators B: Chemical*, 245–252, *96(1–2)*, 2003.
45. H. Tang, M. Yan, H. Zhang, S. Li, *Sensors and Actuators B:Chemical*, 910–915, *114(2)*, 2006.
46. J. Zhang, X. Liu, G. Neri, N. Pinna, *Advanced Material*, 795–831, *28(5)*, 2006.
47. M. Ferroni, D. Boscarino, E. Comini, D. Ganini, V. Guidi, G. Martinelli, P. Nelli, *Sensors and Actuators B: Chemical*, 289–294, *58(1–3)*, 1999.
48. T. Hyodo, J. Ohoka, Y. Shimizu, M. Egashira, *Sensors and Actuators B: Chemical*, 359–366, *117(2)*, 2006.
49. J. A. Dirksen, K. Duval, T. A. Ring, *Sensors and Actuators B: Chemical*, 106–115, *80*, 2001.
50. I. Hotovy, J. Huran, P. Siciliano, S. Capone, L. Spiess, V. Rehacek, *Sensors and Actuators B: Chemical*, 300–311, *103*, 2002.
51. C. Peter, J. Kneer, J. Wollenstein, *Sensor Letters*, 807–811, *9(2*), 2011.
52. H. Long, W. Zeng, H. Zhang, *Journal of Materials in Science Materials in Electronics*, *26(7)*, 2015.
53. L. G. Teoh, Y. M. Hon, J. Shieh, W. H. Lai, *Sensors and Actuators B: Chemical*, 219–225, *96(1–2)*, 2003.
54. C. N. Xu, N. Yamazoe, *Sensors and Actuators B: Chemical*, 163–165, *65(1–3*), 2000.
55. I. Raible, M. Burghard, u. Schlect, A. Yasuda, T. Vossmeyer, *Sensor and Actuator B: Chemical*, 730–735, *106*, 2005.
56. B. Adhikari, S. Majumdar, *Progress in polymer Science*, 699–766, *29(7)*, 2004.
57. J. Kaur, M. C. Bhatnagar, *Sensors and Actuators B: Chemical*, 1090–1095, *123(2*), 2007.
58. C. Jacq, T. Maeder, P. Ryser, *Sadhana, Indian Academy of Science*, 677–687, *34(4)*, 2009.
59. A. Ibrahim, A. Homoudi, J. S. Thakur, R. Naik, G. W. Auner, G. Newaz, Applied Surface Science, 8607–8614, *253*, 2007.
60. J. R. Curtis, *"Design of thick film hybrid amplifiers for wide band high power R.F. Amplifier", ISHM proceedings,* pp. 307, 1983.
61. P. L. Kirby, I. D. Pagan, *Microelectronics International*, 5–7, *4(3*), 1993.

62. E. Mosca, R. Gardella, E. Simonin, E. Varani, *"Surface mounting applications a Comparison between technology", Proc. 5th European Hybrid Microelectronics Conference*, pp. 224, 1985.
63. G. P. Ferraris, A. Tessalvi, *"Fine line photo-processing of thick film resistors for Precision microwave hybrid thin film circuits", Proc. 5th European Hybrid Microelectronics Conference*, pp. 22, 1985.
64. D. P. Amalnekar, M. S. Shetty, S. K. Dake, P. B. Sinha, *Indian Journal of Pure and Applied Physics*, 662–666, *22*, 1984.
65. M. Satyam, *"Overview of hybrid microelectronics", Short term course on thick and thin films hybrid microelectronics IISc, Bangalore*, pp. 1–3, 1986.
66. J. K. Atkinson, S. S. Shahi, M. Varney, N. Hill, *Sensors and Actuators B*, 175–181, *4*, 1991.
67. T. K. Gupta, *Handbook of Thick and Thin-Film Hybrid Microelectronics, New Jersey: John Wiley & Sons*, 2003
68. N. M. White, *"Thick film technology" in Thick Film Sensors, M. Prudenziati, Editor, Elsevier Science B.V., Amsterdam*, 3–33, 1994.
69. M. L. Tofer, *"Thick film microelectronics fabrication, design and applications", Van Nostrand, Reinhold Co. (New York)*, pp. 41, 1971.
70. K. Aguir, C. Lemire, D. B. B. Lollman, *Sensors and Actuators B: Chemical*, 1–5, *84*, 2002.
71. G. Korotcenkov, I. Blinov, M. Ivanov, J. R. Stetter, *Sensors and Actuators B: Chemical*, 679–686, *120*, 2007.
72. M. Akçay, *Journal of molecular structure*, 21–26, *649(1–3)*, 2004.
73. D. E. Tevault, R. E. Pellenbarg, *Science of the total environment*, 65–69, *73(1–2)*, 1988.
74. W. S. Lee, S. C. Lee, S. J. Lee, D. D. Lee, *Sensors and Actuators B: Chemical*, 148–153, *108(1)*, 2009.
75. B. S. Y. Liu, J. J. Belbruno, M. A. Crane, S. E. Tanski, *Nicotine and Tobacco Research*, 1511–1518, *15(9)*, 2013.
76. C. Di Natale, R. Paolesse, E. Martinelli, R. Capuano, *Analytica Chimica Acta*, 1–17, *824C*, 2014.
77. C. Di Natale, A. Di Amico, *Biosensors and Bioelectronics*, 1209–1218, *18(10)*, 2003.

CHAPTER II

1. B. M. White, E. Traversa, *J. Electrochem. Soc.*, J11, *155*, 2008.
2. C. Cantalini, M. Pelino, *Sensors and Actuators B: Chem.*, 112, *35–36*, 1996.
3. J. Tamaki, Z. Zhang, *J. Electrochem. Soc.*, 2207, *141*, 1994.
4. L. Chen, S. C. Tsang, *Sensors and Actuators B: Chem.*, 68, *89*, 2003.
5. B. M. White, F. M. Van Assche, E. Traversa, E. D. Wachsman, *ECS Trans.*, 109, *1*, 2006.
6. T. Morita, M. Miyayama, J. Motegi, H. Yanagida, *Chemical Sensors*, 1993; M. A. Butler, A. J. Ricco, N. Yamazoe, *The Electrochemical Society Proceedings Series*, Pennington, p. 450, *Vol. 93–7*, 1993.
7. M. Penza, C. Martucci, G. Cassano, *Sensors and Actuators B: Chem.*, 52, *50*, 1998.
8. B. White, S. Chatterjee, E. Macam, E.Wachsman, *J. Am. Ceram. Soc.*, 2024, *91*, 2008.
9. E. Macam, B. Blackburn, E. D. Wachsman, *Sensors and Actuators B: Chem.*, 304, *158*, 2011.
10. E. Macam, B. Blackburn, E. D. Wachsman, *Sensors and Actuators B: Chem.*, 353, *157*, 2011.
11. E. R. Macam, B. M. White, B. M. Blackburn, E. D. Bartolomeo, E. Traversa, E. D. Wachsman, *Sensors and Actuators B: Chem.*, 957, *160*, 2011.
12. R. Srivastava, P. Lal, R. Dwivedi, S. Srivastava, *Sensors and Actuators B: Chem.*, 213, *21*, 1994.
13. E. Llobet, R. Ionescu, S. Al-Khalifa, J. Brezmes, X. Vilanova, X. Correig, N. Barsan, J. W. Gardner, *IEEE Sensors Journal*, 207, *1(3)*, 2001.
14. J. Lim, D. Kang, D. Lee, J. Huh, D. Lee, *Sensors and Actuators B: Chem.*, 139, *77*, 2000.
15. S. Roy, S. R. Morrison, *Sensors and Actuators B: Chem.*, 425-440, *12*, 1987.
16. C. Hagleitner, A. Hierlemann, D. Lange, A. Kummer, N. Kerness, O. Brand, H. Baltes, *Nature*, 293-296, *414*, 2001.
17. E. Llobet, R. Ionescu, S. Al-Khalifa, J. Brezmes, X. Vilanova, X. Correig, N. Barsan, J. W. Gardner, *IEEE Sensors Journal*, 207-213, *1(3)*, 2001.
18. S. Roy, W. Sigmund, F. Aldinger, *J. Mater. Res.*, 1524, *14*, 1999.
19. I. Kim, A. Rothschild, H. L. Tuller, *Acta Mater.*, 974, *61*, 2013.
20. M. J. Madou, S. R. Morrison, *Academic Press*, p. 556, 1989.

21. W. Gopel, *Prog. Surf. Sci.*, 9, *20*, 1985.

22. S. M. Kanan, O. M. E. Kadri, I. A. Abu-Yousef, M. C. Kanan, *Sensors*, 8158, *9*, 2009.

CHAPTER III

1. W. Briggs, S. Chatterjee, E. Macam, E. D. Wachsman, *J. Am. Ceram. Soc*., 2024–2031, *91*, 2008**.**
2. M. Williams, R. Minjares, The International Council on Clean Transportation, Washington, June, 2016.
3. D. Jones, Pearson Education (US), United States, 1996.
4. N. Miura, G. Lu, N. Yamazoe, *Solid State Ionics*, 136–137, *533*, 2000.
5. N. Miura, G. Lu, N. Yamazoe, H. Kurosawa, M. Hasei, *Journal of the Electrochemical Society*, L33–L35, *143*, 1996**.**
6. N. F. Szabo, P. K. Dutta, *Solid State Ionics*, 183–190, *171*, 2004.
7. F. Garzon, R. Mukundan, E. Brosha, *Solid State Ionics*, 136–137, *633*, 2000.
8. G. Lu, N. Miura, N. Yamazoe, *Sensors and Actuators B: Chem.*, 35–36, *130*, 1996.
9. N. Miura, G. Lu, N. Yamazoe, *Sensors and Actuators B: Chem.*, 169–178, *52*, 1998.
10. N. Miura, S. Zhuiykov, T. Ono, M. Hasei, N. Yamazoe, *Sensors and Actuators B: Chem.*, 222–229, *83*, 2002.
11. J. Park, B. Yoon, C. Park, W.J. Lee, C. Lee, *Sensors and Actuators B: Chem.*, 516–523, *135*, 2009.
12. V. Plashnitsa, T. Ueda, P. Elumalai, N. Miura, *Sensors and Actuators B: Chem.*, 231–239, *130*, 2008.
13. E. Wachsman, P. Jaiyaweera, *Solid State Ionic Devices II Ceramic Sensors, The Electrochemical Proceedings Series* Vol. PV 2000-32, pp. 298–304, 2000.
14. E. Macam , E. D. Wachsman, *Sensors and Actuators B: Chem.*, 957–963, *160*, 2011**.**
15. E. Di Bartolomeo, M. L. Grilli, E. Traversa, *J. Electrochem. Soc*., H133, *151*, 2004.
16. E. Di Bartolomeo, N. Kaabbuathong, A. D'. Epifanio, M. L. Grilli, E. Traversa, H. Aono, Y. Sadaoka, *Journal of the European Ceramic Society.*, 1187–1190, *24*, 2004.
17. M. L. Grilli, E. Di Bartolomeo, E. Traversa, *J. Electrochem. Soc*., H98, *148*, 2001.
18. A. Ghosh, P. K. Mandal, S. Chatterjee, *Sensor Lett*., 137, *15*, 2017.
19. J. Park, B. Y. Yoon, C. O. Park, W. J. Lee, C. B. Lee, *Sensors and Actuators B: Chem.*, 516, *135*, 2009.
20. N. Miura, G. Lu, N. Yamazoe, H. Kurosawa, M. Hasei, *J. Electrochem. Soc.*, L33, *143*, 1996.

21. N. Miura, H. Kurosawa, M. Hasei, G. Lu, and N. Yamazoe, *Solid State Ionics.*, 1069, *86–88*, 1996.

22. N. F. Szabo, P. K. Dutta, *Solid State Ionics*, 171, *183–190*, 2004.

23. E. L. Brosha, R. Mukundan, R. Lujan, F. H. Garzon, *Sensors and Actuators B: Chem.*, 398–408, *119*, 2006.

24. E. Macam, B. M. Blackburn, E. D. Wachsman, *Sensors and Actuators B: Chem.*, 353–360, *157*, 2011.

25. P. Elumalai, J. Wang, S. Zhuiykov, D. Terada, M. Hasei, N. Miura, *J. Electrochem Soc.*, H95–H101, *152*, 2005.

26. H. T. Giang, H. T. Duy, P. Q. Ngan, G. H. Thai, D. T. A. Thu, D. T. Thu, N. N. Toan, *Sensors and Actuators B: Chem.*, 550–555, *183*, 2013.

27. G. Lu, N. Miura, N. Yamazoe, *J. Mater Chem.*, 1445–1449, *7*,1997.

28. L. P. Martin, A. Q. Pham, R. S. Glass, *Sensors and Actuators B: Chem.*, 53–60, *96*, 2003.

29. E. Di Bartolomeo, N. Kaabbuathong, A. D'Epifanio, M. L. Grilli, E. Traversa, H. Aono, Y. Sadaoka, *Journal of the European Ceramic* Society, 1187–1190, *24*, 2004.

30. P. Elumalai, J. Wang, S. Zhuiykov, D. Terada, M. Hasei, N. Miura, *J. Electrochem. Soc.*, H95–H101, *152*, 2005.

31. P. Elumalai, N. Miura, *Solid State Ionics*, 2517–2522, *176*, 2005.

32. E. Macam, E. D. Wachsman, *Sensors and Actuators B: Chem.*, 353–360, *157*, 2011.

33. M. Breedon, S. Zhuiykov, N. Miura, *Materials Letters*, 5153–5155, *82*, 2012.

34. M. Ando, S. Suto, T. Suzuki, T. Tsuchida, C. Nakayama, N. Miura, N. Yamazoe, *J. Matter. Chem.*, 631–633, *4*, 1994.

35. G. Kuczynski, *Sintering and Catalysis: 10, Springer US*, 1975.

36. G. Sakai, N. Matsunaga, K. Shimanoe, N. Yamazoe, *Sensors and Actuators B: Chem.*, 125–131, *80*, 2001.

37. J. Karger, D. M. Ruthven, D. N.Theodorou, *Diffusion in Nanoporous Materials: Wiley*, 2012

38. Y. Sun, H. Sai, K. A. Spoth, K. A. Tan, U. W. Zwanziger, J. Zwanziger, S. M. Gruner, L. F. Kourkoutis, U. Wiesner, *Nano Lett.*, 651–655, *16*, 2016.
39. R. Schlögl, A. Trunschke, *Lecture Series at Fritz-Haber-Institute Berlin*, 2011.
40. Sing, K.: Adsorption methods for the characterisation of porous materials. Adv. Colloid Interf. Sci. 76–77, 3–11 (1998).
41. E. W. Thiele, *Ind. Eng. Chem*., 916–920, *31*, 1939.
42. C. N. Satterfield, *Mass Transfer in Heterogeneous Catalyst: MIT Press, Cambridge*, 1970.
43. G. Newcombe, M. Drikas, R. Hayes, *Water Research*, 1065–1073, *31*, 1997.
44. S. Brunaur, R. P. H. Emmett, *J. Am. Chem. Soc*., 309–319, 60, 1998.
45. C. Liang, *J. Phys. Chem.*, 84–87, *57*, 1953.
46. S. Roy, W. Sigmund, F. Aldinger, *J. Mater. Res.*, 1524–1531, *14*, 1999.

CHAPTER IV

1. H. Windishmann, P. Mark, *J. Electrochem. Soc.*, 1979, *126*, 627–633.
2. A. Hartmann, M. K. Puchert, R.N. Lamb, *Surface and Interface Analysis*, 1996, *24*, 671–674.
3. K. M. A. Rahman, S. C. Schneider, M. A. Seitz, *J. Am. Ceram. Soc*, 1997, *80*, 1198–1202.
4. A. Ghosh, P. K. Mandal, S. Chatterjee, *Sensor Lett.*, 2017, *15*, 137–141.
5. D. Zappa, A. Bertuna, E. Comini, M. Molinari, N. Poli, G. Sberveglier, *Anal. Methods*, 2015, *7*, 2203–2209.
6. B. White, S. Chatterjee, E. Macam, E. D. Wachsman, *J. Am. Ceram. Soc.*, 2008, *91*, 2024–2031.
7. M. Williams, R. Minjares, *A technical summary of Euro 6/VI vehicle emission standards, The international council on clean transportation*, June 2016.
8. E. D. Bartolomeo, M. L. Grilli, E. Traversa, *J. Electrochem. Soc.*, 2004, *151*, H133–H139.
9. E. D. Bartolomeo, N. Kaabbuathong, A. D'Epifanio, M. L. Grilli, E. Traversa, H. Aono, Y. Sadaoka, *Journal of the European Ceramic Society*, 2004, *24*, 1187–1190.
10. L. Zhao, F. H. Tian, X. Wang, W. Zhao, A. Fu, Y. Shen, S. Chen, S. Yu, *Comput. Mater. Sci.*, 2013, *79*, 691–697.
11. F. Tian, L. Zhao, X. Y. Xue, Y. Shen, X. Jia, S. Chen, Z. Wang, *Appl. Surf. Sci.*, 2014, *311*, 362–368.
12. V. Nagarajan, R. Chandiramouli, *Superlattices Microstruct.*, 2015, *78*, 22–39.
13. F. Wang, C. Di Valentin, G. Pacchioni, *Phys. Rev.*, 2011, *B.84*, 073103.
14. C. Di Valentin, F. Wang, G. Pacchioni, *Topics Catal.*, 2013, *56*, 1404–1419.
15. J . W. Schwank, M. Dibattista, *MRS Bull.*, June 1999, 44.
16. T. Takeuchi, *Sensors and Actuators*, 1998, *14*, 109.
17. K. Nishio, in "*The Fundamentals of Automotive Engine Control Sensors*" (Fontis Media, The Netherlands, 2001).
18. D. E. Williams, *ibid. B*, 1999, *57***,** 1.
19. U. Lampe, M. Fleischer, N. Reitmeier, H. Meixner, in "*Sensors Update*," edited by H. Baltes, W. Gopel, J. Hesse (VCH, New York, 1996).

20. Y. Xu, X. Zhou, O. T. Sorensen, *Sensors and Actuators B*, 2000, *65***,** 2.
21. J . Gerblinger, W. Lohwasser, U. Lampe, H. Meixner, *ibid. B*, 1995, *93*, 26–27.
22. A. Kohli, C. C. Wang, S . A. Akbar, *ibid. B*, 1999, *56*, 121.
23. N. -H. Chan, R. K. Sharma, D. M. Smyth, *J. Electrochem. Soc.*, August 1981, 1762.
24. G. Sberveglieri, *Sensors and Actuators B*, 1995, *23***,** 103.
25. P . T. Moseley, A. J . Crocker, *Sensor Materials* (IOP Publishing, Bristol, 1996).
26. A. M. Azad, S . A. Akbar, S . G. Mhaisalkar, L. D. Birkefeld, K. S . Goto, *J. Electrochem. Soc.*, 1992, *139***,** 3690.
27. A. Takami, *Ceram. Bull.*, 1988, *67*, 1956.
28. D. M. Smyth, "*The Defect Chemistry of Metal Oxides*" (Oxford University Press, New York, 2000).
29. P. K. Clifford, D. T. Tuma, *Sensors and Actuators: B, Chem.*, 1982, *3*, 233–254.
30. J. F. McAleer, P. T. Moseley, J. O. W. Norris, D. E. Williams, B. C. Tofield, *J. Chem. Soc. Faraday Tran.*, 1988, *83*, 1323.
31. B. M. Smith, G. S. V. Coles, G. Williams, *European Patent Application*, EP 0 806 657 A2.
32. N. Murakami, K. Tanaka, K. Sasaki, K. Ihokura, *Anal. Chem. Symp. Ser.*, 1983, *Vol 17 (Chem. Sens)*, p 165.
33. M. Gillet, C. Lemire, E. Gillet, K. Aguir, *Surface Science*, 2003, 532–535.
34. H. Jin, H. Zhou, Y. Zhang, *Sensors*., 2017, *17*, 1898.
35. S. Majidi, A. Achour, D. P. Rai, P. Nayebi, S. Solaymani, N. B. Nezafat, S. M. Elahi, *Results in physics*, 2017, *7*, 3209–3215.
36. M. G. Hutchins, N. A. Kamel, N. Elkadry, A. A. Ramadam, K. Abdel-Hady, *Phys. Stat. Sol. A*, 1999, *175*, 991.
37. J. P. Bonnet, J. F. Marucco, M. Onillon, P. Hagenmuller, *J. Solid State Chem.*, 1981, *40*, 270.
38. S. C. Moulzolf, S. Ding, R. J. Lad, *Sensor and Actuator. B: Chem.*, 2001, *77*, 375.
39. J. Novotny, S. Sloma, Surface and Near Surface Chemistry of Oxide Materials edited by J. Novotny, L. C. Dufour, *Elsevier Science Publishers, United Kingdom*, 1988.

CHAPTER V

1. R. P. Feynman, *Caltech's Engineering and Science Magazine, Reinhold Publishing Corporation*, 1960.
2. R. W. Siegel, G. E. Fougere, *Nanostruct. Mater.*, 1995, *6*, 205–216.
3. J. W. Freeman, L. D. Wright, C. T. Laurencin, S. Bhattacharyya, K. E. Gonsalves, C. R. Halberstadt, C. T. Laurencin, L. S. Nair, *Biomedical Nanostructures*, 2008, 3–24.
4. B. D. Fahlman, *Materials Chemistry*, 2007, ISBN 978-1-4020-6119-6.
5. I. Raiblea, M. Burghardb, U. Schlechtb, A. Yasudaa, T. Vossmeyera, *Sensors and Actuators B*, 2005, *106*, 730–735.
6. A. H. Go´mez, J. Wang, H. Guixian, A. G. Pereira, *Journal of Food Engineering*, 2008, *85*, 625–631.
7. J. Brezmes, E. Llobet, X. Vilanova, J. Orts, G. Saiz, X. Correig, *Sensors and Actuators B*, 2001, *80*, 41–50.
8. C. D. Natale, A. Macagnano, R. Paolesse, A. Mantini, E. Tarizzo, A. D'Amico, F. Sinesio, *Sensors and Actuators B*, 1998, *50*, 246–252.
9. C. D. Natale, A. Macagnano, E. Martinelli, R. Paolesse, E. Proietti, A. D'Amico, *Sensors and Actuators B*, 2001, *70*, 18–26.
10. N. Magan, P. Evans, *Journal of Stored Products Research*, 2000, *36*, 319–340.
11. J. Brezmes, E. Llobet, X. Vilanova, G. Saiz, X. Correig, *Sensors and Actuators B*, 2000, *69*, 223–229.
12. S. Saevels, J. Lammertyn, A. Z. Berna, E. A. Veraverbeke, C. D. Natale, B. M. Nicolai, *Postharvest Biology and Technology*, 2003, *30*, 3–14.
13. H. Young, K. Rossiter, M. Wang, M. Miller, *Journal of Agriculture and Food Chemistry*, 1999, 47, 5173–5177.
14. G. M. Ghimbeu, J. Schoonman, M. Lumbreras, M. Siadat, *Appl. Surf. Sci.*, 2007, *253*, 7483.
15. N. Hidehito, M. Tadatsugu, T. Shinzo, *J. Appl. Phys.*, 1986, *60*, 482.
16. G. S. R. Trivikrama, D. R. Tarakarama, *Sens. Actuators. B*, 1999, *55*, 166.

17. X. L. Cheng, H. Zhao, L. Huo, S. Gao, J. Zhao, *Sens. Actuators. B*, 2004, *102*, 248.

18. D. Paul Joseph, C. Venkateswaran, *Molecular, and Optical Physics*, 2011, 1–7.

19. C. Lia, S. Zhanga, M. Hub, C. Xiea, *Sensors and Actuators B: Chemical*, 2011, *153*, 415–420.

20. M. Ohyama, H. Kozuka, T. Yoko, *J. Am. Ceram. Soc.*, 1998, *81(6)*, 1622.

21. C. Lee, K. Lim, J. Song, *Sol. Energy Mater. Sol. Cells*, 1996, *43*, 37.

22. Y. Yamamoto, K. Saito, K. Takakashi, M. Konagai, *Sol. Energy Mater. Sol. Cells*, 2001, *65*, 125.

23. A. Sanchez-Juarez, A. Tiburcio-Silver, A. Oritz, E. P. Zironi, J. Rickards, *Thin Solid Films*, 1998, *333*, 196–202.

24. M. Abou-Helal, J. W. T. Seeber, *Journal of Non-Crystalline Solids*, 1997, *218*, 139.

25. Y. Natsume, H. Sakata, *Mater. Chem. Phys.*, 2002, *78*, 170–176.

26. B. Sernelius, F. K. Berggren, J. C. Jin, I. Hamberg, C. G. Granqvist, *Phys. Rev.*, 1998, *37*, 10244.

27. J. H. Lee, K. H. Ko, J. B. O. Park, *Cryst. Growth*, 2003, *247*, 119.

28. F. Paraguay, J. Morales, W. Estrada, E. Andrade, M. Miki-Yoshida, *Thin Solid Films*, 2000, *366*, 16.

29. M. Ohyama, H. Kozuka, T. Yoko, S. Saka, *J. Ceram. Soc. Jpn.*, 1996, *104(4)*, 296.

30. P. Nunes, E. Fortunato, P. Tonello, F. B. Fernandes, P. Vilarinho, R. Martins, *Vacuum*, 2002, *64*, 281.

31. O. V. Krylov, *Catalysis by Nonmetals: Rules for Catalyst Selection;Physical Chemistry, a Series of Monographs*, 1970, *Vol. 17*, Academic Press, New York.

32. D. P. Joseph, C. Venkateswaran, *Molecular and Optical Physics*, 2011, 1–7.

33. E. Shim, H. Kang, J. Kang, J. Kim, S. Lee, *Appl.Surf. Sci.*, 2002, *186*, 474.

34. Y. Kashiwaba, F. Katahira, K. Haga, T. Sekiguchi, H. Watanabe, *Cryst. Growth*, 2002, *221*, 431.

35. P. Nunes, D. Costa, E. Fortunato, R. Martins, *Vacuum*, 2002, *64*, 293.

36. M. Kamalasanan, S. Chandra, *Thin Solid Films*, 1996, *288*, 112.

37. F. Paraguay, W. Estrada, D. Acosta, E. Andrade, M. Miki-Yoshida, *Thin Solid Films*, 1996, *350*, 192.

38. N. Bhattacharyya, R. Bandyopadhyay, M. Bhuyan, B. Tudu, D. Ghosh, A. Jana, *IEEE Trans. Instrum. Meas.*, 2008, *57*, 1313–1321.

39. R. Dutta, E. L. Hines, J. W. Gardner, K. R. Kashwan, M. Bhuyan, *Sens. Actuators B*, 2003, *94*, 228–237.

40. V. Kumar, S. Sen, M. Muthe, N. Gaur, S. Gupta, J. Yakhmi, *Sens. Actuat. B*, 2009, *138*, 587–590.

41. A. Barker, S. Crowther, D. Rees, *Sens. Actuators A*, 1997, *58*, 229–235.

42. M. H. Koch, P. Timbrell, R. N. Lamb, *Semicond. Sci. Technol.*, 1995, *10*, 1523–1527.

43. K. Keis, E. Magnusson, H. Lindström, S. Lindquist, A. Hagfeldt, *Sol Energy Mater Sol Cells*, 2002, *73*, 51–58.

44. H. Tang, M. Yan, X. Ma, H. Zhang, M. Wang, D. Yang, *Sens. Actuators B*, 2006, *113*, 324–328.

45. W. Shen, Y. Zhao, C. Zhang, *Thin Solid Films*, 2005, *483*, 382–328.

46. Q. Zhang, C. Xie, S. Zhang, A. Wang, B. Zhua, L. Wang, Z. Yang, *Sensors Actuat. B*, 2005, *110*, 370–376.

47. B. Tudu, B. Kow, N. Bhattacharyya, R. Bandyopadhyay, Int. *J. Smart Sensing and Intelligent System*s, 2009, *2*, 176–189.

48. K. Arshak, E. Moore, G. M. Lyons, J. Harris, S. Clifford, *Sensor Revi*ew, 2004, *24*, 181–198.

49. T. C. Pearce, S. S. Schiffman, H. T. Nagle, J. W. Gardner, *Handbook of Machine Olfaction, Wiley-VCH, Weinheim*, 2003.

50. G. Harsanyi, *Sensor Review*, 2000, *20*, 98–105.

51. Rahman S, Usmani T and Saeed SH (2013)Review Of Electronic Nose And Applications. International Journal of Computational and Corporate research Vol. 3, Issue 2 , 2013

52. S. Borah, E. L. Hines, M. S. Leeson, D. D. Iliescu, M. Bhuyan, J. W. Gardner, *Sens. & Instrumen. Food Qual.*, 2008, *2*, 7–14.

53. Q. Chen, J. Zhao, Z. Chen, L. Hao, Z. De-An, *Sensors and Actuators B: Chemical*, 2011, *159*, 294–300.

54. Y. Huichun, J. Wang, C. Yao, H. Zhang, Y. Yu, *LWT*, 2008, *41*, 1268–1273.

55. B. Tudu, A. Jana, A. Metla, D. Ghosh, N. Bhattacharyya, R. Bandyopadhyay, *Sensors and Actuators B*, 2009, *138*, 90–95.

56. S. Borah, E. L. Hines, M. S. Leeson, D. D. Iliescu, M. Bhuyan, J. W. Gardner, *Sens. & Instrumen. Food Qual.*, 2008, *2*, 7–14.

57. J. Nishino, S. Ohshio, K. Kamata, *J. Am. Ceram. Soc*., 1992, *75 (12*), 3469.

58. I. Petrov, V. Orlinov, A. Misiuk, *Thin Solid Films*, 1984, *120*, 55.

59. S. J. Peartona, D. P. Nortona, K. Ipa, Y. W. Heoa, T. Steiner, *Progress in Materials Science*, 2005, *50*, 293–340.

60. N. F. Mott, E. A. Davis, *Electronic Processes in Non-Crystalline Materials, Second edition, Oxford University Press, New York*, 1997.

61. K. I. Tomlins, A. Mashingaidze, *Food Chemistry*, 1997, *60(4)*, 573–580.

62. G. S. Gill, A. Kumar, R. Agarwal, *Journal of Food Engineering*, 2011, *106*, 13–19.

63. N. Bhattacharyya, S. Seth, B. Tudu, *Sensors and Actuators: B*, 2007, *122*, 627–634.

64. W. He, X. Hu, L. Zhao, X. Liao, Y. Zhang, M. Zhang, J. Wu, *Food Research International*, 2009, *42*, 1462–1467.

65. A. Berna, *Sensors*, 2010, *10*, 3882–3910.

66. H. C. Yu, J. Wang, H. M. Zhang, Y. Yu, C. Yao C, *Sensors and Actuators: B*, 2008, *128 (2)*, 455–461.

Index

A

Activation energy 8,10, 56-57, 59

Adsorption site 2, 48

C

Calcination 19

Chemisorption 11

D

Dopant 2, 7, 65, 76-77

Debye length 6, 7, 26

Density of states 60, 62

Depletion region 4

Defect band 59

Differential electrode equilibria 38

E

E-nose 64-65, 67-69, 73, 79-80, 82, 85

F

Fermi energy 39, 60, 62

G

Grain 3, 7, 9, 40, 60

K

Knudsen diffusion 43

L

Langmuir's isotherm equation 45

M

Microstructure 7, 14, 38-39, 75

Metal oxide sensor 1, 26, 69

Molecular diffusion 43

N

Nanomaterial 1, 64

O

Oxygen vacancies 5, 50, 52, 58, 59

P

Potential barrier 3, 5, 6, 12, 15-16

Porosity 40

Physisorption 11

S

Sensitivity 2, 9-10, 13-15, 17-18, 24, 26, 38-40, 43, 48, 51, 64

Scanning electron microscope 27, 47, 52, 66, 72-74

Selectivity 12, 18, 26, 40, 51

Schottky barrier 6, 9, 10

Stoichiometric 13, 34, 51

Space charge layer 5, 6

Surface diffusion 43

S/N ratio 29

Sensor array 26

T

Transition metal oxide 16, 62, 65

Tranducer 1, 2

Toxic gases 12

V

Volatile organic compound 20, 22, 64-65, 67, 73

Vander Waals interaction 43

X

X-ray diffraction 28, 47, 53, 66, 72, 74-75

Y

YSZ substrate 35, 36, 38, 52

REPRINT OF PAPERS

Role of defects in electron band structure and gas sensor response of La_2CuO_4

Chinmay Roy, Aparna Ghosh and Suman Chatterjee
Department of Physics, University of North Bengal, Darjeeling, India

Abstract

Purpose – This paper aims to estimate the relationship between defect structure with gas concentration for use as a gas sensor. The change in defect concentration caused a shift in the Fermi level, which in turn changed the surface potential, which is manifested as the potentiometric response of the sensing element.

Design/methodology/approach – A new theoretical concept based on defect chemistry and band structure was used to explain the experimental gas response of a sensor. The theoretically simulated response was compared with experimental results.

Findings – Understanding the origin of potentiometric response, through the generation of defects and a corresponding shift in Fermi level of sensing surface, by the adsorption of gas. Through this understanding, the design of a sensor with improved selectivity and stability to a gas can be achieved by the study of defect structure and subsequent band analysis.

Research limitations/implications – This paper provides information about various types of surface defects and numerical simulation of material with defect structure. The Fermi energy of the simulated value is correlated with the potentiometric sensor response.

Practical implications – Gas sensors are an integral part of vehicular and industrial pollution control. The theory developed shows the origin of response which can help in identifying the best sensing material and its optimum temperature of operation.

Social implications – Low-cost, reliable and highly sensitive gas sensors are highly demanded which is fulfilled by potentiometric sensors.

Originality/value – The operating principle of potentiometric sensors is analyzed through electron band structure analysis. With the change in measured gas concentration, the oxygen partial pressure changes. This results in a change in defect concentration in the sensing surface. Band structure analysis shows that change in defect concentration is associated with a shift in Fermi level. This is the origin of the potentiometric response.

Keywords Defects behavior, Oxygen vacancy, Partial pressure, Points defects, Semiconductor sensor, Sensor response

Paper type Research paper

Introduction

Defects in oxide semiconductors

Defects in metal oxide semiconductors have been studied for many years for controlling their behavior through various forms of defects techniques, including novel techniques such as co-implantation, millisecond annealing, photo-stimulation and surface engineering (Noh, 2010). At the beginning of this century, the first invention of semiconductor gas sensors was made from two pioneer research groups led by Seiyaman and Taguchi in 1962 (Taguchi, 1962; Sugiyama *et al.*, 1962). These types of metal oxide semiconductors are used in many industrial and commercial purposes, involving monitoring and controlling the environment, chemical gas detectors, medical field, etc. The release of various chemical pollutants from industries, automobiles and homes into the atmosphere has been causing global environmental issues such as acid rain, the global greenhouse effect and ozone depletion (Michaels, 1999; Close *et al.*, 1980). Hazardous and toxic gases from auto and industrial exhausts are polluting the environment. To measure and control these gases, one should know the amount and nature of gases present in the environment. Thus, the need to monitor and control these gases has led to research and development of a wide variety of sensors. This was done by using different materials and technologies that increase the efficiency, capability, cost reduction, shape, size, weight, etc. (Graham Solomons and Fryhle, 2004; Tinashue *et al.*, 1996). Many researchers have given attention to the importance of the metal oxide semiconductor gas sensor in the past decades. Researchers have invested their knowledge in the new generations of sensors, such as semiconducting bulks (Kocemba *et al.*, 2001), thick films (Singh *et al.*, 2014; Choi and Oh, 2013; Hübner *et al.*, 2012; Liu *et al.*, 2011; Bârsan *et al.*, 2011; Oprea *et al.*, 2009), thin films (Malagù *et al.*, 2005; Ansari *et al.*, 1997; Zhao *et al.*, 2016; Marikkannan *et al.*, 2015; Lim *et al.*, 2014; Zeng *et al.*, 2012; Brunet *et al.*, 2012; Korotcenkov *et al.*, 2009) and nanostructure composites (Lee *et al.*, 2008; Korotcenkov *et al.*, 2001; Brown *et al.*, 2000; Zhao *et al.*, 2010; Gong *et al.*, 2011; Zhai *et al.*, 2016), which were made of different materials. The most common metal oxide semiconductor is La_2CuO_4 used in gas sensors; this is a perovskite metal oxide. It has some flexibility that allows for

The current issue and full text archive of this journal is available on Emerald Insight at: **https://www.emerald.com/insight/0260-2288.htm**

Sensor Review
 [ISSN 0260-2288]
[DOI 10.1108/SR-12-2019-0319]

The authors gratefully acknowledge the financial assistance of the University Grants Commission, India through the Major Research Project and University of North Bengal for carrying out the research work.

Received 18 December 2019
Revised 14 September 2020
Accepted 30 September 2020

controlling of the transport and catalytic properties, which are important for improving sensing performance (Miller *et al.*, 2014). The sensor mechanism for different types of sensor works is based on its conductivity. Ionic conductors are often used as high-temperature sensors in the auto-ignition. Pure ionic conductors are used in potentiometric, mixed-potential or amperometric sensors (Fergus, 2007; Yamazoe and Miura, 1998). But mixed conductors are used in semiconductor-based sensors (Miura *et al.*, 2000; Azad *et al.*, 1992; Lee, 2006). The response of oxide semiconductor gas sensors is dependent on oxygen partial pressure and points defects.

Kroger–Vink notations are typically used to depict the atomic defects with charges. Some general notations are used in defects given in the following Table 1. Here in the case of stoichiometric (La_2CuO_4) metal oxide, the dominant defects are La^{3+}, Cu^{2+}, O^{2-}, V_{La}'', V_{Cu}'' and $V_O^{\cdot\cdot}$. In sensor response, the point defects O^{2-}, $V_O^{\cdot\cdot}$ and O play the main role.

Effect of defect in resistivity

As mentioned earlier, defects concentration depends on the partial pressure of the target gas and it was known that the electrical resistance of a sensor R is related to the partial pressure of the target gas by the following equation (Moseley, 1992):

$$R = aP^{n};\ \text{or}\quad \log R = a' + n\log P \tag{1}$$

Where a, a' and n are constants. This sensor resistance and the corresponding sensor response are well correlated with the oxygen vacancy by the following equations (Rao *et al.*, 2014):

$$R = R_0 \exp\left(q^2 w^2 N_v/\varepsilon kT\right) \tag{2}$$

$$S = \exp\left(\alpha q^2 w^2 N_v/\varepsilon kT\right) \tag{3}$$

Where R_0 is the resistance under flat-band condition; q, ϵ and K are the elemental charge of the electron, the permittivity of La_2CuO_4 and the Boltzmann constant, respectively; T is the operating temperature; W is the width of the depletion layer; α denotes the percentage of electrons released back to the depletion layer during gas detection; and N_v is the oxygen vacancies in the semiconductor. These three equations indicate that the resistance and responses are greatly influenced by the partial pressure of the target gas as well as the oxygen vacancies that originate within the metal oxide semiconductor substance. It was also determined that the sensitivity, known as the power-law exponent for gas sensors. Power laws have been used to show the variation of sensor resistance as well as conductivity with the concentration of oxygen partial pressure (Moseley, 1992). To understand the sensor response during gas detection of metal oxide, semiconductor gas sensors can be summarized shortly as follows. Every sensor possesses three parts, which are, namely, the receptor function, the transducer function and the utility factor (Rao *et al.*, 2014). The core sensing body of the semiconductor gas sensor contained millions of tiny semiconducting grains. The receptor function describes how a single grain responds to oxygen in the aerial atmosphere and stimulant gases (Yamazoe and Shimano, 2009; Yamazoe *et al.*, 2012; Yamazoe and Shimano, 2011). It has been reported that the sintered semiconductor grains of La_2CuO_4 are stoichiometric, which contained inherent oxygen vacancies within the systems (Yamazoe and Shimano, 2009). The defects on the surface of the grain provide adsorption sites for aerial oxygen. The types of adsorbed oxygen are found to be O, O_2 and O^{2-}, which are dependent on the operating temperature. The adsorbed oxygen can seize quasi-free electrons near the surface of grains and produce a depletion layer (Fonstad and Rediker, 1971; Morrison, 1987) as shown in Figure 5. This results in a change of resistance and Fermi energy of the sensing element.

Table 1 Kroger–Vink notations for different point defects

Category of defect	Kroger–Vink notation
Charge oxygen vacancy	$V_o^{\cdot}$ or $V_o^{\cdot\cdot}$
Charge metal vacancy	V_M' or V_M''
Charge metal or oxygen vacancies	$V_i^{\cdot\cdot}$ and O_i''
Electron and holes	e' and $h^{\cdot}$
Normal cation or anion with zero effective charges in and oxide	M_M^X or O_O^X

Note: Dot (˙) represents the positive charge and prime (′) represent the negative charge

Resistivity and sensor response

When underexposed to air, oxygen is adsorbed on the grain as anionic species O^-, inducing an electron depletion layer to increase the surface potential and work function. The transducer function indicates how the response of each grain is transuded into device resistivity. As the grains are connected through grain boundaries, because of the effect of migration of electrons, a potential barrier called the double Schottky barrier is set up across the grain boundary (Figure 1).

The height of the Schottky barrier plays an important role in determining the resistance of the sensing substrate which therefore changes in the gas detection. When a reducing gas interacts with the surface of the sensor element, the oxygen adsorbates are consumed, leading to mitigation in a potential barrier and also the resistivity (Yamazoe *et al.*, 1979). Thus, resistivity decreases with increasing partial pressure (P_{O2}). On the other side, interaction with oxidizing gas such as CO_2 and NO_2 in air, oxygen is adsorbed competitively as anionic ions on the same grains. If the adsorption of the target gas is stronger than that of oxygen, the surface potential barrier will increase upon exposure to the target gas, increasing the resistivity. The gas diffusion theory (Mitsufuji, 1975; Yamazoe and Shimano, 2011; Sakai *et al.*, 2001) was proposed to formulate the utility factor of semiconducting thin film gas sensors, which are the best-understood parts of a gas sensor (Matsunaga *et al.*, 2002; Gong *et al.*, 2009).

Figure 1 Barrier formation in the grain boundary

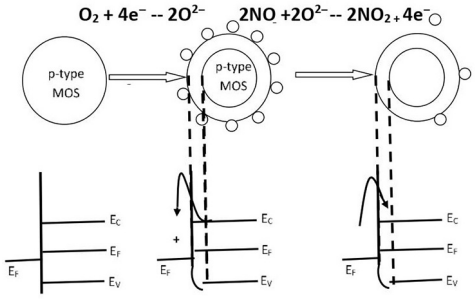

More attention has been given in this paper about the effects and behaviors of oxygen vacancies within the semiconducting metal oxide sensing substance. The defects concentration differently depends on the partial pressure oxygen for stoichiometric and non-stoichiometric metal oxides. In the stoichiometric sensor, the oxygen vacancy was found to be the predominant defect which is independent of oxygen partial pressure. At low oxygen partial pressure, the oxygen vacancy formation enthalpy decreases and produces heat (Liu *et al.*, 2009). Oxygen vacancies at the surface of the sensor initiated to oxygen adsorption and the gas sensor response were significantly increased by defects (Lambert-Mauriat *et al.*, 2012). A special chemical environment is created by the oxygen vacancy around the surface of the grain that improved the gas adsorption and enhanced the charged transfer from the grain surface to the adsorbates (Wu *et al.*, 2014). This causes an increase in the sensor response.

Experimental

Fabrication of sensor element

Tape cast YSZ substrates of dimension (20 × 10 × 0.15 mm) were used for sensor fabrication. Pt paste was screen-printed on one side of the substrate and the ceramic electrode on the other. Thin platinum wires were connected to both the electrodes using Pt paste for ohmic contact. For the fabrication of the sensing electrode material, La_2CuO_4 perovskite oxides, prepared in the laboratory, were mixed with appropriate amounts of solvents and ball-milled for 10 h. The slurry thus obtained was screen-printed on one face of the substrate. Finally, after the drying of the printed electrode slurry, the sensor was sintered at an appropriate temperature.

Simple La_2CuO_4 compounds were prepared through the auto-ignition technique (Zeng *et al.*, 2012), where nitrate salts of constituent elements were taken and citric acid is added in appropriate proportion and subsequently heated with thorough mixing to form a gel, which was burnt to ashes. The nature of burning depends on the citrate–nitrate ratio and is the key parameter in determining the powder morphology.

Characterization of sensing element through X-ray diffraction and scanning electron microscopy

X-ray diffraction (XRD) patterns of powders prepared shows the minimum temperature of complete phase formation by calcination at 600°C for 10 h, as presented in Figure 2.

Table 2 shows the characteristics of powders synthesized through different routes. Brunauer–Emmett–Teller (BET) surface area analysis shows the highest surface area for the powders prepared through the auto-ignition technique and is shown in Table 2. Average particle size distribution, as determined from stereological analysis of scanning electron microscopy (SEM) micrographs of calcined powders, also confirms very small particle size for the powders prepared through the auto-ignition technique.

The microstructure of the sensing material La_2CuO_4 largely depends on the powder preparation technique and firing temperatures. SEM micrographs sensor surfaces for samples prepared through the auto-ignition technique and fired at a sintering temperature of 800°C are presented in Figure 3. Powders prepared through the auto-ignition process show the finer microstructure with an average particle size of 0.1–0.3 μm. with a flaky microstructure.

Figure 2 Unit cell structure adopted for Density functional calculations for La_2CuO_4 (a) without and (b) with one La vacancy

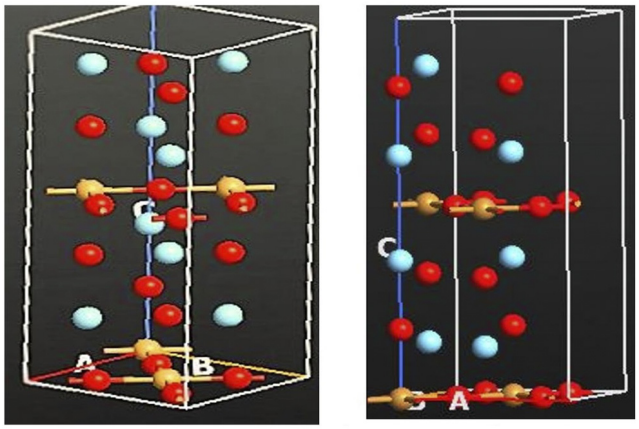

(a) (b)

Notes: (a) Bulk structure of La_2CuO_4 without vacancy; (b) La_2CuO_4 with one la vacancy

Table 2 Characteristics of prepared powders

Powder preparation route	Calculations temperature	Average grain size (from SEM)	Morphology (appearance)	BET surface area
Auto-ignition	600°C/10 h	0.2 μm	Flakey	16.7

The appropriate calcination temperature was determined through phase identification of the perovskite oxides by the XRD analysis. XRD patterns showed only the peaks of orthorhombic perovskite-type La_2CuO_4 phases, for powders calcined in air at 600°C for auto-ignited powders and 650°C for 10 h for co-precipitated and Pechini powders. The BET surface area was studied to find the surface area of the powder synthesized. Microstructures of the electrodes were observed by SEM.

La_2CuO_4 perovskite powder was prepared and systematically evaluated for NO reduction activity in a typical combustion environment, simulated by adding oxygen (3%), CO_2 (16%) and NO_2 (100 ppm) in nitrogen as the carrier gas. Sensing experiments were carried out in a computer-controlled gas-flow system with a controlled heating facility. The sensors were exposed to step change of 50, 100, 200, 400 and 650 ppm of the NO gas to be sensed, in a simulated combustion environment, at the total flow rate of 300 ml/min, in the temperature range between 400 and 700°C. Electromotive force (EMF) measurements were performed between the two electrodes of the sensors using a digital voltmeter. During the EMF measurements, the electrode with the oxide coating was always kept at the positive terminal of the electrometer and both the electrodes were exposed to the same gas environment.

Results and discussion

Defect structure of La_2CuO_4

The approach is to formulate the defect structure of La_2CuO_4 and calculate the activation energy for the individual defect

Figure 3 Change of resistance with oxygen partial pressure at a fixed temperature

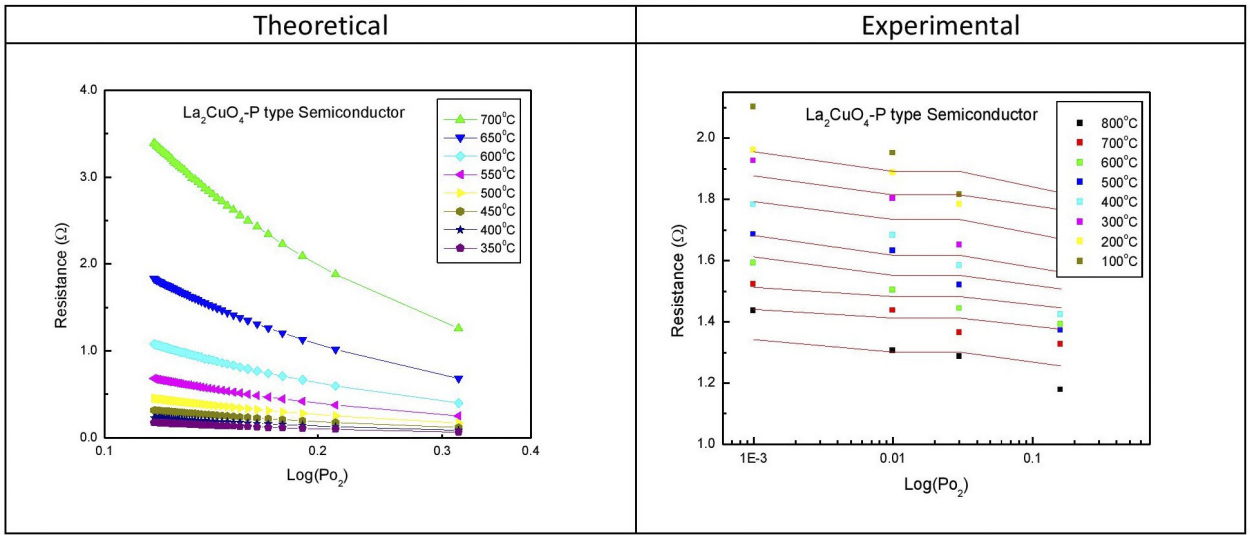

equation and derive the theoretical change in conductivity. This result is correlated with the experimental conductivity data.

Defect chemistry and electrical properties of La_2CuO_4

The oxidation reaction dominates at low temperatures and the reduction reaction dominates at a higher temperature.

Oxidation reaction

The thermodynamic stability of various point defects can be realized by the defects equilibrium chemical reactions for the formation of these defects. To analysis, the defects chemistry, the mass action laws and charge neutrality condition play an important role. Several defects occurred in La_2CuO_4, namely, O_i, O_i^{2-} and $V_O^{\cdot\cdot}$. Another most importance defect is known as an electronic defect in the electron-hole formation (Table 3). The low values of hole formation energies are approximately 2 eV for oxidative non-stoichiometry in La_2CuO_4. Here, for samplings, the following three oxidation reactions (Allan and Mackrodt, 1988) are considered as important:

$$La_{La}{}^{x} + 3/4O_2(g) = V_{La}{}''' + 3h + La_{La}{}^{\cdots} + 3/2O_o{}'' \quad (4)$$

$$Cu_{Cu}{}^{x} + 1/2O_2(g) = V_{Cu}{}'' + 2h + Cu_{Cu}{}^{\cdot\cdot} + O_O{}'' \quad (5)$$

$$V_O{}^{x} + 1/2O_2(g) = O_O{}'' + 2h \quad (6)$$

With the associated defect formation energy, E_a, E_b and E_c (Allan and Mackrodt, 1988) are considered in the orthorhombic structure (Table 4).

Reduction reaction

The reduction equation plays an important role in understanding the dependency of the partial oxygen pressure to the defect concentration. These types of defects occurred in oxygen-deficient oxides. The following reduction reaction takes place in the La_2CuO_4:

$$V_{La}{}''' + 3/2O_O{}^{x} = 1/2O_2(g) + 3e \quad (7)$$

$$V_{Cu}{}'' + O_O{}^{x} = 1/2O_2(g) + 2e \quad (8)$$

$$O_O{}^{x} = 1/2O_2(g) + 2e + V_O{}^{\cdot} \quad (9)$$

With defect formation energy, E_d, E_e and E_f, respectively (Allan and Mackrodt, 1988), are given in the following Table 5.

Table 3 Different point defects for La_2CuO_4

Traditional notation	Description	Kroger–Vink notation
$La_{La}{}^{3+}$	La^{3+} ion in a lanthanum lattice site	$La_{La}{}^{\times}$
$La_{La}{}^{2+}$	$La_{La}{}^{2+}$ ion in the lanthanum site	e'
V_{La}	Lanthanum vacancy	$V_{La}{}'''$
$La_{La}{}^{3+}$	La^{3+} in the interstitial site	$La_i{}^{\cdot\cdot\cdot}$
$Cu_{Cu}{}^{2+}$	Cu^{2+} ion in the copper lattice site	$Cu_{Cu}{}^{\times}$
$Cu_{Cu}{}^{2+}$	Cu^{2+} in the interstitial site	$Cu_i{}^{\cdot\cdot}$
V_{Cu}	Copper vacancy	$V_{Cu}{}''$
$O_O{}^{2-}$	$O_O{}^{2-}$ ion in the oxygen lattice site	$O_O{}''$
V_O	Oxygen vacancy	$V_O{}^{\cdot\cdot}$
$O_O{}^{-}$	$O_O{}^{-}$ ion in the oxygen lattice site	$h^{\cdot}$

Table 4 Defect formation energies (eV) in La_2CuO_4

Energy (eV)	Orthorhombic
E_a	2.2
E_b	4.0
E_c	−1.7

Table 5 Defect formation energies (eV) in La_2CuO_4

Energy (eV)	Orthorhombic
E_d	10.4
E_e	4.4
E_f	10.1

Among these different reduction equations, the more important equations are the formation of an oxygen vacancy by losing oxygen to the atmosphere, formation of electron-hole pair and formation of oxygen interstitial.

Variation of defect concentration with oxygen partial pressure:

From equations (4)–(6), it can be seen that the oxygen in the lattice can be compensated by oxygen interstitials (O_O'') and cation vacancies, respectively. In every case, neutral oxygen goes into the lattice (substrate surface) by picking up 3, 2 and 2 electrons, respectively, from the metal valance band to become an oxide ion, as a result creating 3, 2 and 2 holes, respectively, in each case. Hence the substrate becomes a *p*-type electronic conductor with increasing Po_2.

In an oxygen-deficient condition, there is a loss of neutral oxygen which gives 3, 2 and 2 electrons in each case in the lattice, which are shown by equations (7)–(9). Hence the materials become *n*-type electronic conduction with decreasing oxygen partial pressure Po_2 as shown in Figure 1.

From mass action and electro-neutrality equations corresponding to equation (6), it has been derived that:

$$[V_O^{\cdot}] = K_1(P_{O2})^{-1/8} \tag{10}$$

at a fixed temperature. Whereas for the formation of oxygen interstitial equation:

$$1/2O_2(g) \leftrightarrow O_i'' + 2h, \tag{11}$$

This gives the oxygen partial pressure dependence relation by the equation:

$$[O_i''] = K_2(P_{O2})^{1/8} \tag{12}$$

Where $[V_O^{\cdot\cdot}]$ is the oxygen vacancy concentration and $[O_i'']$ is the oxygen interstitial concentration.

Electron-hole formation equation

$$\text{Null} \leftrightarrow e^- + h \tag{13}$$

Where $[e^-]$ and $[h]$ are the concentrations of electron and hole, respectively. This formation reaction does not depend on oxygen partial pressure. But significantly the energy required for this reaction is equal to the bandgap energy (E_g) of this oxide. For La_2CuO_4, in orthorhombic lattice structure band gap, energy is 2.4 eV.

The variation of defects concentration with oxygen partial pressure in the bulk surface of La_2CuO_4 with the partial pressure for the above mathematical equation is plotted theoretically in Figure 4.

$$R = R_0\exp\left(q^2w^2N_v/\varepsilon kT\right) \tag{14}$$

$$R = (1/\sigma)L/A \tag{15}$$

Where σ is the conductivity of the sensing substrates which changes because of the variation of formation of oxygen vacancies as well as oxygen interstitials by the relation:

$$\sigma = a\exp(-E_a/KT)\,(P_{O2})^n \tag{16}$$

where a is a constant, E_a is the activation energy for the conduction band, P_{O2} is the oxygen partial pressure and n is a numerical constant that takes the different value on the base of dominant defect nature present in the bulk. The above graph defect concentration vs P_{O2} shows three regimes:

1 a reduced regime with slope −1/8;
2 neutral regime; and
3 an oxidized regime with slope +1/8.

In a reduced regime, La_2CuO_4 suffers from a lack of oxygen and behaves like an *n*-type semiconductor because of electron movement. Whereas in the oxidizing regime, it shows *p*-type semiconductivity. This change occurs by the change in oxygen partial pressure of La_2CuO_4, which changes from *n*-type to a *p*-type semiconductor. In this case, the number of available electrons in the conduction and valence band changes in Figure 5.

Resistance with oxygen partial pressure at a fixed temperature

As seen in Figure 5, at low temperatures, there is very little change in resistance by change of oxygen partial pressure. At low temperature, oxidation reaction dominates, which has no charge carriers associated [equations (4)–(6)]. So there are limited responses observed at low temperatures. At higher temperatures, the dominant reaction is the reduction reaction, which involves electrons as charge carriers. And so for *p*-type semiconductors, by variation of NO concentration, the resistivity decreases with increasing partial pressure.

Resistance with the temperature at fixed O_2 concentration

We calculated the oxygen partial pressure generated by changing the NO gas concentration. As plotted in Figure 6, at a fixed P_{O2}, the defect reaction depends on the temperature. The Arrhenius plot shows the variation of activation energy with gas concentration.

The Arrhenius plot of the sensing electrode material is plotted with changing O_2 concentration in Figure 7. It was observed in this figure that there is a sudden change in the slope of the response curve between low- and high-temperature ranges. This is because of the conversion of the sensing element

Figure 4 The Band structure and DOS through Density functional calculations for La_2CuO_4 (a) without and (b) with one La vacancy

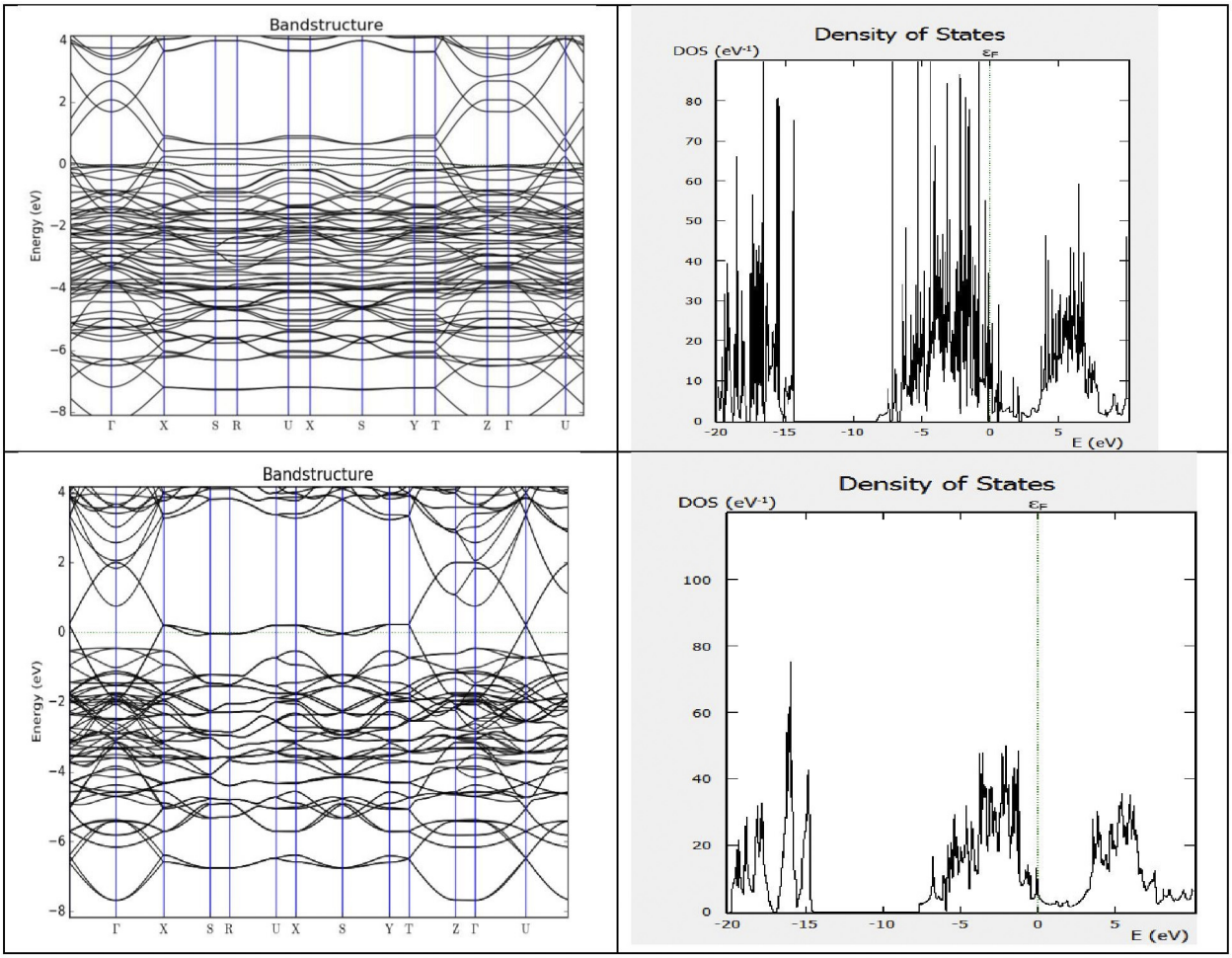

Figure 5 The microstructure of sensing electrode material prepared through the auto-ignition process and sintered at (a) 700°C (b) 800°C (c) 900°C each for 10 hrs

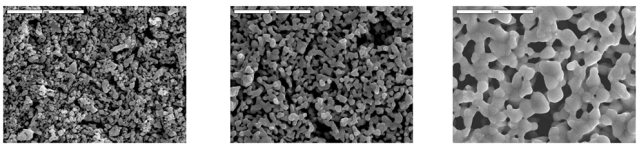

from *n*-type to *p*-type. Our theoretical results are in the low-temperature range and so they lie only in the *n*-type region.

Experimentally, the activation energy was found out by changing the temperature over a wider range. This shows that there is different activation energy at a higher temperature which corresponds to the reduction reaction [equations (8)–(10)].

Whenever a sensing surface in an experimental setup is exposed to oxygen partial pressure Po_2 (or other gas pressure) at a certain working temperature, two defect equilibrium equations take place. In the present case, oxygen loss is compensated by oxygen vacancies ($V_O^{\cdot\cdot}$) and cation interstitials ($M^{\cdot\cdot}_i$) are shown in the following equations, respectively:

Figure 6 The variation of defects concentration with oxygen partial pressure

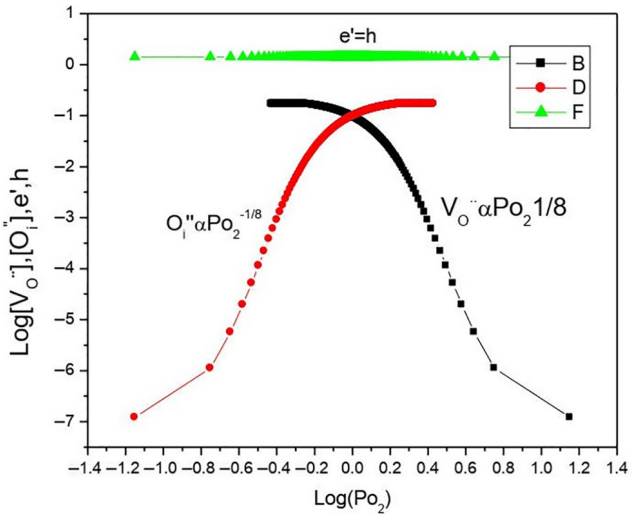

Figure 7 Resistive response and response sensitivity of the prepared sensor element

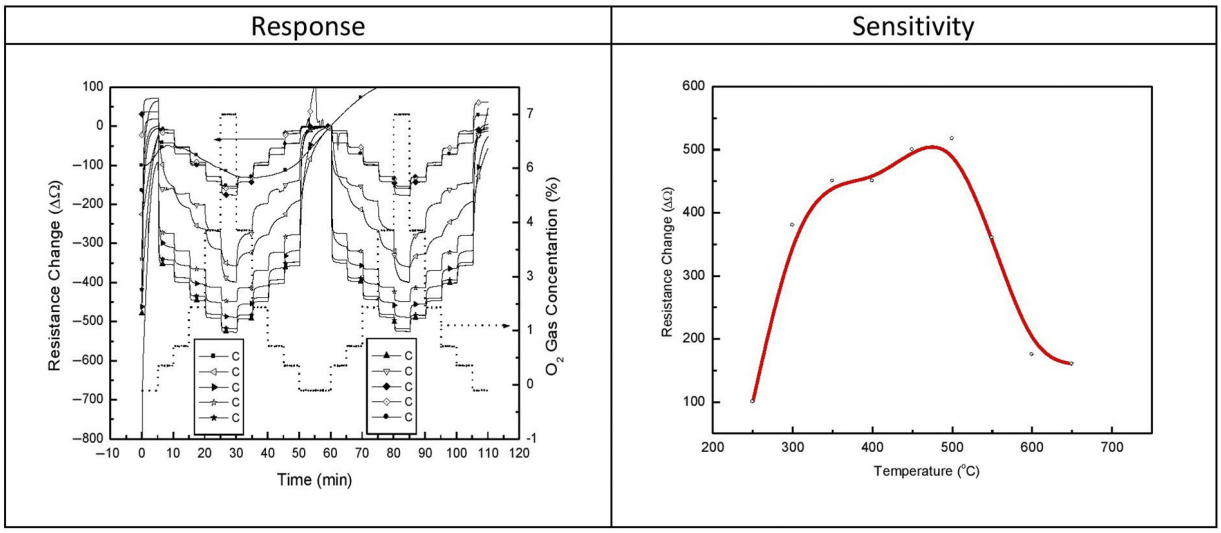

$$O_O{}^{x} = 1/2O_2(g) + 2e + V_O{}^{\cdot\cdot} \quad (17)$$

$$MO = 1/2O_2 + M_I^{\cdot\cdot} + 2e \quad (18)$$

Where M_i indicates the metal ions La^{3+} and Cu^{2+}. It can be seen from the graph that there are two different slopes, indicating the presence of two different activation energies (Table 6), one at the low-temperature region and the other in the high-temperature region. At low temperatures, the equation having smaller activation energy [equation (17)] dominates. And at high temperatures, the equation having higher activation energy [equation (18)] dominates.

Density functional calculations

Explanations of band structure calculation and its consequences

La_2CuO_4 structure is form based on the following consideration (Figure 8):

1 Space group-69: Fmmm;
2 Structure – orthorhombic;
3 Unit cell dimensions: a = 5.363 Å; b = 5.409 Å; c = 13.17 Å; and $\alpha = \beta = \gamma = 90°$; and
4 The cell contains four La_2CuO_4 unit cells.

The electron density at a particular energy level determines the availability of electrons. However, by the adsorption of gas molecules, the availability of electron in the conduction band changed and is reflected in the density of states diagram. In the defect-free La_2CuO_4 structure, as shown in

Table 6 Theoretical and experimental value of activation energies in different reactions

Activation energy	Oxygen expulsion reaction [equation (17)]	Metal dissociation reaction [equation (18)]
Theoretical	0.20 eV	0.12 eV
Experimental	0.18 eV	0.11 eV

Figure 8 La_2CuO_4 changes from n-type to a p-type semiconductor by changing oxygen partial pressure

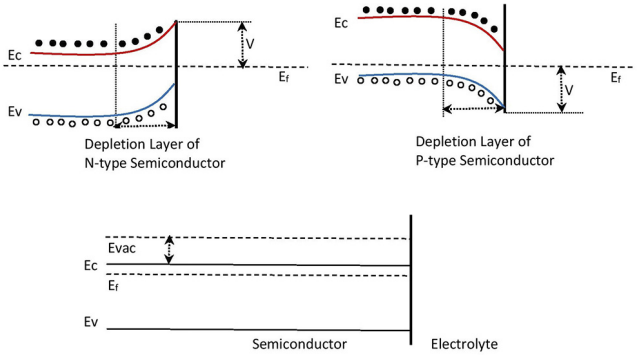

Figure 9 XRD Pattern of powders prepared through the auto-ignition process and calcined at two different temperatures showing complete phase formation at 600°C

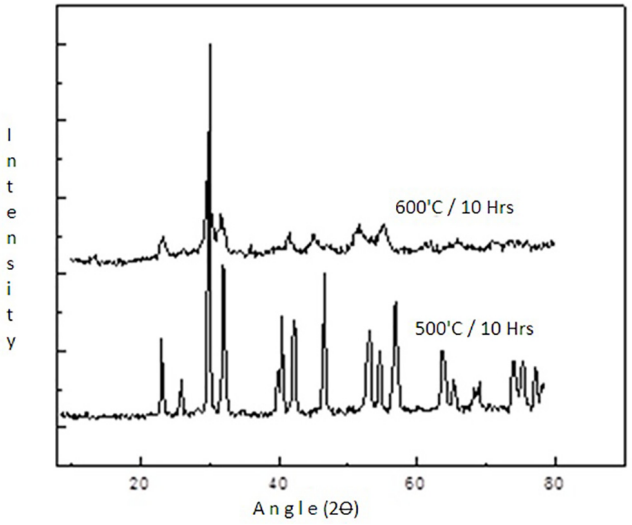

Figure 9(a), the number of available electrons is fixed. However, this number changes when it is added with an electron defect caused by gas adsorption as shown in Figure 9(b). The added defects provide an electron of higher energy, going to the conduction band, resulting in a rise in the Fermi level of the sensing surface. This change in the Fermi energy can be seen in the band diagram with and without defect, as shown in Figure 9(b). This causes a change in the relative potential between the sensing and counter electrodes. Thus, when the counter electrode is grounded, the potential of sensing electrodes is the indicator of gas concentration. As a result, the resistivity in the system changes proportionally with the gas concentration.

In the analysis of electron band structure, it was found that for perfect structure, the Fermi level is positioned at 2.45 eV, and for structure with the defect, it is positioned at 1.24 eV. This shift in Fermi energy is because of the creation of a large number of an electron at the conduction band of metal after the formation of an oxygen-deficient surface. Practically, when reducing gas, NO is exposed on a transition metal oxide La_2CuO_4-based sensing material and it becomes oxidized to NO_2 gas by creating an oxygen vacancy on the surface and thereby forming an oxygen-deficient surface and releasing electrons. The total number of oxygen vacancies is strongly related to defect density and so the sensor output must depend on these defects formed. Here, we generate a 5% oxygen vacancy by removing oxygen atoms and one La from La_2CuO_4 surface that gives a change in Fermi level between perfect crystal without and with defects, whose value is the difference, i.e. 1.21 eV.

Actually, after the creation of oxygen vacancy, the density of states changes around Fermi energy, and Fermi level shifts toward higher energy states because of a large concentration of electrons at the conduction band. As a result, several partly occupied energy bands appeared at the Fermi level. The change in the Fermi level is responsible for sensor output. However, the concentration of the defects also depends on the particular gas species. Gases with higher electronegativity cause a larger change in Fermi energy causing a higher magnitude of response.

Sensor response calculation

It is a very important characteristic of any sensor. In the literature, it has been defined as the percentile change of resistance with the initial resistance of the sensor when exposed without target gas. It is given by the following equation (19).

$$\text{Response} = (R/R_0 - 1) * 100\% \tag{19}$$

Where R is the measured resistance at present of target gas and R_0 is the resistance in the absence of the target gas. In general, R_0 is smaller than the R, which gives the larger change in the measured R. The sensor response very much depends on the defect concentration and the partial pressure of the oxygen.

As shown in Figure 10, the sensor response is very small at low temperature and the response magnitude decreases at high temperature. It has significant value in the intermediate range. The minimum temperature of response was 290°C while the measurement at a higher temperature up to 500°C was possible for the resistive mode of operation. The interaction between the sensor and the gas phase may involve physical adsorption (physisorption), chemical adsorption (chemisorption) (Allan and Mackrodt, 1988) and the formation or annihilation of surface and bulk defects (Chen *et al.*, 2013). The prevailing effect or dominant reaction depends on temperature, for the interaction between oxygen and the surface of La_2CuO_4 (He *et al.*, 2020). This characteristic behavior is typical for many semiconducting metal oxides, with the transition from one region to another occurring at different temperatures for different materials. For most gas sensors operating at elevated temperatures, chemisorption is the dominant effect controlling the sensing mechanism typically between 100 and 500°C. The *p*-type material span on maximum response is larger for the reason that, NO being a reducing gas, can deliver electron more easily to the substrate and *p*-type substrate can more easily adsorb this electron resulting in a higher span of measurement for the *p*-type substrate.

Figure 10 (a) Change of resistance with the temperature at different NO concentration and (b) change of resistance with the temperature at different O2 concentration

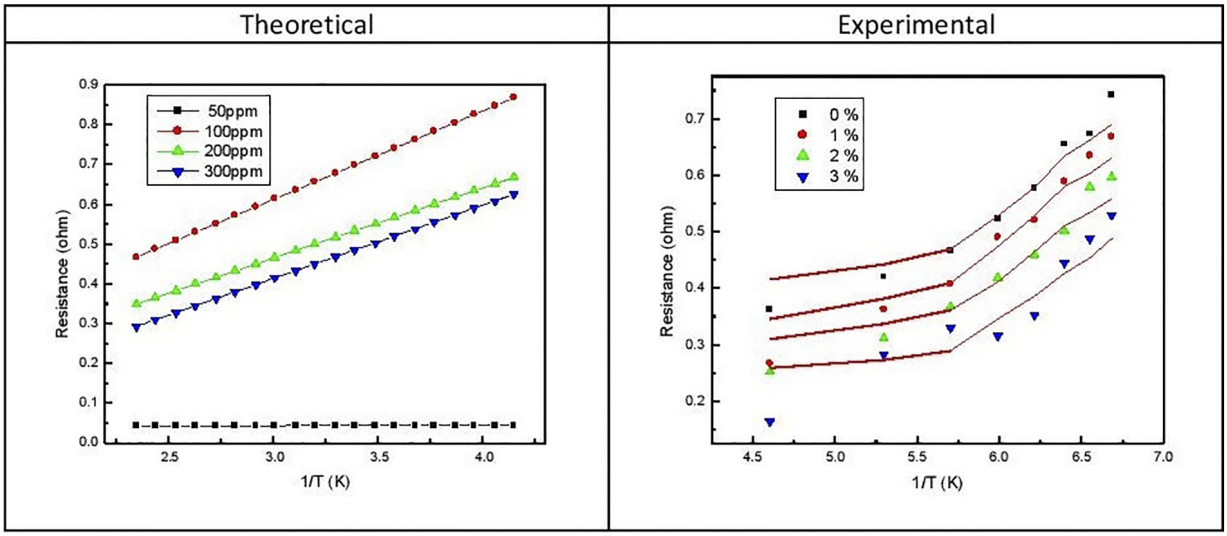

Conclusion

Defects in the semiconducting sensor elements affect the electrical transport by changing the bandgap and density of states of sensing material. At a fixed temperature, the toxic gas concentration in the sensing environment was varied and change in defect concentration with Oxygen partial pressure was calculated. This change in defect concentration shifts the Fermi level, which is manifested in the resistance drop across the sample. The experimentally observed resistance drops were compared with the simulated values obtained analytically. The sensor is less sensitive below the temperature of 290°C and above 500°C for reduction gas adsorption. By the adsorption of gas, there occurs a change in the Fermi level of sensing surface based on the electronegativity value of the gas. Gases with higher electronegativity cause a larger change in Fermi energy causing a higher magnitude of response. Through this understanding, the design of a sensor with improved selectivity and stability to a gas can be achieved by the study of defect structure and subsequent band analysis.

References

Allan, N.L. and Mackrodt, W.C. (1988), "The calculated defect properties of La_2CuO_4 related to high $-T_c$ superconductivity", *Philosophical Magazine A* , Vol. 58 No. 4, pp. 555-569.

Ansari, S., Boroojerdian, P., Sankar, S., Karekar, R., Aiyer, R. and Kulkarni, S. (1997), "Grain size effects on H2 gas sensitivity of thick film resistor using SnO2 nanoparticles", *Thin Solid Films*, Vol. 295 Nos 1/2, pp. 271-276.

Azad, A.-M., Akbar, S., Mhaisalkar, S.G., Birkenfeld, L.D. and Goto, K.S. (1992), "Solid-state gas sensors: a review", *Journal of the Electrochemical Society*, Vol. 139 No. 12, pp. 3690-3704.

Bârsan, N., Hübner, M. and Weimar, U. (2011), "Conduction mechanisms in SnO2 based polycrystalline thick film gas sensors exposed to CO and H2 in different oxygen backgrounds", *Sensors and Actuators B: Chemical*, Vol. 157 No. 2, pp. 510-517.

Brown, J.R., Haycock, P.W., Smith, L.M., Jones, A.C. and Williams, E.W. (2000), "Response behavior of tin oxide thin film gas sensors grown by MOCVD", *Sensors and Actuators B: Chemical*, Vol. 63 Nos 1/2, pp. 109-114.

Brunet, E., Maier, T., Mutinati, G.C., Steinhauer, S., Köck, A., Gspan, C. and Grogger, W. (2012), "Comparison of the gas sensing performance of SnO2 thin film and SnO2 nanowire sensors", *Sensors and Actuators B: Chemical* , Vol. 165 No. 1, pp. 110-118.

Chen, D., Wang, J., Chen, T. and Shao, L. (2013), "Defect annihilation at grain boundaries in alpha-Fe, scientific report, 22 March".

Choi, J.Y. and Oh, T.S. (2013), "CO sensitivity of La2O3-doped SnO2 thick film gas sensor", *Thin Solid Films*, Vol. 547, pp. 230-234.

Close, L.G., Catlin, F.I. and Cohn, A.M. (1980), "Acute and chronic effects of ammonia burns of the respiratory tract", *Archives of Otolaryngology – Head and Neck Surgery*, Vol. 106 No. 3, pp. 151-158.

Fergus, J.W. (2007), "Perovskite oxides for semiconductor-based gas sensors", *Sensors and Actuators B: Chemical*, Vol. 123 No. 2, pp. 1169-1179, doi: 10.1016/j.snb.2006.10.051.

Fonstad, C. and Rediker, R. (1971), "Electrical properties of high-quality stannic oxide crystals", *Journal of Applied Physics*, Vol. 42 No. 7, pp. 2911-2918.

Gong, S., Liu, J., Quan, L., Fu, Q. and Zhou, D. (2011), "Preparation of tin oxide thin films on silicon substrates via sol-gel routes and the prospects for the H2S gas sensor", *Sensor Letters*, Vol. 9 No. 2, pp. 625-628.

Gong, S., Liu, J., Xia, J., Quan, L., Liu, H. and Zhou, D. (2009), "Gas sensing characteristics of SnO2 thin films and analyses of sensor response by the gas diffusion theory", *Materials Science and Engineering: B*, Vol. 164 No. 2, pp. 85-90.

Graham Solomons, T.W. and Fryhle, C.B. (2004), *Org. Chem*, (8th ed.), 497-498.

He, L., Fan, Y., Bellettre, J., Yue, J. and Luo, L. (2020), "A review on catalytic methane combustion at low temperatures: catalysts, mechanisms, reaction conditions and reactor designs", *Renewable and Sustainable Energy Reviews*, Vol. 119, p. 109589.

Hübner, M., Bârsan, N. and Weimar, U. (2012), "Influences of Al, Pd and Pt additives on the conduction mechanism as well as the surface and bulk properties of SnO2 based polycrystalline thick film gas sensors", *Sens. ActuatorB Chem*, Vol. 171, pp. 172-180.

Kocemba, I., Szafran, S., Rynkowski, J.M. and Paryjczak, T. (2001), "Sensors based on SnO2 as a detector for CO oxidationin air", *Reaction Kinetics and Catalysis Letters*, Vol. 72 No. 1, pp. 107-114.

Korotcenkov, G., Han, S.-D., Cho, B. and Brinzari, V. (2009), "Grain size effects in sensor response of nanostructuredSnO2-and In2O3-based conductometric thin film gas sensor", *Critical Reviews in Solid State and Materials Sciences*, Vol. 34 Nos 1/2, pp. 1-17.

Korotcenkov, G., Brinzari, V., Schwank, J., DiBattista, M. and Vasiliev, A. (2001), "Peculiarities of SnO2 thin film deposition by spray pyrolysis for gas sensor application", *Sensors and Actuators B: Chemical*, Vol. 77 Nos 1/2, pp. 244-252.

Lambert-Mauriat, C., Olson, V., Saadi, L. and Aguirre, K. (2012), "Ab initio study of oxygen point defects on tungsten trioxide surface", *Surface Science*, Vol. 606 Nos 1/2, pp. 40-45.

Lee, S.P. (2006), "Electrical behavior in the gas-solid interface of gas sensors based on oxide semiconductors", *International Journal of Applied Ceramic Technology*, Vol. 3 No. 3, pp. 225-229.

Lee, Y., Huang, H., Tan, O. and Tse, M. (2008), "Semiconductor gas sensor based on Pd-doped SnO2 nanorod thin films", *Sensors and Actuators B: Chemical*, Vol. 132 No. 1, pp. 239-242.

Lim, S.P., Huang, N.M., Lim, H.N. and Mazhar, M. (2014), "Aerosol assisted chemical vapor deposited (AACVD) ofTiO2 thin film as a compact layer for dye-sensitized solar cell", *Ceramics International*, Vol. 40 No. 6, pp. 8045-8052.

Liu, J., Gong, S., Xia, J., Quan, L., Liu, H. and Zhou, D. (2009), "The sensor response of tin oxide thin films to

different gas concentration and the modification of the gas diffusion theory".

Liu, H., Wu, S., Gong, S., Zhao, J., Liu, J. and Zhou, D. (2011), "Nanocrystalline In2O3-SnO2 thick films for low-temperature hydrogen sulfide detection", *Ceramics International*, Vol. 37 No. 6, pp. 1889-1894.

Malagù, C., Carotta, M., Gherardi, S., Guidi, V., Vendemiati, B. and Martinelli, G. (2005), "AC measurements and modeling of WO3 thick film gas sensors", *Sensors and Actuators B: Chemical*, Vol. 108 Nos 1/2, pp. 70-74.

Marikkannan, M., Vishnukanthan, V., Vijayshankar, A., Mayandi, J. and Pearce, J.M. (2015), "A novel synthesis of tin oxide thin films by the sol-gel process for optoelectronic applications", *AIP Advances*, Vol. 5 No. 2, p. 027122.

Matsunaga, N., Sakai, G., Shimano, K. and Yamazoe, N. (2002), "Diffusion equation-based study of thin-film semiconductor gas sensor-response transient", *Sensors and Actuators B: Chemical*, Vol. 83 Nos 1/3, pp. 216-221.

Michaels, R.A. (1999), *Environmental Health Perspectives*, Vol. 107 No. 8, pp. 617-627.

Miller, D.R., Akbar, S.A. and Morris, P.A. (2014), "Nanoscale metal oxide-based heterojunctions for gas sensing: a review",

Mitsufuji, H. (1975), *Keiso (in Japanese)*, Vol. 18, p. 15.

Miura, N., Lu, G. and Yamazoe, N. (2000), "Progress in mixed-potential type devices based on solid electrolytes for sensing redox gases", *Solid State Ionics*, Vol. 136-137 Nos 1/2, pp. 533-542.

Morrison, S.R. (1987), "Mechanism of semiconductor gas sensor operation", *Sensors and Actuators*, Vol. 11 No. 3, pp. 283-287.

Moseley, P.T. (1992), "Material selection for semiconductor gas sensors", *Sensors and Actuators B: Chemical*, Vol. 6 Nos 1/3, pp. 149-156.

Noh, K.W. (2010), "Defect engineering of metal oxide semiconductors", pp. 10-11, avliable at: www.ideals.illinois.edu/handle/2142/15964

Oprea, A., Gurlo, A., Barsan, N. and Weimar, U. (2009), "Transport and gas sensing properties of In2O3 nano-crystalline thick films: a hall effect-based approach", *Sensors and Actuators B: Chemical*, Vol. 139 No. 2, pp. 322-328.

Rao, Y., Inwati, G., Kumar, A., Meena, J. and Singh, M. (2014), "Metal oxide-based nanoparticles use for pressure sensor", *International Journal of Current Engineering and Technology*, Vol. 4 No. 4, pp. 2492-2498.

Sakai, G., Matsunaga, N., Shimano, K. and Yamazoe, N. (2001), "Theory of gas-diffusion controlled sensitivity for thin film semiconductor gas sensor", *Sensors and Actuators B: Chemical*, Vol. 80 No. 2, pp. 125-131.

Singh, S., Verma, N., Singh, A. and Yadav, B.C. (2014), "Synthesis and characterization of CuO–SnO2 nanocomposite and its application as a liquefied petroleum gas sensor", *Materials Science in Semiconductor Processing*, Vol. 18, pp. 88-96.

Sugiyama, T., Kato, A., Fujii, K. and Nagatani, M. (1962), "Anew detector for gaseous components using semiconductive thin films", *Anal. Chem*, Vol. 34, pp. 1502-1503.

Taguchi, N. (1962), A Metal Oxide Gas Sensor. Japanese Patent 45-38200,

Tinashue, Z., Ruifang, Z., Yusheng, S. and Xingqin, L. (1996), *Sens. Actuators B: Chem*, Vol. 32, pp. 185-189.

Wu, J., Huang, Q., Zeng, D., Zhang, S., Yang, L., Xia, D., Xiong, Z. and Xie, C. (2014), "Al-doping induced formation of oxygen-vacancy for enhancing gas-sensing properties of SnO2 NTs by electrospinning", *Sensors and Actuators B: Chemical*, Vol. 198, pp. 62-69.

Yamazoe, N. and Miura, N. (1998), "Potentiometric gas sensors for oxidic gases", *Journal of Electroceramics*, Vol. 2 No. 4, pp. 243-255.

Yamazoe, N. and Shimano, K. (2009), "New perspectives of gas sensor technology", *Sensors and Actuators B: Chemical* , Vol. 138 No. 1, pp. 100-107.

Yamazoe, N. and Shimano, K. (2009), "Receptor function of small semiconductor crystals with clean and electron-traps dispersed surfaces", *Thin Solid Films*, Vol. 517 No. 22, pp. 6148-6155.

Yamazoe, N. and Shimano, K. (2011), "Theoretical approach to the gas response of oxide semiconductor film devices under the control of gas diffusion and reaction effects", *Sensors and Actuators B: Chemical*, Vol. 154 No. 2, pp. 277-282.

Yamazoe, N., Suematsu, K. and Shimano, K. (2012), "Extension of receptor function theory to include two types of adsorbed oxygen for oxide semiconductor gas sensors", *Sensors and Actuators B: Chemical*, Vol. 163 No. 1, pp. 128-135.

Yamazoe, N., Fuchigami, J., Kishikawa, M. and Sugiyama, T. (1979), "Interactions of tin oxide surface with O_2, H_2O and H_2", *Surface Science*, Vol. 86, pp. 335-344.

Zeng, J., Hu, M., Wang, W., Chen, H. and Qin, Y. (2012), "NO2-sensing properties of porous WO3 gas sensor based on anodized sputtered tungsten thin film", *Sensors and Actuators B: Chemical*, Sensors 2017, 17, 1852 24 of 27, Vol. 161 No. 1, pp. 447-452.

Zhai, Z., Liu, J., Jin, G., Luo, C., Jiang, Q. and Zhao, Y. (2016), "Characterization and gas sensing properties of copper-doped tin oxide thin films deposited by ultrasonic spray pyrolysis", *Mater. Sci*, Vol. 22, pp. 201-204.

Zhao, X., Shi, W., Mu, H., Xie, H. and Liu, F. (2016), "Templated bicontinuous tin oxide thin film fabrication and the NO2 gas sensing", *Journal of Alloys and Compounds*, Vol. 659, pp. 60-65.

Zhao, J., Wu, S., Liu, J., Liu, H., Gong, S. and Zhou, D. (2010), "Tin oxide thin films prepared by aerosol-assisted chemical vapor deposition and the characteristics on gas detection", *Sensors and Actuators B: Chemical*, Vol. 145 No. 2, pp. 788-793.

Further reading

Korotcenkov, G. (2020), "Practical aspects in the design of one-electrode semiconductor gas sensors: status report, sens. Actuators B".

Park, C.O. and Akbar, S.A. (2003), "Ceramics for chemical sensors", *Journal of Materials Science*, Vol. 38 No. 23, pp. 4611-4637.

Park, C.O., Akbar, S.A. and Weppner, W. (2003), "Ceramic electrolytes, and electrochemical sensors", *Journal of Materials Science*, Vol. 38 No. 23, pp. 4639-4660.

Weppner, W. (1987), "Solid-state electrochemical gas sensors", *Sensors and Actuators*, Vol. 12 No. 2, pp. 107-119.

About the authors

Chinmay Roy has completed his B.Sc. in Physics from Balurghat College, Dakshin Dinajpur in 2011 and M.Sc. in Physics in 2013 from University of North Bengal. He is currently working as a Research Fellow at the Department of Physics, University of North Bengal.

Aparna Ghosh has completed her B.Sc. in Physics from A.B. N. Seal College, Coochbehar in 2010 and M.Sc. in Physics in 2012 from University of North Bengal. She is currently working as a Research Fellow at the Department of Physics, University of North Bengal.

Suman Chatterjee obtained his PhD from Jadavpur University in the 1996. Subsequently, he was employed as Post-doctoral Fellow in various universities in Brazil, Canada and USA. He works as an Associate Professor in Department of Physics, University of North Bengal. His areas of interest are electro-ceramic and organic devices and sensors. Suman Chatterjee is the corresponding author and can be contacted at: suman_chatterjee@hotmail.com

SENSOR LETTERS
Vol. 15, 1–5, 2017

Temperature Dependence of Semiconducting Gas Sensors in Potentiometric and Resistive Modes of Measurement

Aparna Ghosh*, P. K. Mandal, and Suman Chatterjee

Department of Physics, University of North Bengal, Siliguri 734013, India

(Received: xx Xxxx xxxx. Accepted: xx Xxxx xxxx)

This paper presents a study of the responses with temperature of a *p*-type, La_2CuO_4 and a *n*-type, WO_3 semiconducting sensing element fabricated over YSZ substrate in NO gas atmosphere. The measurements in potentiometric and resistive modes revealed that for potentiometric mode the peak of the response curve shifts toward lower temperature region and for resistive mode the peak shifts towards higher temperature region which confirms more sensitivity of potentiometric mode at lower temperature region compared to resistive mode for both kind of sensing materials.

Keywords: Potentiometric, Resistive, Nitric Oxide (NO), Semiconductor, *n*-Type, *p*-Type.

RESEARCH ARTICLE

1. INTRODUCTION

Air pollution is a serious problem in many heavily populated and industrialized areas. Economic growth and industrialization are proceeding at a rapid pace, accompanied by increasing emissions of air pollutants. Furthermore, since the kinds and quantities of pollution sources have also increased dramatically, the development of methods to monitor the pollutants has become even more important. To prevent or minimize the damage caused by atmospheric pollution, suitable monitoring systems are required that can rapidly and reliably detect and quantify air pollutants. Nitric Oxide is one of the major air pollutant component which is heavily produced by many industrial systems. Metal oxide semiconductor gas sensors are utilized in a variety of different roles and industries. They are relatively inexpensive compared to other sensing technologies. They are also robust, lightweight, long lasting and beneficial from high material sensitivity and quick response times. That is why they have been used extensively to measure and monitor trace amounts of environmentally important gases such as carbon monoxide (CO), nitrogen dioxide (NO_2), Nitric Oxide (NO) etc. From literature survey, it has been shown that NO gas effects the conductivity of both the semiconductor sensing materials La_2CuO_4 and WO_3.[1–4] It is reported that sensors of the form La_2CuO_4|YSZ|Pt and WO_3|YSZ|Pt are very sensitive to NO in the temperature range of 400 °C–600 °C[5] and 150–250 °C[6, 7] respectively. Various works involving La_2CuO_4 electrodes for non-Nernstian potentiometric sensors with La_2CuO_4 electrodes illustrating the effect of the sensing electrode with varying grain size,[8] area[9] and thickness,[10] on the response of the potentiometric sensor are well reported. The effect of electrical contact configuration for the La_2CuO_4 sensing electrodes on the sensor response has also been studied.[11] But the comparative study of temperature sensitivity of these semiconducting sensing materials in Resistive and Potentiometric mode is not studied yet. Here we report a comparative study of Resistive and Potentiometric mode to find out the minimum temperature of operation for pollution monitoring. Out of these above said two methods we found that Potentiometric mode is more sensitive at lower temperature towards NO gas.

2. EXPERIMENTAL DETAILS

2.1. Synthesis of the Material

La_2CuO_4 powder was synthesized by the auto ignition technique.[12] A stoichiometric mixture of $La(NO_3)_3 \cdot 6H_2O$ (Kanto chemical co., 99.99%) and $Cu(NO_3)_2 \cdot xH_2O$ (Alfa Aesar, 99.999%) was dissolved in deionized water and 0.25 mole% citric acid (Alfa Aesar, 99.5%) was added to the mixture subsequently. The solution was heated at 70 °C with constant stirring until a precipitate was formed, and

*Corresponding author; E-mail: aparnaghosh26091989@gmail.com

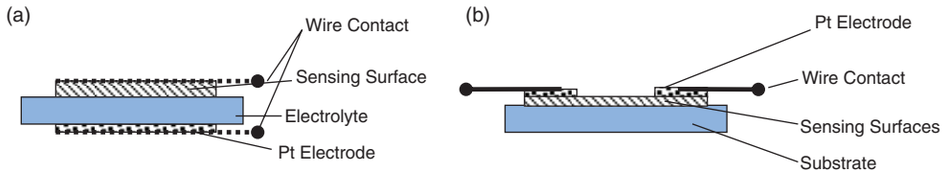

Fig. 1. Schematic diagram of sensor designs (a) potentiometric and (b) resistive.

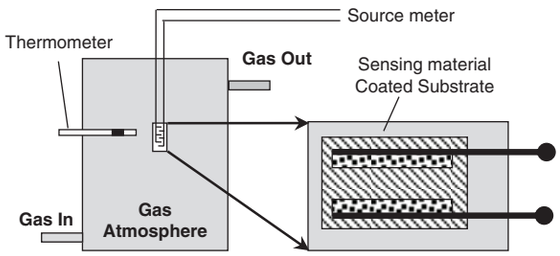

Fig. 2. Schematic diagram of the measurement setup.

the precipitate was then auto ignited with further heating at 90 °C. The resulting powder was calcined at 600 °C for 10 h.

Tungsten oxide (WO_3, 99.8% purity, Alfa Aesar) powder was purchased and the powder was dispersed in ethanol with polyethylene glycol 400 (PEG-400, Avocado Research Chemicals Ltd.), and mixed in a mortar for 3 h. The mixed slurry was then heated at 60 °C for 10 h to remove the ethanol completely.

2.2. Sensor Electrode Preparation

For the preparation of a sensing electrode, Tungsten oxide or La_2CuO_4 powder was mixed thoroughly with solvent ethanol and plasticizer (0.01%) ethylene glycol. The slurry was screen printed over one face of a Zirconia substrate.

For Potentiometric measurement, a square electrode of the sensing material was screen printed on one side of a YSZ substrate and a Pt electrode was printed directly opposite the sensing electrode. After that thin Pt wires were connected to both electrodes and finally, both the prepared sensors (La_2CuO_4 and WO_3) were sintered at 750 °C for 10 h and at 400 °C for 12 hours respectively.

For resistive measurement, a square electrode of the sensing material was printed on one side of an YSZ substrate and it was fitted with Pt electrodes. In this case both the electrodes were in the same side. Finally, both the prepared sensors (La_2CuO_4 and WO_3) were sintered at 750 °C for 10 h and at 400 °C for 12 hours respectively.

2.3. Experimental Setup

Sensing experiments were carried out with a gas flow system connected to a quartz tube which was inside of a furnace. Then the sensors were exposed to NO gas. For Potentiometric and resistive measurement, the voltage and change in resistance between the two sensor electrodes was monitored using a digital source meter (2400 Keithley source meter) respectively.

3. RESULTS AND DISCUSSION

3.1. Sensor Fabrications and Characterizations

The morphology of the samples was observed using a Scanning electron microscope (SEM).

Figure 3 shows the microstructure of two sensing surfaces. The particle size was around $\sim$1 μm of both the films; however, for WO_3 the particle size appears to be smaller. For La_2CuO_4, the particles appear to be sintered a little more than WO_3. The BET surface area of powders was found to be 16.3 for La_2CuO_4 and 11.2 for WO_3 powders.

X-ray diffraction patterns of both the sensing materials WO_3 and La_2CuO_4 were collected in the 2θ range of 5° to

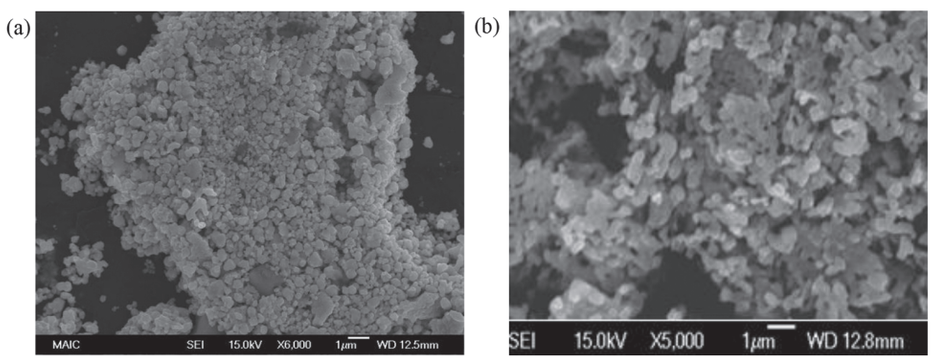

Fig. 3. SEM micrograph of sensing surfaces (a) WO_3 and (b) La_2CuO_4.

RESEARCH ARTICLE

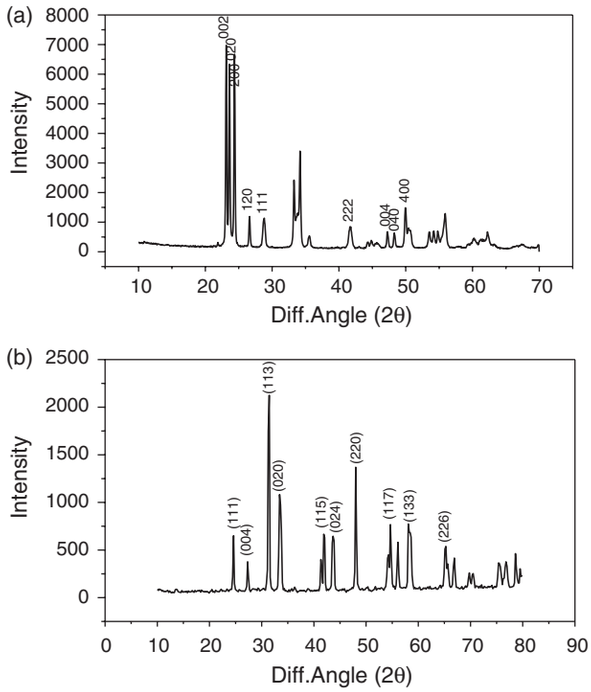

Fig. 4. X-ray diffraction pattern of sensing surfaces (a) WO_3 and (b) La_2CuO_4.

70° and 10° to 80° respectively using a diffractometer as shown in Figure 4. However, no departure was observed from pure substances.

The response characteristics for one *p*-type and one *n*-type sensor in Potentiometric and Resistive mode of detection have been presented in the figures below. The voltage and resistance change is detected when NO gas (in N_2) concentration is raised from 0 to 650 ppm. The sensitivity of the maximum response shows that the response is much higher for Potentiometric mode of measurement for two types of sensors. It also shows that the response for *n*-type and *p*-type materials are opposite in magnitude for both types of measurements. The response characteristics at different temperature in Potentiometric mode indicates that stability of response improves at lower temperature of operation. From Table I we observed that S/N ratio is small for Resistive mode where as it is high for Potentiometric mode. Very small value of S/N ratio

Table I. Sensing parameters of sensing surfaces WO_3 and La_2CuO_4 in resistive and potentiometric modes.

	Resistive	Potentiometric
n-type		
Sensitivity	3.02	4.35
Stability (S/N ratio)	60.185	77.89
Response time (90%)	2.17 min	38.4 sec
p-type		
Sensitivity	5.72	6.63
Stability (S/N ratio)	2.64	66.95
Response time (90%)	4.68 min	4.36 min

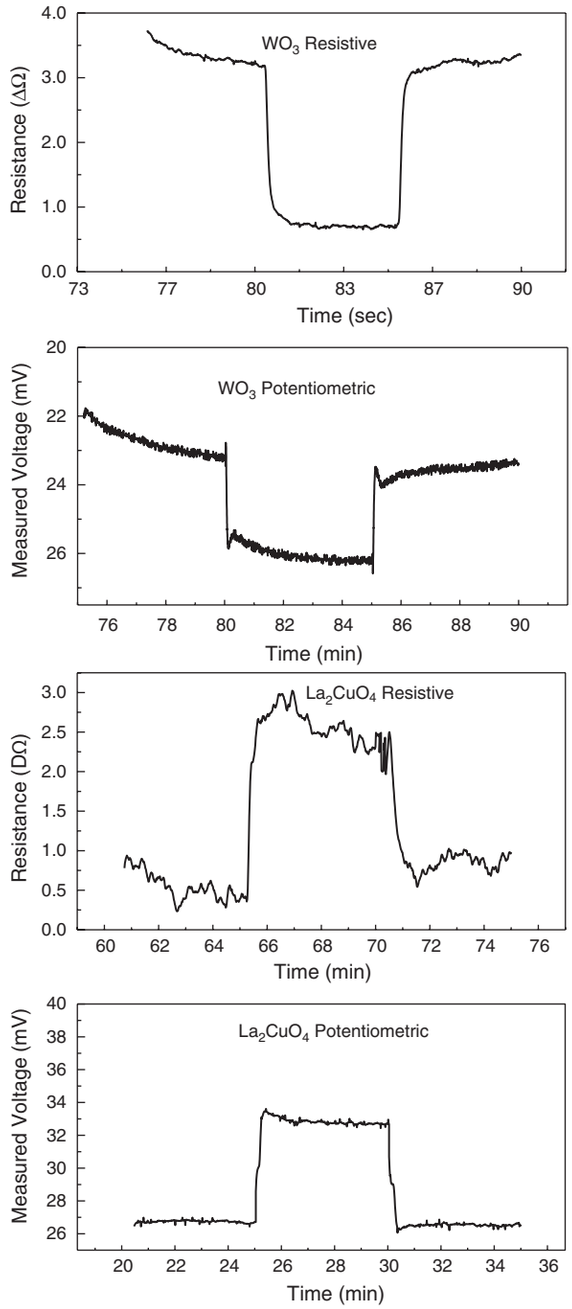

Fig. 5. Response characteristics of sensing surfaces WO_3 and La_2CuO_4 in resistive and potentiometric modes.

in case of *p*-type Resistive mode was obtained. The reason behind this small value of S/N ratio may be due to some fabrication error during screen-printing of the sensing substrate or Counter electrode. The high magnitude of response indicates higher response sensitivity of the sensing element to NO. In this experiment La_2CuO_4 in Potentiometric mode shows the higher response sensitivity to NO. While Response time (time in which response reaches 90% of its maximum value) is higher in Resistive

RESEARCH ARTICLE

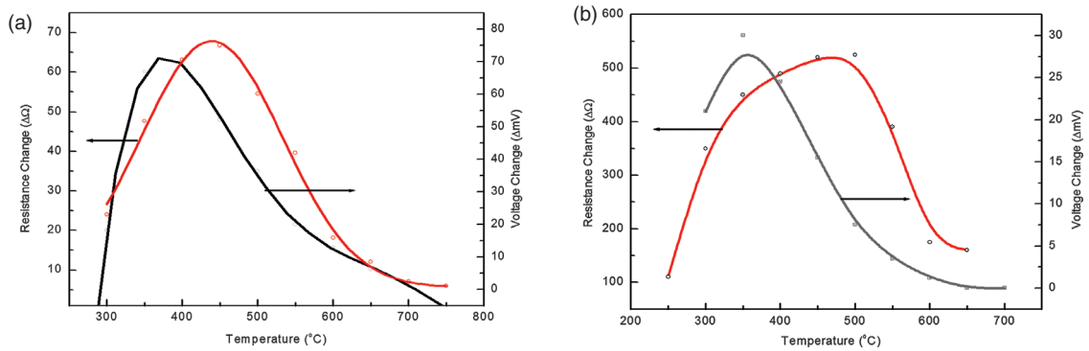

Fig. 6. Response with temperature of sensing surfaces (a) WO_3 and (b) La_2CuO_4 in resistive and potentiometric modes.

Table II. Span of temperature for high response of sensing surfaces WO_3 and La_2CuO_4 in resistive and potentiometric modes.

Sensing material	Mode of operation	Minimum temperature (°C)	Maximum temperature (°C)	Span of measurement (°C)	Reported in literature (°C)
WO_3, *n*-type	Potentiometric	325	410	85	100 (Ref. [16])
	Resistive	400	500	100	250 (Ref. [7])
La_2CuO_4, *p*-type	Potentiometric	290	420	130	450–600 (Ref. [5])
	Resistive	320	530	210	–

mode for both *n*-type and *p*-type material but it is lower in Potentiometric mode for both the material. Among two type of material in Potentiometric mode, *n*-type material shows the minimum response time.

In case of La_2CuO_4 sensing element, for Potentiometric mode, the minimum temperature of response was 290 °C and for Resistive mode it was 320 °C while maximum temperature of response for Potentiometric and Resistive modes were around 420 °C and 530 °C respectively. Similarly, for WO_3 sensing element the minimum temperature of responses was 325 °C and 400 °C for Potentiometric and Resistive modes of operation respectively. While maximum temperature of responses was around 410 °C for Potentiometric mode of operation and the measurement at higher temperature up to 500 °C was possible for resistive mode of operation as shown in table below.

The interaction between the sensor and the gas phase may involve physical adsorption (physisorption), chemical adsorption (chemisorption),[13] and formation or annihilation of surface and bulk defects.[14] The prevailing effect, or dominant reaction, depends on temperature, for the interaction between oxygen and the surface of ZnO.[15] This characteristic behavior is typical for many semiconducting metal oxides, with the transition from one region to another occurring at different temperatures for different materials. For most gas sensors operating at elevated temperatures, typically between 100 and 500 °C, chemisorption is the dominant effect controlling the sensing mechanism, while for resistive oxygen sensors operating at higher temperatures (typically above 700 °C), oxygen incorporation into the lattice is the dominant mechanism. This is beyond our measurement region.

For the *n*-type material span on maximum response is less for both Potentiometric and resistive mode. This is because, NO being a reducing gas, can deliver electron more easily to the substrate. A *p*-type substrate can more easily adsorb this electron delivered by the NO gas. So, the span of measurement is higher for *p*-type substrate.

While comparing Potentiometric and resistive modes, for resistive mode of measurement, span of maximum response is wider. This is because, for Potentiometric mode the conductivity of electrolyte plays an important role, which diminishes at lower temperature, resulting in a shorter span of response. Whereas for resistive mode conductivity of the substrate play almost no significant role on the response. So, it gives high response for the entire range of temperature where gas adsorption is present.

Peak response for both *n*-type and *p*-type materials was found to be shifted towards lower temperature range in the Potentiometric mode. This is because for Potentiometric mode the physisorbed gas molecules only donate electrons for conduction through the substrate, while the chemisorbed molecules have bound electrons which do not take part in ionic conduction. The resistive mode of measurement gives higher response at higher temperature due to electrons contributed by the chemisorbed gas molecules.

4. CONCLUSION

This work has been attempted to compare the response curve shifts with temperature of the *p*-type, La_2CuO_4 and the *n*-type, WO_3 semiconducting sensing element

RESEARCH ARTICLE

fabricated over YSZ substrate in NO gas atmosphere. For La_2CuO_4 based sensing element, in Potentiometric mode, the minimum temperature of response was 290 °C and in Resistive mode it was 320 °C while maximum temperature of response for Potentiometric and Resistive modes were around 420 °C and 530 °C respectively. In case of WO_3 based sensing element the minimum temperature of responses was 325 °C for Potentiometric mode and for Resistive modes it was 400 °C. While maximum temperature of response was around 410 °C for Potentiometric mode and the measurement at higher temperature up to 500 °C was possible for resistive mode of measurement. From the experimental data, it has been observed that among Potentiometric and resistive mode Potentiometric mode was more sensitive at lower temperature range. Whereas for the resistive mode the sensors can be well operated upto higher temperature. Thus, Potentiometric mode of operation can be used at lower temperature and the resistive mode can be utilized for higher temperature to detect the NO gas.

Acknowledgment: The authors gratefully acknowledge the financial assistance of the University Grants Commission, India through the Major Research Project.

References and Notes

1. B. M. White and E. Traversa, *J. Electrochem. Soc.* 155, J11 **(2008)**.
2. C. Cantalini and M. Pelino, *Sens. Actuators B* 35–36, 112 **(1996)**.
3. J. Tamaki and Z. Zhang, *J. Electrochem. Soc.* 141, 2207 **(1994)**.
4. L. Chen and S. C. Tsang, *Sens. Actuators B* 89, 68 **(2003)**.
5. B. M. White, F. M. Van Assche, E. Traversa, and E. D. Wachsman, *ECS Trans.* 1, 109 **(2006)**.
6. T. Morita, M. Miyayama, J. Motegi, and H. Yanagida, *Chemical Sensors* **(1993)**; M. A. Butler, A. J. Ricco, and N. Yamazoe (eds.), *The Electrochemical Society Proceedings Series*, Pennington, PV **(1993)**, Vol. 93–7, p. 450.
7. M. Penza, C. Martucci, and G. Cassano, *Sens. Actuators B: Chem.* 50, 52 **(1998)**.
8. B. White, S. Chatterjee, E. Macam, and E. Wachsman, *J. Am. Ceram. Soc.* 91, 2024 **(2008)**.
9. E. Macam, B. Blackburn, and E. D. Wachsman, *Sens. Actuators B: Chem.* 158, 304 **(2011)**.
10. E. Macam, B. Blackburn, and E. D. Wachsman, *Sens. Actuators B: Chem.* 157, 353 **(2011)**.
11. E. R. Macam, B. M. White, B. M. Blackburn, E. D. Bartolomeo, E. Traversa, and E. D. Wachsman, *Sens. Actuators B: Chem.* 160, 957 **(2011)**.
12. S. Roy, W. Sigmund, and F. Aldinger, *J. Mater. Res.* 14, 1524 **(1999)**.
13. I. Kim, A. Rothschild, and H. L. Tuller, *Acta Mater.* 61, 974 **(2013)**.
14. M. J. Madou and S. R. Morrison, Academic Press **(1989)**, p. 556.
15. W. Gopel, *Prog. Surf. Sci.* 20, 9 **(1985)**.
16. S. M. Kanan, O. M. E. Kadri, I. A. Abu-Yousef, and M. C. Kanan, *Sensors* 9, 8158 **(2009)**.

RESEARCH ARTICLE

SENSOR LETTERS
Vol. 16, 1–7, 2018

Fabrication and Characterization of NO_x Gas Sensor Based on Lanthanum Copper Oxide (La_2CuO_4) Nanoparticles Annealed at Different Temperatures

Suman Chatterjee* and Aparna Ghosh

Department of Physics, University of North Bengal, Siliguri 734013, India

(Received: 22 January 2018. Accepted: 22 January 2018)

The detection limit of solid state gas sensors are dependent on the size and average pore diameter of the sensing material which can be varied by sintering the materials at appropriate temperatures. In this paper, we report the fabrication and characterization of a potentiometric NO_x gas sensor based on La_2CuO_4 nanoparticles as efficient electrode material annealed at different temperatures. The synthesized nanoparticles were characterized by scanning electron microscopy (SEM) and X-ray diffraction (XRD) which revealed that the particle size of the prepared nanomaterials increases with increasing the sintering temperature. It was observed that the smaller nanoparticles increases the contact surface area of the gas–solid interface and exhibited higher sensitivity at low gas concentrations. From voltage response curve, it has been observed that range of detection was maximum at intermediate particle size diameter and became least at large diameter nanoparticles. Planar sensor elements were fabricated over tape cast YSZ substrate with both the ceramic and metal electrodes screen printed on either side of the substrate. The dependence of sensitivity at different range of gas concentration with the pore size distribution of the sensing electrode has been studied in this investigation.

Keywords: La_2CuO_4 Nanoparticles, NO_x Gas Sensors, Sintering Temperature, Potentiometric Method.

RESEARCH ARTICLE

1. INTRODUCTION

Metal oxide semiconductor gas sensor with finer microstructures are ideal candidates for low range detection because of its larger contact surface area between gas–solid interface. From the view point of today's demand, development of sensors, suitable for low range detection are necessary because of increase in environmental pollutants from different industrial exhaust and automobiles. There are already some legislation[1] based on low limit values for CO, NO_x and HCs from automotive emission. Several earlier investigations reported that sensitivity and response time depends on gas concentration profile.[2] The dependence of sensitivity at different range of gas concentration with the pore size distribution of the sensing electrode of YSZ based Potentiometric sensor has been studied in this investigation. Two theories have been proposed to explain the working mechanism of the potentiometric sensors: Mixed Potential Theory and Differential Electrode Equilibria Theory. Among them, Mixed Potential Theory originates from corrosion theory,[3] in which a pair of reduction and oxidation (redox) electrochemical reactions occur simultaneously to establish an equilibrium and there by produces a corrosion potential.[13] This concept was first introduced in order to address potentiometric responses that deviated from the Nernst Equation.[4–12] According to Mixed Potential Theory, multiple gas reactions simultaneously come to equilibrium over the electrodes and each electrode establishes a mixed potential based on the equilibrium and rates of these reactions. For a NO sensor, the following equations represents the corresponding redox reactions:

$$2NO + 2O^{2-} \rightarrow 2NO_2 + 4e^- \quad (1)$$

$$O_2 + 4e^- \rightarrow 2O^{2-} \quad (2)$$

Since it measures the equilibrium level of NO, cannot describe NO sensing accurately. There are two limitations

*Corresponding author; E-mail: suman_chatterjee@hotmail.com

in Mixed Potential Theory, one of them is that NO does not come to thermodynamic equilibrium at sensor operating conditions because of the kinetic limitations and other is that at least one of the electrodes in a sensor must be a semiconducting material. To overcome these discrepancy Wachsman et al. introduced the idea of Differential Electrode Equilibria[14] to the gas sensing mechanism which is a more inclusive theory that takes into account multiple contributions as a cause for the difference in potential between two electrodes. Besides them additional contributions, namely the adsorptive and catalytic properties of semiconducting oxides, including La_2CuO_4, have been thoroughly studied to potentiometric sensitivity in NO_x sensors. Upon adsorption of gas, semiconductors exhibit a change in Fermi Energy which lies between the valence and conduction bands and tends to bend under development of charge on the surface due to the adsorption.[15] Since Fermi Level is the localized electrochemical potential of electrons ($\mu_e = E_F$), the output (i.e., the difference between two electrodes) of a potentiometric sensor is affected by this phenomenon. Mixed Potential Theory that occurs over electrodes also does not take account for gas phase catalysis. So, sensitivity of semiconducting gas sensors in potentiometric mode can be explained with adsorption kinetics.

Earlier investigations with Potentiometric gas sensors indicate that electrode's microstructure affect the sensitivity and response time of the sensor[16–18] due to a large number of adsorption sites of microstructure electrode element which increases the surface to bulk ratio of microstructure electrode that extend the surface charging into the core of the microstructure. In previous work it was reported that response time decreases with microstructure of electrodes.[19] The NO_x sensors based on YSZ as a solid electrolyte has been reported in many publications.[20–28] From literature survey it has been observed that there are various sensors for NO_x detection in the form of Cr_2O_3 |YSZ| Pt,[29] $La_{0.8}Sr_{0.2}FeO_3$ |YSZ| Pt,[30] NiO |YSZ| Pt,[31,32] $La_{0.8}Sr_{0.2}CrO_3$ |YSZ| Pt,[33] La_2CuO_4 |YSZ| Pt,[34] CuO |YSZ| Pt,[35] possess maximum range of detection 500 ppm, 20–1000 ppm, 10–400 ppm, 0–500 ppm, 50–400 ppm, 10–100 ppm respectively. But dependence of electrode's pore size with range of detection of a sensor is not discussed properly yet. Here we will discuss how detection of ultra-low ppm range is possible by using nano-crystalline microstructure electrode.

The experimental curve and simulated curve in this study both provide proofs of *s*-type nature of sensitivity with gas concentration with a definite shift in sensing range with average pore size of sensing layer. Microporous La_2CuO_4 based NO_x sensor also exhibit higher sensitivity at low gas concentration and low range (ppm) detection capability.

2. EXPERIMENTAL DETAILS

In this study to fabricate a sensor, tape cast YSZ (20 mm × 10 mm × 0.15 mm) was taken as substrate and La_2CuO_4 as one of the electrode which were prepared through Auto-ignition technique,[36] where nitrate salts of constituent elements were taken and citric acid was added in appropriate proportion and subsequently heated with thorough mixing to form a gel, which was burnt to ashes which depends on the citrate-nitrate ratio, and was the key parameter in determining the powder morphology and the prepared La_2CuO_4 were calcined in air at 750 °C, 800 °C and 1000 °C and mixed with appropriate amounts of solvents and ball-milled for 10 hrs. The slurry thus obtained was screen-printed on one face of the substrate and Pt was pasted on the other. Thin platinum wires were connected to both the electrodes using Pt paste for ohmic contact. Finally, after drying of the printed electrode slurry, the sensor was sintered at appropriate temperature. The synthesized nanoparticles were characterized by X-ray diffraction (XRD) (Fig. 1) and scanning electron microscopy (SEM) (Fig. 2), which revealed that the particle size of the prepared nano materials increases with increasing the annealing temperature. The phase identification of all three perovskite oxides showed only the peaks of orthorhombic perovskite-type La_2CuO_4 phases.

Prepared La_2CuO_4 perovskite-based sensor was systematically evaluated for NO reduction activity in Nitrogen (N_2) as carrier gas and the sensing experiments were carried out in a gas-flow system with a controlled heating facility. The sensors were exposed to step change of 50, 100, 200, 400 and 650 ppm of the NO gas to be sensed, in simulated combustion environment, at the total flow rate of 300 ml/min, in the temperature range between 400 and 700 °C. Electromotive force (EMF) measurements were performed between the two electrodes of the sensors using a Keithley 2400, digital voltmeter. During the EMF measurements, the electrode with the oxide coating was always kept at the positive terminal of the electrometer

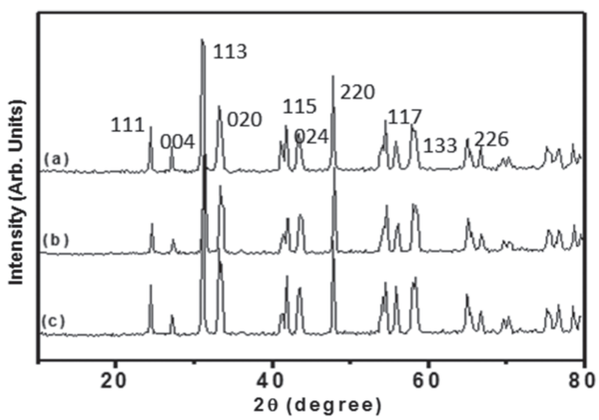

Fig. 1. X-ray diffraction pattern for the prepared La_2CuO_4 nanoparticles sintered at (a) 750 °C, (b) 800 °C and (c) 900 °C.

RESEARCH ARTICLE

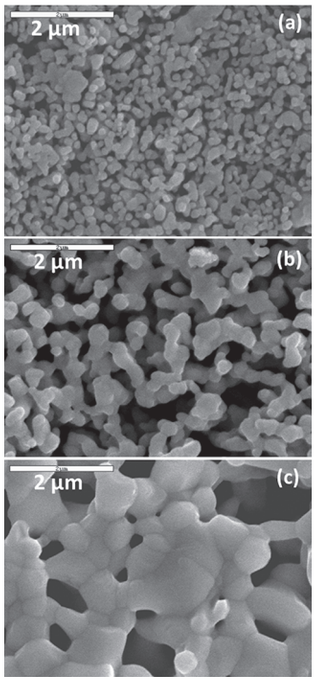

Fig. 2. Typical SEM images of prepared La_2CuO_4 nanoparticles sintered at (a) 750 °C, (b) 800 °C and (c) 900 °C.

and both the electrodes were exposed to the same gas environment.

3. RESULTS AND DISCUSSION

Figure 2 revels that powder sintered at 750 °C, 800 °C and 1000 °C exhibit tiny, intermediate and macro grains respectively. Again, it was observed from earlier literature that pores were usually comparable to their grainsizes.[37] With increasing sintering temperature, grains as well as pores began to fuse together,[38] produces a reduction of total porosity of the sensing material because of decreased surface area and modified surface structure.[39] In this regard, we optimized the sintering temperature at 1000 °C for macro pore and that sintered at 750 °C to yield micro pore, while 800 °C to yields mesoporous sensing surface.

3.1. Change of Response Magnitude with Gas Concentration

The NO gas response of the potentiometric sensing element has been shown in Figure 3 where the response voltage is presented with changing gas concentrations in steps of 0, 50, 100, 200, 500 and 650 ppm. Under exposure of 650 ppm NO gas on the three types of porous sensing surfaces, gas response at a fixed temperature (450 °C) are different in magnitude and it is maximum for sensor which exhibit tiny pore, sintered at 750 °C and is minimum for that which exhibit macropore, sintered at 1000 °C. However, under close observation it was seen that the sensitivity is not always same and it indicates a larger variation at

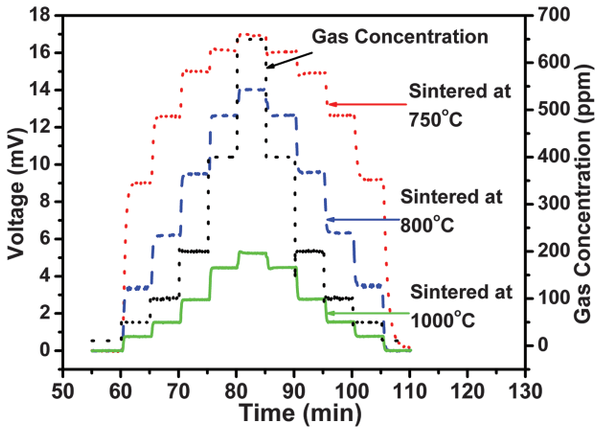

Fig. 3. Voltage response of three different types of prepared La_2CuO_4 nanoparticles sintered at 750 °C, 800 °C and 900 °C with step change in gas concentration.

the beginning for micropores and smaller variation at the beginning for macro-pores. In order to understand the variation more closely, the sensitivity of three types of sensing surfaces are plotted in Figure 4.

3.2. Sensitivity with Pore Size

Actually, with the increase in pore size following three types of diffusion occur at sensing material such as surface diffusion, Knudsen diffusion and molecular diffusion respectively,[40] which are responsible for gas sensing at different types of porous surfaces. For microporous material, pore sizes are too small to adsorb multiple layers of gas molecules and also, the pore edges are sharp. Due to these factors, the gas adsorption or surface forces are dominant so that adsorbed gas molecule cannot escape from force field of the surface. Due to small volume of pores, saturation of gas adsorption occurs at lower gas concentration

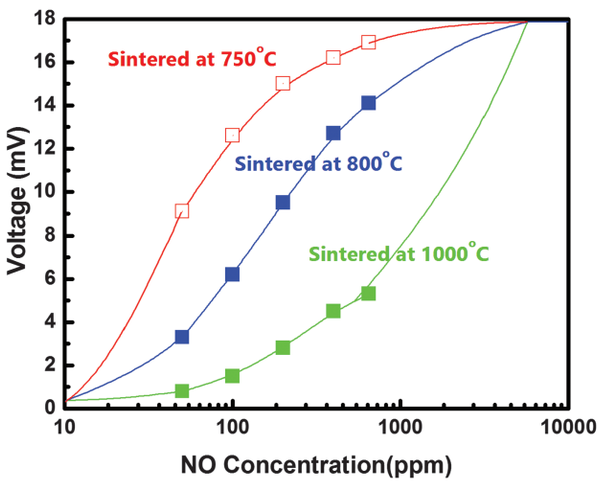

Fig. 4. Voltage response of three different types of prepared La_2CuO_4 nanoparticles sintered at 750 °C, 800 °C and 900 °C with gas concentration at 450 °C.

RESEARCH ARTICLE

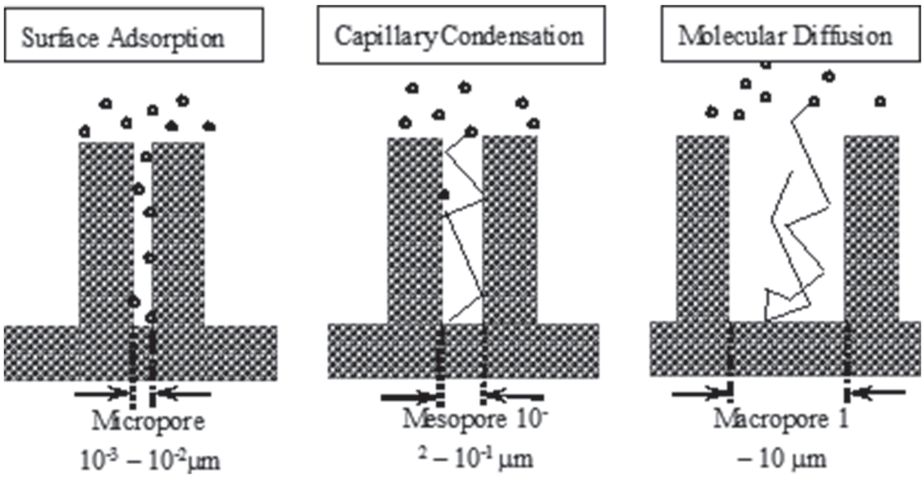

Fig. 5. Schematic diagram of gas diffusion through different porous sensing surface.

ranges. This variation can be explained with the help of diffusion theory in nano porous media.[41] On the other hand, for mesoporous range, as the pore sizes are comparatively larger, capillary forces dominate over surface forces for their sensitivity in which pore condensation occur after multilayer adsorption of gas on the sensing material, as a result free volume of a mesopore decreased slowly than micropore after sorption treatment.[42,43] Again, from literature survey, Nitrogen adsorption isotherm for active charcoal showed that Nitrogen uptake at low relative pressure was mainly due to filling of micropores.[44] So, in case of mesoporous surface, sensitivity is smaller than that for microporous sensor in the low concentration range. The reason behind this may be due to an increased number of Vander-waals interactions between gas molecules inside the confined space of capillary. For macro pore, molecular diffusion is responsible for their sensitivity,[45] in which transport properties of gas molecules through the macro pore is large but gas adsorption capacity is very small, and in this case interaction between gas molecules is significantly larger than the interaction between gas molecule to pore wall, that's why it exhibits a smallest sensitivity among them as shown in Figure 5. This can be explained with the concept of mean free path length.

The gas diffusion coefficient is related linearly with its pore diameter as given in equation

$$D_K = 4/3r\sqrt{\frac{2RT}{\pi M}} \tag{3}$$

By using this diffusion constant and by solving the diffusion equation, one can estimate the amount of gas adsorbed (C_A) inside the sensing surface.

$$\frac{\partial C_A}{\partial t} = D_K \frac{\partial^2 C_A}{\partial x^2} - kC_A \tag{4}$$

$$C_A = C_{AS} \frac{\cosh[(L-x)\sqrt{k/D_K}]}{\cosh[L\sqrt{k/D_K}]} \tag{5}$$

Where, C_{AS} is the gas concentration outside the sensing layer, and L and x is the thickness of sensing layer and the diffusion length respectively. The different range of detection for micro, meso and macro-porous sensing surface can be explained with the help of this gas concentration profile inside this sensing surface, which again depends on pore size (from Eq. (3)) as well as surface reaction and rate of diffusion on surface of sensing material.[46,47] The gas concentration reduces with decrease in pore diameter. For micropores, volume of gas adsorbed is sufficiently low. This results in the gas molecules to reside closely near the sensing surface and further diffusion is restricted, reducing the chances of multilayer adsorption. Since micropores are in the range of <1 nm so it is assumed that a small concentration of target gas is sufficient to fill the pore,[48] so saturation region in this case came earlier than meso and macro-porous surfaces.

For macro-porous surfaces, the amount of gas adsorbed in sensing layer is sufficiently large, increasing the collision probability between gas molecules, results in lowering of mean free path length $\lambda_M = 2kT/(\pi d^2 P)$, where d and P are the pore diameter and pressure concentration of applied gas. So, a large number of multilayer adsorption is required to fill up the pore volume of the sensing material. In macro pores, diffusion occurs mainly by bulk or molecular diffusion mechanism in which diffusion coefficient is inversely proportional to square of its pore diameter as given in Eq. (6) below,

$$D_M = 2/3\sqrt{\frac{kT}{\pi m}}\frac{kT}{\pi d^2 P} \tag{6}$$

So, with increasing pore diameter, rate of diffusion decreases and as a result high concentration of target gas is required to fill all the pores of bulk region. For this reason, saturation occur at high concentration range of the target gas.

RESEARCH ARTICLE

In mesopore region, both the surface reaction as well as capillary forces are responsible for their wide detection range. In this case, the pore size is in intermediate range and so the volume of gas adsorbed will also be intermediate. Again, from Eq. (5), it can be observed that the adsorbed gas concentration (C_A) decreases from surface after few diffusion layers. So, adsorption starts at higher gas concentration than microporous surface and saturation occurs after a small number of multilayer adsorption. Here the mean free path length for mesopore is $\lambda_m = 1/(\sqrt{2}\pi\sigma^2)V/N_A$, where V is the gas molar volume at particular pressure and σ is the molecular cross section. In this case, collision probability between gas molecules are lower compared to collision probability with pore walls.

The profile of distribution of adsorbed molecules in subsequent layers can be obtained from Langmuir's isotherm equation for monolayer adsorption.[49] Considering evaporation in one layer and condensation in subsequent layer, the Langmuir's isotherm equation can be modified for nth layer as.

$$v = \frac{v_m cx}{(1-x)}\left[\frac{1-(n+1)x^n + nx^{n+1}}{1+(c-1)x - cx^{n+1}}\right] \quad (7)$$

Where, v is the volume of gas adsorbed when the entire adsorbent surface is covered with a complete unimolecular layer, $x = P/P_0$ and n is the number of layers of adsorbent v_m is the volume of the adsorbed gas in a monolayer of adsorbent. With the help of Eq. (7), the s-type nature of our experimental graph could be simulated and is presented in Figure 6. To explain the exponential rise in sensitivity at very low gas pressure range, following factors may be responsible. It is highly probable that some surface complex containing carbon, hydrogen, and oxygen remained at the sensing surface. These can decompose into

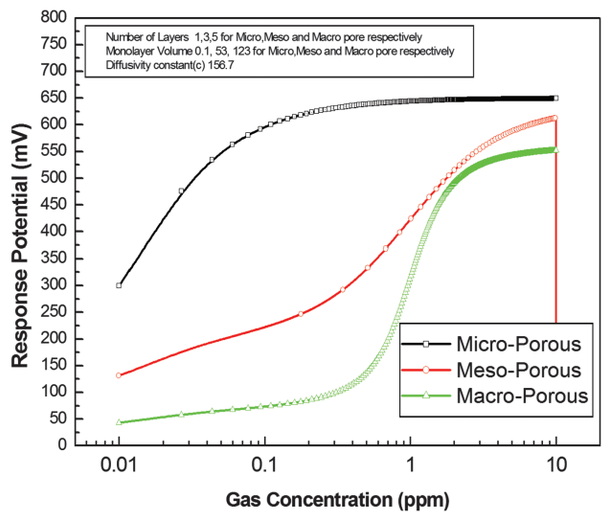

Fig. 6. Simulation of the sensitivity range for small, medium and large sized pores of sensing material.

CO_2, CO, and H_2 by continued thermal treatment. Some of this complex could be removed during the outgassing at 450 °C, but an appreciable portion always remained in the adsorbent. The presence of this residual complex could have a major influence on the observed steady-state pressure in the range of very low pressures. The experimental results suggest that one of the factors responsible for the behaviour observed at low pressures may be directly related to the residual complex. Another factor of influence is associated with the diffusion of gas molecules at low pressures. Because of the intricate structure of the porous material, more time is required for the adsorbate to locate the adsorption sites of minimum potential energy which reduces the surface coverage. A similar argument may be valid in connection with surface diffusion phenomena. This helps to explain the fact that even relatively well out gassed adsorbents (400 °C for 16 hr) required long periods to attain equilibrium in the low-pressure range.[50] With larger pore sizes, this equilibration time should be much larger. More and more be the gas pressure, the equilibration time became faster.

4. CONCLUSION

In conclusion, this study shows that the sensitivity of different microstructures are different in magnitude and they exhibit a shift in detection range, which has got definite correlation with pore size of the sensing layer. Larger pores have got higher sensitivity at higher concentration of gas whereas smaller pores have higher sensitivity at lower concentration of gas. Considering adsorption in one layer and condensation in subsequent layers and mean free path of gas molecules, we simulated the sensitivity profile. Simulation shows s-type nature of sensitivity with gas concentration with a definite shift in sensing range with average pore size of sensing layer. It was concluded that very large pore diameter reduced the adsorption sites and very small pore diameter reduced the probability of penetration. So, for the detection of higher concentrations one may use sensing material with larger pores and for low ppm detection one may use the sensor with micro pores.

Acknowledgments: The authors gratefully acknowledge University Grants Commission, India for financial support through the Major Research Project Grant No. F 41-841/2012 (SR) and UGC for awarding National fellowship to one of the authors.

References and Notes

1. W. Briggs, S. Chatterjee, E. Macam, and E. D. Wachsman, Effect of electrode microstructure on the sensitivity and response time of potentiometric NO_x sensors. *J. Am. Ceram. Soc.* 91, 2024 (**2008**).
2. M. Williams and R. Minjares, A technical summary of Euro 6/VI vehicle emission standards, The International Council on Clean Transportation, Washington, June (**2016**).
3. D. Jones, Principles and Prevention of Corrosion, Pearson Education (US), United States (**1996**).

RESEARCH ARTICLE

4. N. Miura, G. Lu, and N. Yamazoe, Progress in mixed-potential devices based on solid electrolyte for sensing redox gases. *Solid State Ionics* 136–137, 533 **(2000)**.

5. N. Miura, G. Lu, N. Yamazoe, H. Kurosawa, and M. Hasei, Mixed potential type NO_x sensor based on stabilized zirconia and oxide electrode. *Journal of the Electrochemical Society* 143, L33 **(1996)**.

6. N. F. Szabo and P. K. Dutta, Correlation of sensing behavior of mixed potential sensors with chemical and electrochemical properties of electrodes. *Solid State Ionics* 171, 183 **(2004)**.

7. F. Garzon, R. Mukundan, and E. Brosha, Solid-state potential gas sensors: Theory, experiments and challenges. *Solid State Ionics* 136.

8. G. Lu, N. Miura, and N. Yamazoe, High-temperature hydrogen sensor based on stabilized zirconia and a metal oxide electrode. *Sens. Actuators B Chem.* 35–36, 130 **(1996)**.

9. N. Miura, G. Lu, and N. Yamazoe, High-temperature potentiometric/amperometric NO_x sensors combining stabilized zirconia with mixed-metal oxide electrode. *Sens. Actuators B Chem.* 52, 169 **(1998)**.

10. N. Miura, S. Zhuiykov, T. Ono, M. Hasei, and N. Yamazoe, Mixed potential type sensor using stabilized zirconia and $ZnFe_2O_4$ sensing electrode for NO_x detection. *Sens. Actuators B Chem.* 83, 222 **(2002)**.

11. J. Park, B. Yoon, C. Park, W.-J. Lee, and C. Lee, Sensing behvior and mechanism of mixed potential NO_x sensors using NiO(YSZ) and CuO oxide electrodes. *Sens. Actuators B Chem.* 135, 516 **(2009)**.

12. V. Plashnitsa, T. Ueda, P. Elumalai, and N. Miura, NO_2 sensing performances of sensor using stabilized zirconia and thin-NiO sensing electrode. *Sens. Actuators B Chem.* 130, 231 **(2008)**.

13. N. Miura, G. Lu, N. Yamazoe, H. Kurosawa, and M. Hasei, Mixed potential type NO_x sensor based on stabilized zirconia and oxide electrode. *J. Electrochem. Soc.* 143, L33 **(1996)**.

14. E. Wachsman and P. Jaiyaweera, Selective detection of NO_x by differential electrode equilibria, *Solid State Ionic Devices II-Ceramic Sensors, The Electrochemical Proceedings Series*, edited by W. Weppner, E. Traversa, M. Liu, P. Vanysek, and N. Yamazoe, Pennington, NJ **(2000)**, Vol. PV 2000-32, pp. 298–304.

15. E. Macam and E. D. Wachsman, La_2CuO_4 sensing electrode configuration influence on sensitivity and selectivity for a multifunctional potentiometric gas sensor. *Sensors and Actuators: B Chemical* 160, 957 **(2011)**.

16. E. Di Bartolomeo, M. L. Grilli, and E. Traversa, Sensing mechanism of potentiometric gas sensors based on stabilized zirconia with oxide electrodes: Is it always mixed potential? *J. Electrochem. Soc.* 151, H133 **(2004)**.

17. E. Di Bartolomeo, N. Kaabbuathong, A. D'. Epifanio, M. L. Grilli, E. Traversa, H. Aono, and Y. Sadaoka, Nano-structured perovskite oxide electrodes for planar electrochemical sensors using tape casted YSZ layers. *Journal of the European Ceramic Society* 24, 1187 **(2004)**.

18. M. L. Grilli, E. Di Bartolomeo, and E. Traversa, Electrochemical NO_x sensors based on interfacing nanosized $LaFeO_3$ perovskite-type oxide and ionic conductors. *J. Electrochem. Soc.* 148, 98 **(2001)**.

19. A. Ghosh, P. K. Mandal, and S. Chatterjee, Temperature dependence of semiconducting gas sensors in potentiometric and resistive modes of measurement. *Sensor Lett.* 15, 137 **(2017)**.

20. J. Park, B. Y. Yoon, C. O. Park, W. J. Lee, and C. B. Lee, Sensing behaviour and mechanism of mixed potential NO_x sensors using NiO, NiO(YSZ) and CuO oxide electrodes. *Sensors Actuators, B* 135, 516 **(2009)**.

21. N. Miura, G. Lu, N. Yamazoe, H. Kurosawa, and M. Hasei, Mixed potential type NO_x sensor based on stabilized zirconia and oxide electrode. *J. Electrochem. Soc.* 143, L33 **(1996)**.

22. N. Miura, H. Kurosawa, M. Hasei, G. Lu, and N. Yamazoe, Stabilized zirconia-based sensor using oxide electrode for detection of NO_x in high-temperature combustion-exhausts. *Solid State Ionics* 86–88, 1069 **(1996)**.

23. N. F. Szabo and P. K. Dutta, Correlation of sensing behaviour of mixed potential sensors with chemical and electrochemical properties of electrodes. *Solid State Ionics* 171, 183 **(2004)**.

24. E. L. Brosha, R. Mukundan, R. Lujan, and F. H. Garzon, Mixed potential NO_x sensors using thin film electrodes and electrolytes for stationary reciprocating engine type applications. *Sensors Actuators B Chemical* 119, 398 **(2006)**.

25. E. Macam, B. M. Blackburn, and E. D. Wachsman, The effect of La_2CuO_4 sensing electrode thickness on a potentiometric NO_x sensor response. *Sensors and Actuators B: Chemical* 157, 353 **(2011)**.

26. P. Elumalai, J. Wang, S. Zhuiykov, D. Terada, M. Hasei, and N. Miura, Sensing characteristics of YSZ-based mixed-potential-type planar NO_x sensors using NiO sensing-electrodes sintered at different temperatures. *J. Electrochem. Soc.* 152, H95 **(2005)**.

27. H. T. Giang, H. T. Duy, P. Q. Ngan, G. H. Thai, D. T. A. Thu, D. T. Thu, and N. N. Toan, High sensitivity and selectivity of mixed potential sensor based on Pt/YSZ/$SmFeO_3$ to NO_2 gas. *Sensors Actuators B* 183, 550 **(2013)**.

28. G. Lu, N. Miura, and N. Yamazoe, High-temperature sensors for NO and NO_2 based on stabilized zirconia and spinel-type oxide electrodes. *J. Mater. Chem.* 7, 1445 **(1997)**.

29. L. P. Martin, A. Q. Pham, and R. S. Glass, Effect of Cr_2O_3 electrode morphology on the nitric oxide response of a stabilized zirconia sensor. *Sensors Actuators B: Chemical* 96, 53 **(2003)**.

30. E. Di Bartolomeo, N. Kaabbuathong, A. D'Epifanio, M. L. Grilli, E. Traversa, H. Aono, and Y. Sadaoka, Nano-structured perovskite oxide electrodes for planar electrochemical sensors using tape casted YSZ layers. *Journal of the European Ceramic Society* 24, 1187 **(2004)**.

31. P. Elumalai, J. Wang, S. Zhuiykov, D. Terada, M. Hasei, and N. Miura, Sensing characteristics of YSZ-based mixed-potential-type planar NO_x sensors using NiO sensing electrodes sintered at different temperatures. *J. Electrochem. Soc.* 152, H95 **(2005)**.

32. P. Elumalai and N. Miura, Performances of planar NO_2 sensor using stabilized zirconia and NiO sensing electrode at high temperature. *Solid State Ionics* 176, 2517 **(2005)**.

33. E. L. Brosha, R. Mukundan, R. Lujan, and F. H. Garzon, Solid-state mixed potential gas sensors: Theory, experiments and challenges. *Sensors Actuators B: Chemical* 119, 398 **(2006)**.

34. E. Macam and E. D. Wachsman, The effect of La_2CuO_4 sensing electrode thickness on potentiometric NO_x sensor response. *Sensors and Actuators: B Chemical* 157, 353 **(2011)**.

35. M. Breedon, S. Zhuiykov, and N. Miura, The synthesis and gas sensitivity of CuO micro-dimensional structures featuring a stepped morphology. *Mater. Lett.* 82, 5153 **(2012)**.

36. S. Roy, W. Sigmund, and F. Aldinger, Nanostructured yttria powders via gel combustion. *J. Mater. Res.* 14, 1524 **(1999)**.

37. M. Ando, S. Suto, T. Suzuki, T. Tsuchida, C. Nakayama, N. Miura, and N. Yamazoe, H_2S-sensitive thin film fabricated from hydrothermally synthesized SnO_2 sol. *J. Matter. Chem.* 4, 631 **(1994)**.

38. G. Kuczynski, Sintering and Catalysis 10, Springer, US **(1975)**.

39. G. Sakai, N. Matsunaga, K. Shimanoe, and N. Yamazoe, Theory of gas-diffusion controlled sensitivity for thin film semiconductor gas sensor. *Sensors and Actuators B: Chemical* 80, 125 **(2001)**.

40. G. Sakai, N. Matsunaga, K. Shimanoe, and N. Yamazoe, Theory of gas-diffusion controlled sensitivity for thin film semiconductor gas sensor. *Sensors and Actuators B: Chemical* 80, 125 **(2001)**.

41. J. Karger, D. M. Ruthven, and D. N. Theodorou, Diffusion in Nanoporous Materials, Wiley **(2012)**.

42. Y. Sun, H. Sai, K. A. Spoth, K. A. Tan, U. W. Zwanziger, J. Zwanziger, S. M. Gruner, L. F. Kourkoutis, and U. Wiesner, Stimuli-responsive shapeshifting mesoporous silica nano-particles. *Nano Lett.* 16, 651 **(2016)**.

43. R. Schlögl and A. Trunschke, Modern methods in heterogeneous catalysis, diffusion in porous media measurement and modelling, Lecture Series, Fritz-Haber-Institute, Berlin **(2011)**.

44. K. Sing and J. Rouquerol, Adsorption at the Gas–Solid and Liquid–Solid Interface, Elsevier **(1982)**.
45. R. Schlögl and A. Trunschke, Modern methods in heterogeneous catalysis, diffusion in porous media measurement and modelling, Lecture Series, Fritz-Haber-Institute, Berlin **(2011)**.
46. E. W. Thiele, Relation between catalytic activity and size of particle. *Ind. Eng. Chem.* 31, 916 **(1939)**.
47. C. N. Satterfield, Mass Transfer in Heterogeneous Catalyst, MIT Press, Cambridge, MA **(1970)**.
48. G. Newcombe, M. Drikas, and R. Hayes, Influence of characterised natural organic material on activated carbon adsorption: II. Effect on pore volume distribution and adsorption of 2-methylisoborneol. *Water Research* 31, 1065 **(1997)**.
49. S. Brunaur, R. P. H. Emmett, and Edware, Adsorption of gases in multimolecular layers. *Am. Chem. Soc.* 60, 309 **(1998)**.
50. C. Liang, A study of physical adsorption at low coverages. *J. Phys. Chem.* 57, 84 **(1953)**.

SENSOR LETTERS
Vol. 16, 1–6, 2018

Investigation of Sensing Mechanism of NO Oxidation on WO_3 Surface Using Density Functional Analysis

Suman Chatterjee*, Aparna Ghosh, and Chinmay Roy

Department of Physics, University of North Bengal, Siliguri, 734013

(Received: xx Xxxx xxxx. Accepted: xx Xxxx xxxx)

The mechanism of NO adsorption on the WO_3 surface to improve the performance of gas sensing has been studied from a theoretical view point based on Density Functional Study. Different activation energies of the defect directly affect the surface chemistry of the sensing material. Here, the adsorption behaviour of NO on the sensor surface, including the perfect and WO_3 surfaces with defects have been studied. In this study it was revealed that surface oxygen vacancies induced by the adsorption of NO molecule on the defect free WO_3 surface increased the surface conductance of the sensing material. The WO_3 surface with defects was re-oxidized by the atmospheric O_2 molecules. During this step, charge transfer from the surface to O_2 molecule generates an active O_2 species which results in reduction of surface conductivity. This active O_2 species tends to react with the NO molecule and releases NO_2 molecule with the reproduction of perfect WO_3 surface. The difference between Fermi levels associated with above surface reactions were determined with the help of Density Functional study and was found to be 1.54 eV.

Keywords: Defects, Activation Energy, Nyquist Diagram, Oxygen Partial Pressure, Conductivity, Fermi Energy.

RESEARCH ARTICLE

1. INTRODUCTION

For environmental pollution levels measurement, gas sensors are hopeful candidates because of their low cost, fast response, high sensitivity, and direct electronic interface. Metal oxides are used as gas sensitive materials, due to their reproducibility and typical surface properties which are suitable for gas detection. They are robust, lightweight, long lasting and beneficial from high material sensitivity and quick response times and also relatively inexpensive compared to other sensing technologies. Tungsten oxide (WO_3) is one of these oxide elements studied extensively as NO_x sensors.[1] The functioning of these sensing devices can be attributed to the defects present in the surface of the material.[2,3] Material and surface properties are strongly dependent on the nature, concentration, and arrangement of defects like pores, voids, impurities, and vacancies. In our early studies we have presented *n*-type, WO_3 semiconducting sensing element fabricated over YSZ substrate in NO gas atmosphere,[4] since NO is one of the major air pollutant gas and also reducing in nature. To analyze the air quality, the development of NO sensing materials has become an important subject of current research. Concentration of electrons increases when a reducing gas is exposed on an *n*-type semiconductor surface. The change of resistivity of sensor surface is associated with oxidation–reduction kinetics of adsorbed gas.[5] It has been shown in earlier literature that NO gas affects the conductivity of the semiconductor sensing materials WO_3.[6–9] So, a theoretical study is very essential to understand the sensing mechanism of metal oxide material WO_3 with oxidation of NO on the surface. However, such theoretical analysis, compared with experimental results are lacking so far. Recently Tian's group have performed a series of first principle calculations.[10,11] Recent theoretical studies mainly focus on the adsorption behaviour of NO at WO_3 surfaces,[12] where surface resistivity of sensing material is related to the change of oxygen vacancy concentration ($V_o^{\cdot\cdot}$). A dramatic effect on the electronic structure of WO_{3-x} has observed at higher $V_o^{\cdot\cdot}$ concentration (4%) where defect states become dispersed and then merge with the conduction band, that gives the metallic character of the sensing material.[13,14] In this work, the role of oxygen vacancies ($V_o^{\cdot\cdot}$) on the performance of NO sensing by through the material WO_3 have been studied.

*Corresponding author; E-mail: suman_chatterjee@hotmail.com

2. EXPERIMENTAL DETAILS

2.1. Synthesis of Sensing Material and Device Fabrication

For the preparation of a sensing electrode, Tungsten oxide powder was mixed thoroughly with solvent ethanol and plasticizer (0.01%) ethylene glycol. For resistive measurement, a square electrode of the sensing material was printed on one side of an YSZ substrate and it was fitted with Pt electrodes. In this case both the electrodes were in the same side. Finally, the prepared sensors sintered at 400 °C for 12 hours. To study the sensing mechanism with the help of density functional theory, we remove one oxygen atom from WO_3 to produce defect with creation of single oxygen vacancy.

2.2. Characterization of Sensing Elements

The morphology of the sample was observed using a Scanning electron microscope (SEM). Figure 1 shows the microstructure of sensing surfaces.

The particle size was around ~100 nm for the films. The BET surface area of powders was found to be 11.2 for WO_3 powders. X-ray diffraction patterns of both the sensing materials WO_3 was collected in the 2θ range of 5 °C to 70 °C which shows complete formation of WO_3 phase.

2.3. Fabrication and Measurements

Sensing experiments were carried out with a gas flow system connected to a quartz tube which was inside of a furnace. Then the sensors were exposed to NO gas. For resistive measurement, the change in resistance between the two sensor electrodes was monitored using a digital source meter (2400 Keithley source meter). Computational methods using density functional analysis are taken to illustrate the experimental output.

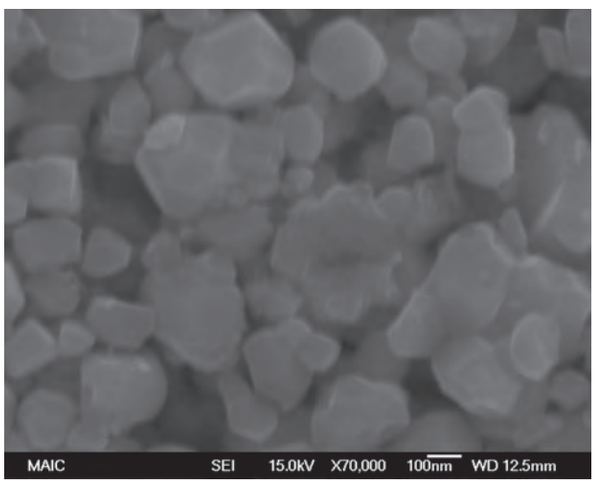

Fig. 1. SEM micrograph of sensing surface WO_3.

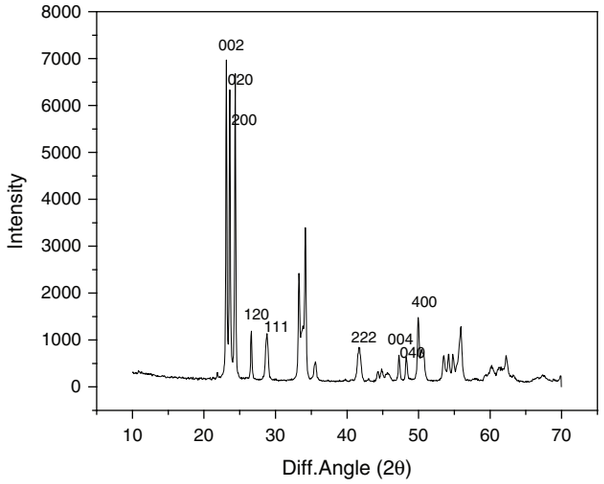

Fig. 2. X-ray diffraction pattern of sensing surface WO_3.

3. RESULTS AND DISCUSSION

3.1. Dependence of Oxygen Partial Pressure on Sensor Output

The defect phenomena at two temperature ranges results in introduction of defect only in high temperatures and defect free substrate at low temperatures. This is further confirmed through impedance analysis.

Figures 3(a) and (b), represent the variation of $\mathrm{Im}(x)$ with $\mathrm{Re}(x)$ at different partial pressure at two different temperature, is a circle whose right intercept with the x axis represent device resistance at $\omega \to 0$ and it is related by an equation

$$\mathrm{Re}(x) = R/(1+\omega^2 R^2 C^2) \tag{1}$$

From Figures 3(a) and (b), it is seen that with increasing partial pressure of oxygen, resistance of the sample increases which is also true for Figure 3(c) and it agrees with the relation[15–18]

$$R = R_{\mathrm{O}} P_{\mathrm{O2}}^{\beta} \tag{2}$$

where R_{O} is the sensor resistance in pure O_2 and β is the power law coefficient, which demands that the sensing material is n-type. And it is also seen that at temperature 450 °C the value of real part of resistance is much larger than that at 650 °C. It implies that at 450 °C, oxygen adsorption plays a significant role in sensing mechanism than at higher temperature 650 °C. Actually, at low P_{O2}, there occurs a loss of oxygen from semiconductor bulk and at high temperature there occur a lattice vacancy by releasing conduction band electrons. From Figure 3(c), it is seen that, slope of the resistivity versus log (P_{O2}) graph at 450 °C is much higher than that at 650 °C, which implies that at low temperature region activation energy is higher than that at high temperature region, where the relation between conductivity and P_{O2} with E_{g} at a fixed temperature is given by

$$\sigma \infty P_{O_2}^{-1/6} \times e^{-E_{\mathrm{g}}/kT} \tag{3}$$

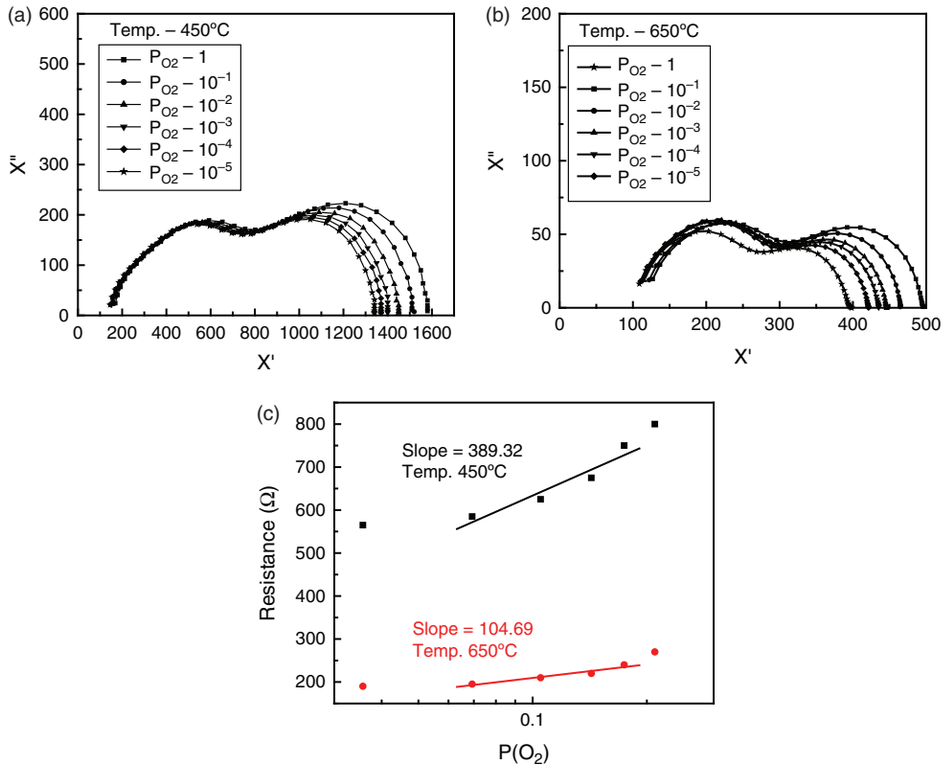

Fig. 3. (a) Nyquist diagrams of WO_3 films in different P(O_2) at 450 °C. (b) Nyquist diagrams of WO_3 films in different P(O_2) at 650 °C. (c) Variation of resistance as a function of P(O_2) plotted on logarithmic axes.

This difference in activation energies at two temperature ranges results in introduction of defects only in high temperatures and defect free substrates in low temperatures.

3.2. Resistivity of WO_3 Thin Film with Reducing Gas

Figure 4(a) shows the resistance variation with temperature at a gas concentration of 650 ppm of NO, for WO_3 film fired between 300 °C to 800 °C temperature in NO gas atmosphere. Variation of resistance with temperature obeys the relation

$$R = R_0 e^{(-\Delta E/KT)} \tag{4}$$

and this curve consist of three distinct regions indicating different conduction regions with different slopes. At the high temperature range, the decrease in resistance with increasing temperature indicates the semiconductor behavior of the WO_3 thin film.[19]

Figure 4(b) shows the activation energy derived from Figure 4(a). From Figure 4(a), we see that at very low

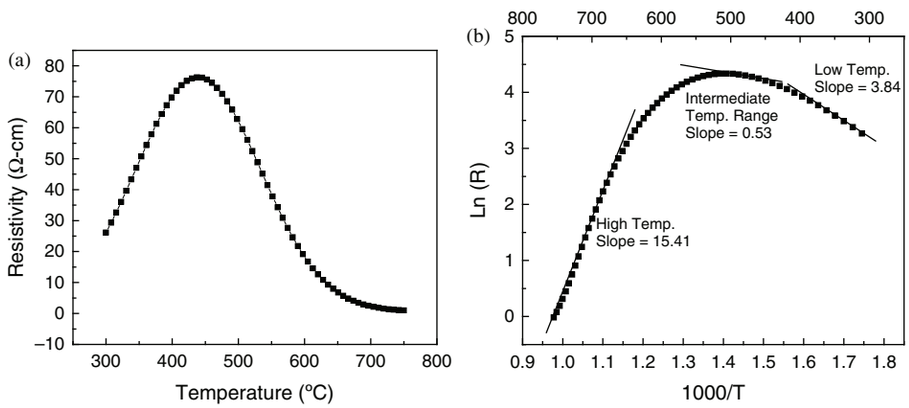

Fig. 4. (a) Response with temperature of WO_3 sensing surfaces in resistive mode and (b) corresponding arrhenius plot.

RESEARCH ARTICLE

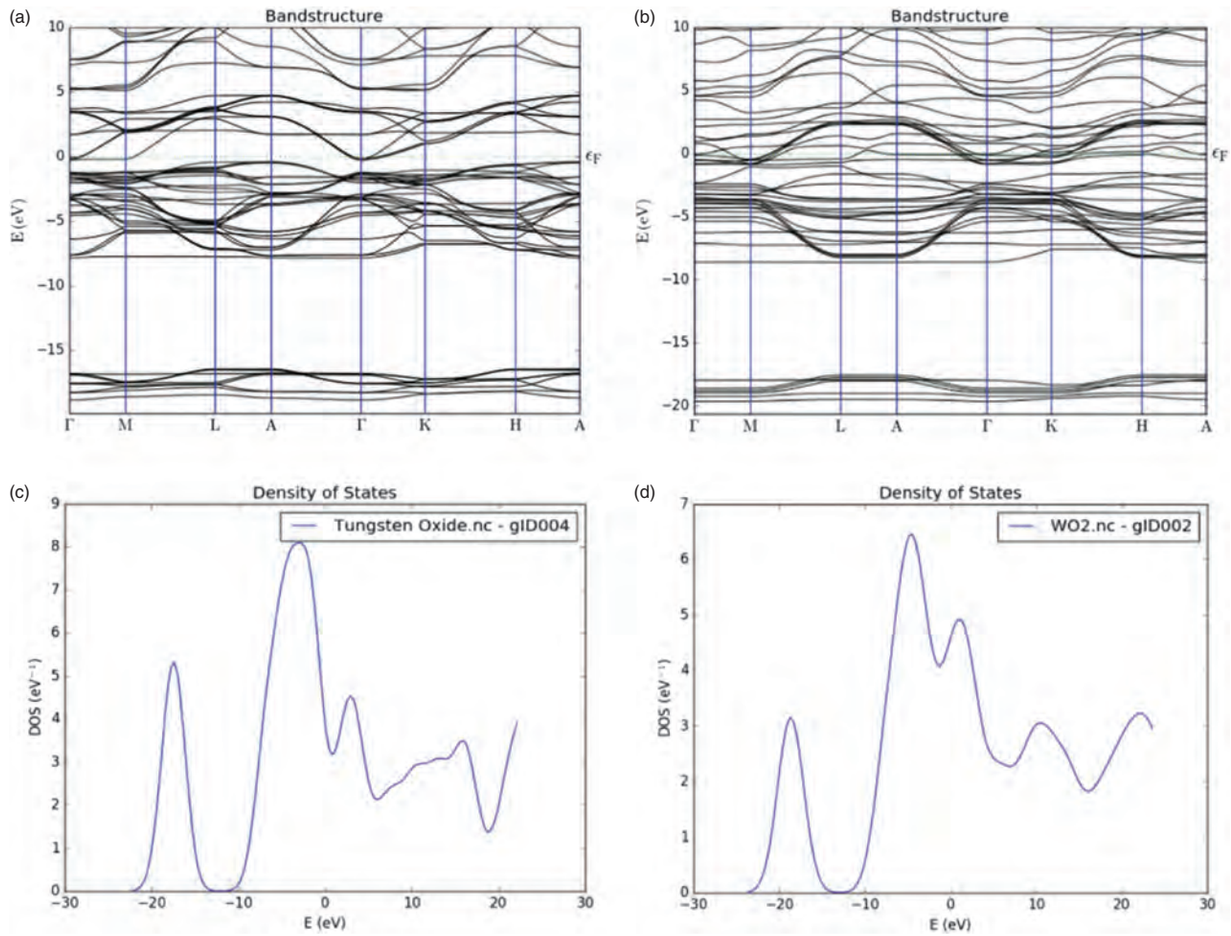

Fig. 5. (a) Band structure of WO_3 (Fermi level = −6.41 eV). (b) Band structure of W_nO_{3n-1} (Fermi level = −4.87 eV). (c) Variation of DOS with energy for WO_3 structure. (d) Variation of DOS with energy for WO_3 with 5 percent defect surface states.

temperature region, between 300 °C to 450 °C, the resistivity of sensing material is high. This is due to oxygen atoms pre-adsorbed on the surface which can be explained by the equation

$$(WO_3 + e^-) + 1/2O_2 WO_3(O^-)_{ad} \quad (5)$$

and further NO adsorption is not possible so high activation energy is required in this region. In the intermediate range, between 450 °C to 600 °C, the activation energy is lower, allowing NO adsorption by replacing oxygen atoms on surface which can be explained by the equation

$$WO_3(O^-)_{ad} + NO \rightarrow (WO_3 + e^-) + NO_2 \quad (6)$$

From Eq. (5) it is clear that the ionosorption of atmospheric oxygen consume conduction band electrons which again become free by removal of O^- surface species by reducing gas NO. The net rate of return of electrons to the conduction band depends on oxygen partial pressure by a relation

$$\frac{dn}{dt} = K_2 P_{NO} - K_1 \sqrt{P_{O2}} \quad (7)$$

where K_1 and K_2 are rate constant for the processes involved in Eqs. (5) and (6) respectively. This equation again confirms that with decreasing P_{O2} the net rate of return of electrons to the conduction band must increase, provided P_{NO} remains constant. Whereas, at high temperature range, between 600 °C to 800 °C, the activation again rises (Fig. 4(b), as all gas molecules gets expelled from the surface and conductivity is determined by solid-state ionic equilibria.

The reduction of activation energy in the intermediate temperature range which is mainly due to the release of electron[20] which can be further explained with the help of defect equation,

$$W_nO_{3n} + NO = W_nO_{3n-1} + V_{O'} + NO_2 + e^- \quad (8)$$

Accumulation of these electrons create a donor level which reduces the activation energy.

The WO_3 surface with defect was further re-oxidized by the atmospheric O_2 molecules following the defect equation

$$W_nO_{3n-1} + NO + O_2 = W_nO_{3n} + NO_2 \quad (9)$$

RESEARCH ARTICLE

at very high temperature region. During this step, charge transfer from the surface to O_2 molecule generates an active O_2 species resulting in a reduction in surface conductivity. This active O_2 species tends to react with the NO and releases NO_2 with the reproduction of perfect WO_3 surface. With increasing concentration of gas, the number of oxygen vacancy is increased and such oxygen vacancies changes of the surface structure significantly.[21]

Resistivity of WO_3 thin films against the reciprocal temperature are represented by Arrhenius curves, the slopes of which depend on environment conditions of the sample. And the variation of conductivity σ with temperature is normally interpreted using Arrhenius equation

$$\sigma = \sigma_o \exp(-E_o/Kt) \tag{10}$$

where σ is the conductivity and E_o, the activation energy for electrical conduction and K the Boltzmann constant. The activation energy deduced from this equation corresponds to the slopes of the Arrhenius curves.

The conductivity of tungsten oxide films is controlled by the non-stoichiometry of n-type WO_3 and originates only from oxygen vacancies was assumed. The creation of oxygen vacancies in WO_3 can be expressed by a chemical equilibrium,

$$O_o^x \Leftrightarrow V_o^x + \left(\frac{1}{2}O_2\right)_g \tag{11}$$

Where, O_o^x is the neutral oxygen atom in an oxide site and V_o^x is the neutral oxygen vacancy with two trapped electrons giving rise to a donor level in the gap. When the temperature is increased, the donors are successively ionized with an activation energy E_a, generating free electrons e in the conduction band. This process is expressed by

$$V_o^x \Leftrightarrow V_o^{2+} + 2e^- \tag{12}$$

Where, V_o^{2+} represents a doubly ionized oxygen vacancy and subsequently, the total equilibrium for carrier generation is

$$O_o^x \Leftrightarrow V_o^x + 2e + \left(\frac{1}{2}O_2\right)_g \tag{13}$$

When the defect levels concentration increases, the donor orbitals overlap and lead to the formation of band which lessens the gap required for carrier ionization. For high defect concentration the "defect band" broadens sufficiently so that the gap disappears. Such a "defect band" model can be applied to the conductivity results that we obtain on WO_3 where the defects are surface oxygen vacancies. When the oxygen pressure decreases the density of oxygen vacancies, increases up to a $c(2 \times 2)$ structure for some parts of the sample. So according to the model of "defect band" the activation energy for electron generation decreases as the density of vacancies increase with decreasing oxygen partial pressure and drop to zero when the WO_3 sample is annealed in vacuum.[22–25]

In fact, there are many other parameters consider, in particular the grain size with the barrier at the grain boundaries should play an important role in the conduction mechanism. However, we suppose that the most important phenomenon in our experimental conditions is the oxygen vacancy formation.

3.3. Explanation with Band Structure Calculations

From Band structure it was noted that the Fermi level lies above the band gap for both the defect free and WO_3 structure with oxygen vacancies and hence the material is n-type all through the concentration level of the adsorbed gas. There is a clear rise in the Fermi energy for WO_3 with defect surface ($E_F = -4.87$ eV) than WO_3 with defect free surface formed ($E_F = -6.41$ eV) due to gas adsorption and creation of donor levels. From the DOS it was seen that the density of states near the Fermi level is quite large for samples with defect. This variation of DOS plays a significant role in sensor output.

4. CONCLUSION

Our work demand that defect may affect the electrical transport by changing the band gap and density of states (DOS) of sensing material. For perfect structure the Fermi level positioned at -6.41 eV and for defect structure that positioned at -4.87 eV. This shift in Fermi energy is due to creation of large number electron at the conduction band of metal after formation of oxygen deficient surface. Practically when reducing gas (NO) exposed on a transition metal oxide (WO_3) based sensing material it become oxidized to NO_2 gas by creating oxygen vacancy on the surface and there by formed oxygen deficient surface and release electrons. The total number of oxygen vacancies is strongly related with defect density. So, sensor output must depend on defect density. Here, we generate 5% oxygen vacancy by removing oxygen atoms from WO_3 surface that gives a change in Fermi level between perfect and structure with defects, whose value is 1.54 eV. Actually, after creation of oxygen vacancy, magnitude of DOS decreases and Fermi level shifts towards higher energy states due to large concentration of electrons at conduction band of metal so that several partly occupied energy bands appeared at the Fermi level. These differences in Fermi level and DOS are responsible for resistive sensor output.

RESEARCH ARTICLE

References and Notes

1. H. Windishmann and P. Mark, A model for the operation of a thin film SnOx conductance modulation carbon monoxide sensor. *J. Electrochem. Soc.* 126, 627 (**1979**).
2. A. Hartmann, M. K. Puchert, and R. N. Lamb, Influence of copper dopants on the resistivity of ZnO films. *Surf. Interface Anal.* 24, 671 (**1996**).
3. K. M. Anisur Rahman, Susan C. Schneider, and Martin A. Seitz, *J. Am. Ceram. Soc.* 80, 1198 (**1997**).

4. A. Ghosh, P. K. Mandal, and S. Chatterjee, Temperature dependence of semiconducting gas sensors in potentiometric and resistive modes of measurement. *Sensor Lett.* 15, 137 **(2017)**.

5. D. Zappa, A. Bertuna, E. Comini, M. Molinari, N. Poli, and G. Sberveglier, Tungsten oxide nanowires for chemical detection. *Anal. Methods* 7, 2203 **(2015)**.

6. B. White, S. Chatterjee, E. Macam, and E. D. Wachsman, Effect of electrode microstructure on the sensitivity and response time of potentiom etric NO_X sensors. *J. Am. Ceram. Soc.* 91, 2024 **(2008)**.

7. M. Williams and R. Minjares, A technical summary of euro 6/VI vehicle emission standards, The International Council on Clean Transportation, June **(2016)**.

8. E. D. Bartolomeo, M. L. Grilli, and E. Traversa, Sensing mechanism of potentiometric gas sensors based on stabilized zirconia with oxide electrodes: Is it always mixed potential? *J. Electrochem. Soc.* 151, H133 **(2004)**.

9. E. D. Bartolomeo, N. Kaabbuathong, A. D'Epifanio, M. L. Grilli, E. Traversa, H. Aono, and Y. Sadaoka, Nano-structured perovskite oxide electrodes for planar electrochemical sensors using tape casted YSZ layers. *J. Eur. Ceram. Soc.* 24, 1187 **(2004)**.

10. L. Zhao, F. H. Tian, X. Wang, W. Zhao, A. Fu, Y. Shen, S. Chen, and S. Yu, Mechanism of CO adsorption on hexagonal WO_3 (001) surface for gas sensing: A DFT study. *Comput. Mater. Sci.* 79, 691 **(2013)**.

11. F. Tian, L. Zhao, X. Y. Xue, Y. Shen, X. Jia, S. Chen, and Z. Wang, DFT study of CO sensing mechanism on hexagonal WO_3 (001) surface: The role of oxygen vacancy. *Appl. Surf. Sci.* 311, 362 **(2014)**.

12. V. Nagarajan and R. Chandiramouli, DFT investigation on CO sensing characteristics of hexagonal and orthorhombic WO_3 nanostructures. *Superlattices Microstruct.* 78, 22 **(2015)**.

13. F. Wang, C. Di Valentin, and G. Pacchioni, Semiconductor to metal transition in WO_{3-x}: Nature of the oxygen vacancy. *Phys. Rev. B* 84, 073103 **(2011)**.

14. C. Di Valentin, F. Wang, and G. Pacchioni, Tungsten oxide incatalysis and photocatalysis: Hintsfrom DFT. *Topics Catal.* 56, 1404 **(2013)**.

15. P. K. Clifford and D. T. Tuma, Characteristics of semiconductor gas sensors I. Steady state gas response. *Sensors and Actuators* 3, 233 **(1982–83)**.

16. J. F. McAleer, P. T. Moseley, J. O. W. Norris, D. E. Williams, and B. C. Tofield, *J. Chem. Soc. Faraday Trans.* 1.83, 1323 **(1988)**.

17. B. M. Smith, G. S. V. Coles, and G. Williams, Tin oxide gas sensors, European Patent Application, EP 0 806 657 A2.

18. N. Murakami, K. Tanaka, K. Sasaki, and K. Ihokura, *Anal. Chem. Symp. Ser. (Chem. Sens.)* 17, 165 **(1983)**.

19. M. Gillet, C. Lemire, E. Gillet, and K. Aguir, The role of surface oxygen vacancies upon WO_3 conductivity. *Surface Science* 532 **(2003)**.

20. H. Jin, H. Zhou, and Y. Zhang, Insight into the mechanism of CO oxidation on WO_3 (001) surfaces for gas sensing: A DFT study. *Sensors* 17, 1898 **(2017)**.

21. S. Majidi, A. Achour, D. P. Rai, P. Nayebi, S. Solaymani, N. B. Nezafat, and S. M. Elahi, Effect of point defects on the electronic density states of SnC nanosheets: First-principles calculations. *Results in Physics* 7, 3209 **(2017)**.

22. M. G. Hutchins, N. A. Kamel, N. Elkadry, A. A. Ramadam, and K. Abdel-Hady, *Phys. Stat. Sol. A* 175, 991 **(1999)**.

23. J. P. Bonnet, J. F. Marucco, M. Onillon, and P. Hagenmuller, *J. Solid State Chem.* 40, 270 **(1981)**.

24. C. Scott, Moulzolf, S.-A. Ding, and R. J. Lad, *Sensor. Actuator. B* 77, 375 **(2001)**.

25. J. Novotny and S. Sloma, Surface and Near Surface Chemistry of Oxide Materials, edited by J. Novotny and L. C. Dufour, Elsevier Science Publishers **(1988)**.